"Mimicking the abrasion resistant sandfish epidermis"

Von der Fakultät für Mathematik, Informatik und Naturwissenschaften der RWTH Aachen University zur Erlangung des akademischen Grades eines Doktors der Naturwissenschaften genehmigte Dissertation.

vorgelegt von

Boštjan Vihar, M.Sc.

Aus Maribor, Slowenien

Berichter: Universitätsprofessor Prof. Dr. Peter Bräunig
Universitätsprofessor Prof. Dr. Werner Baumgartner

Tag der mündlichen Prüfung: 7. September 2015

"L'essentiel est invisible pour les yeux."
Antoine de Saint-Exupéry

Abstract

The sand inhabiting skink *Scincus scincus* has due to its sand swimming behaviour gained some attention by the research community in recent years. The sand swimming creates ample stress on the outer layers of its skin, generating the prospect of wear. The skin itself is however very resilient towards abrasion and even facilitates smoother movement by reducing friction against the sharp sand particles. Past research has concentrated much on the characterization of structure and surface properties of the skin, however, a complete understanding of its properties is lacking up to date. In this work, a review of known data is done in addition to new measurements concerning surface properties, composition, ultrastructure and mechanics, but also other feats such as optical properties. Replication of "anti-adhesive" properties on existing technical materials was tested along with the development of new techniques for such endeavour. Chemical and structural analysis shows the epidermis of the sandfish is very homogeneous and is mainly composed of compact bundles of β keratins, which are possibly interlinked by a matrix composed of α keratins. Strong glycosylation of the keratins was shown, confirming previous studies, and five glycan structures were observed in the analysis. The occurrence of glycans could also be linked with the surface properties concerning surface energy and adhesion of the epidermis towards sand. Mechanical properties of the sandfish epidermis were shown to be similar to some artificial polymers which will be interesting for the replication of the sandfish epidermis from artificial materials. The surface micro structure of the sandfish epidermis has been shown to promote diffraction of light. This might suggest possible light trapping or dispersion behaviour, which could not be conclusively confirmed. Finally, we propose a hypothesis on abrasion resistance and friction reduction, which is possibly the result of an interplay between mechanical and chemical properties of both keratins and glycans. However, additional research will be required to confirm the proposed mechanism.

Acknowledgements

I would like to express my sincere gratitude to my mentor, Prof. Dr. Werner Baumgartner, for the chance to work on this project and the guidance I needed during the process. I thank Prof. Dr. Peter Bräunig for taking responsibility on and being an expert witness of my work. I also thank Prof. Dr. Lothar Elling for the valuable discussions, scientific input and for being an expert witness to this work. Special thanks goes to Agnes Weth, whose methodological expertise enabled me to do things, I otherwise could not. I thank Christian Effertz, Dennis Hirtz, Prof. Dr. Franz Georg Hanisch, Matic Tement, Umut Cakmak, Christian Reißecker, Prof. Dr. Johannes Heitz, Lisa Maria Uiberlacker, Markus Himmelsbach and Lucas Sternbauer for their indispensable cooperative work on the project, which I was not capable of doing myself. Much appreciation goes to the DFG (the German Research Foundation) and the Bionik Graduate school Bonn - Aachen - Jülich, which financed the project and without which this work was not possible. I owe thankfulness to all my colleagues at RWTH Aachen and JKU Linz, who often gave council, provided ideas for the research and created a pleasant working atmosphere. Special thanks also goes to my family and friends, who supported and motivated me to achieve my goals.

Contents

List of Figures

Chapter 1 - General introduction

1.1 About the Sandfish

Scincus scincus, first described by Linnaeus (1758), is a desert inhabiting lizard and one of the few squamates which have adapted to life under sand. The fish-like locomotion of some closely related lizards has earned these sand swimming animals the common name "sandfish" which is literally translated from the Arabic سمكة الرمال (pronounced "smkh arlm-al"). In this work, the name sandfish will be used exclusively for *Scincus scincus*, which was the main object of research in our lab. The genus *Scincus* (first termed by Garsault, 1764) today has four species, several subspecies (Arnold & Leviton 1977) and the family of skinks (*Scincidae*) is with roughly 1200 species the most diverse family of lizards we know today (Sever & Hopkins, 2005). The full taxonomical classification after Welsch & Storch (2003) is shown below:

Phylum:	Chordata
Subphylum:	Vertebrata
Class:	Sauropsida
Order:	Squamata
Suborder:	Lacertilia
Superfamily:	Scincomorpha
Family:	Scincidae
Subfamily (Greer, 1970):	Scincinae
Genus:	*Scincus*
Species:	*Scincus scincus*

1.1.1 Basic description

An adult sandfish has a body length of about 20cm, including a 5 - 8cm tail and can weigh from 25 to 30 grams. Around the neck and tail, local accumulations of adipose tissue are found beneath the skin, making these regions very wide and creating a smooth transition to other body parts (Arnold & Leviton, 1977). As a result, the body has a streamlined form, contributing to improved gliding through powdery materials (Arnold & Leviton, 1977). The lateral and dorsal

Figure 1.1: *Scincus scincus* in its natural environment. Photo by Chris Mattison/FLPA (2009).

skin coloration is yellow with dark transversal stripes. The head and the ventral side of the body have a lighter beige to greyish color. While body shape and coloration are fairly common among members of the same species, local variations do exist (Arnold & Leviton, 1977). The frontal cross section of the body has a pentagonal shape, which is the result of a flat ventral side and a slight dorsal elevation along the vertebral column. The head is semi-conical, continuing the body form into the tip of the snout. Its eyes are small and can be closed with eyelids to prevent irritation by the sand. The ears are covered with scales, likely for the same reason, although some authors suggest this might also improve subterranean hearing by increasing vibrational translation (Arnold & Leviton, 1977; Hetherington, 1989). To actually be able to move through the densely packed sand bed, the body musculature needs to be sufficiently strong (Maladen et al., 2009), but the limbs also play an important role in the locomotion (Hartmann, 1989; Baumgartner et al., 2008). The digits are flat and covered with extended scales which reduce the spaces in-between and increase the contact surface to sand and movement control (Arnold & Leviton, 1977). In contrast, the scales on the body are compactly aligned, making particle accumulation between them impossible. The skin feels very smooth to touch and has a clear optical shine.

1.1.2 Ecology

The sandfish inhabits sandy deserts of North Africa and a large part of the Middle East, its main habitat being loose sand with minimum vegetation like grass or dry shrubs (Hartmann, 1989). The sandfish can be found throughout the Atlantic coast of Africa in the west, the Atlas Mountains and the Mediterranean Sea to the north, the savanas and rain forests in the south and the Arabian sea in the east, see figure 1.2 (Arnold & Leviton, 1977; Baumgartner et al., 2007; Map of Life, 2011).

The sandfish is an omnivorous animal, feeding on grass fruits and seeds, but mainly on desert

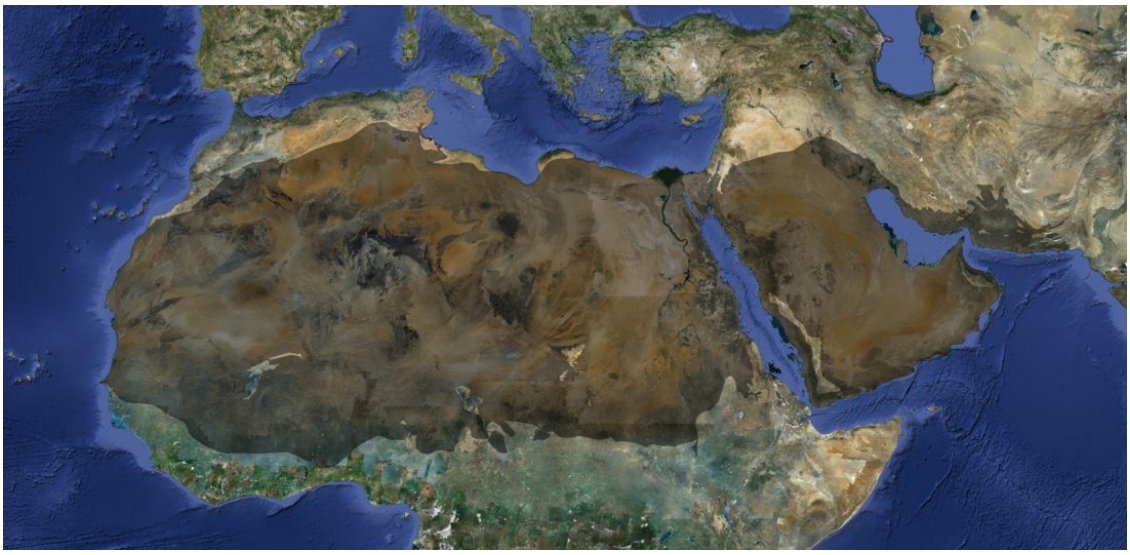

Figure 1.2: Geographic distribution of *S. scincus*. Sandfish populations can be found in all corners of the Sahara desert, the Arabian peninsula and southern Iran, Map of Life (2011).

insects, like orthopters (Hartmann, 1989). Even though it occurs occasionally, because of the general lack of liquid water in its environment, the sandfish must rely on extracting water from its animalic prey (Hartmann, 1989). The food is swallowed whole, digesting larger chunks is therefore done in cycles with intermediary pauses (Hartmann, 1989), probably for breathing. The sandfish is a diurnal animal and strongly depends on the photoperiode for its day/night rhythm (Hartmann, 1989). It remains buried for the most part of the day and emerges mostly for feeding and reproduction, but also for vitamin D production (Hartmann, 1989). Male as well as female animals share common sand dunes and both tolerate other subjects in their vicinity most of the time, except during the mating season, when the males are more aggressive and try to fend off other males (Hartmann, 1989).

Sandy deserts offer very specific habitats, and the loose sand, which is also the home of the sandfish has some interesting properties. Sand typical for the sandfish's habitat varies somewhat in particle size from 0.06 to 0.5mm in diameter. The major part is represented by particles with approximately 0.12mm in diameter, smaller grains making up less than 10% of the overall mass of the sandbed (Hartmann, 1989). On sunny days, where air temperatures can rise above 50°C, the sand surface can become even hotter. Because the sand particles are irregularly shaped, the sand bed is a porous medium, filled with many air pockets (Holdich, 2002). Heat conduction to lower layers is therefore slow and a gradient is created in the vertical direction, with a constant temperature in a specific depth (Nofziger, 2003). During night time, when air temperature can drop even below 0°C, the gradient is flipped and changes like these could be hostile for most animals. On the other hand, due to the temperature gradients and deep areas with more constant temperatures, sand dwelling animals have an opportunity to move from layer to layer and thereby passively regulate their body temperature.

As a habitat, a finely particulate sand medium can also be challenging from other perspectives. Once compact, it may create a resistance to chest expansion of a buried animal, preventing

respiratory ventilation (Vihar, 2012). The fine sand particles may also enter the respiratory system, thus blocking the airways and preventing gas exchange (Vihar, 2012), also, the fine, sharp particles could damage the delicate olfactory and respiratory surfaces (Vihar, 2012). High airflow resistance and prolonged lingering in the same position can create local depletion of oxygen and accumulation of carbon dioxide. However, experiments and simulations have shown that the metabolic rate of the sandfish is low enough to sustain physiological conditions (Vihar, 2012). Studies also suggest that the ventilation dynamics and the anatomy of the nasal cavity may create a solution for filter less particle removal (Vihar, 2012).

From a technological perspective, a very interesting and also one of the most studied features of the sandfish is its subterranean locomotion - sand swimming. Different modes of movement were described by different research groups. Maladen et al. (2009) have observed locomotion in plastic granulate where the animal presses its limbs to the body and moves by propagating an undulatory travelling wave. Baumgartner et al. (2008), on the other hand, have recorded swimming in sand where the animal also used its limbs. Trotting movements with a frequency of approximately 3Hz thereby seemed to promote local sand decompaction, making the medium behave as a fluid.

Due to the mostly buried state, yet predatory feeding and somewhat communal social way of life, questions arise about under-sand orientation and location of prey, predators and other things. In general, reptiles tend to have a weak sense of hearing, yet exhibit a strong sense for vibrations which are translated over the skeleton and processed by the auditory system (Vitt & Caldwell, 2014). Orientation by echolocation has been known in other animals (Simmons & Stein, 1980; Pack & Herman, 1995; Payne, 1971), and does seem advantageous in compact sand, but could not be verified up to date for the sandfish in any way.

1.1.3 Motivation

As shown above, studying the sandfish is interesting from many aspects, however, this work mainly concentrates on the skin and its anti abrasive, low friction properties. The fact that the skin is indeed smooth and shiny despite constant scraping by the sharp sand particles, is what motivated early biomimetic research on this group of animals. When in contact with sand, the skin surface shows very low friction and abrasion, when compared to other materials like glass or polished steel (Rechenberg & Khyari, 2004; Baumgartner et al., 2007). The abrasion resistance is indeed so advanced, that despite constant exposure to abrasion and rare moulding (shedding), which occurs evenly through a period of approximately 3 months (Hartmann, 1948), the epidermis keeps its surface intact (Rechenberg & Khyari, 2004; Baumgartner et al., 2007). Even the exuviae remain this way long after the process.

1.2 Project goals

The aim of this project was to continue the previous work of Saxe (2010) and Staudt (2012) and thereby further investigate the characteristics of the sandfish epidermis. In this regard, more details were to be acquired, specifically concerning friction reduction, abrasion resistance and a detailed characterization of the elements composing the epidermis which are responsible for the observed skin properties. Ultimately, the goal of the project was to fully comprehend the effect, create a working biomimetic prototype and devise a strategy for industrial production of meaningful applications.

Chapter 2 - What do we know about the adhesion and friction reduction, abrasion resistance and what do these have in common?

2.1 Introduction

2.1.1 From interaction to friction

The sandfish skin has remarkable properties concerning friction and abrasion, both of which prevent the surface from being damaged and enable smooth gliding through sand. Abrasion is the mechanical removal of material and will be discussed later on. Friction is defined as the resisting force of surfaces or fluid layers in relative motion to each other. In 1699 Guillaume Amontons postulated 3 laws which apply to dry friction:

1. The force of friction is directly proportional to the applied load. (Amontons' 1st Law)
2. The force of friction is independent of the apparent area of contact. (Amontons' 2nd Law)
3. Kinetic friction is independent of the sliding velocity. (Amontons's 3rd, also Coulomb's Law of friction)

For dry interfaces, friction can be divided into static and dynamic friction. Dynamic friction is the force needed to maintain the sliding, while static friction is the minimal lateral force needed to initiate it (Zhang et al., 2007). When two very close surfaces (or molecules) are at their lowest energy state, a critical finite force is required to initiate motion. This equals the potential energy barrier of the interface and is the result of change in interactions. The change depends on the spatial gradient of the motion. For example parallel separation - sliding (creates friction), or perpendicular (full) separation (creates adhesion). Because separation varies as a function of direction, sliding (friction) is not necessarily equally energy demanding as full separation (adhesion), but is related to it in terms of the nature of interaction (Zhang et al, 2007). Unlike chemisorption (ionic, covalent or metallic bonds), intermolecular or Van der Waals forces (Zangwill, 1988; Parsegian, 2005) occur between separate entities and are divided into three types, depending on the nature of attraction (ordered from strong to weak):

- Between permanent dipoles (Keesom forces) - two close dipoles will turn in the opposite direction to create an attraction.
- Between a permanent and an induced dipole (Debye forces) - A dipole will induce polarity on a nearby non polar molecule in the attractive direction.
- Between transient dipoles (London, or dispersive forces) - Due to their motion, electrons in every molecule will create transient dipoles. In close molecules, these form in an attractive manner.

The interaction potential (w) between two particles increases in proportion to the coefficient C, which is interaction specific (Keesom/Debye/London) and decreases in proportion to distance r to the 6th power. The resulting Van der Waals force (F) is a gradient of the Van der Waals potential:

$$w_{VdW} = -\frac{C}{r^6} \qquad \vec{F}_{VdW} = -\nabla w_{VdW}(\vec{r}) \tag{2.1}$$

Following DLVO (Derjauguin-London-Verwey-Overbeek) theory, which was developed for colloids, but is also applicable for flat interfaces, the stability of an interaction is determined by the sum of Van der Waals attractive forces and electrostatic repulsive forces (Parsegian, 2005), see Figure 2.1.

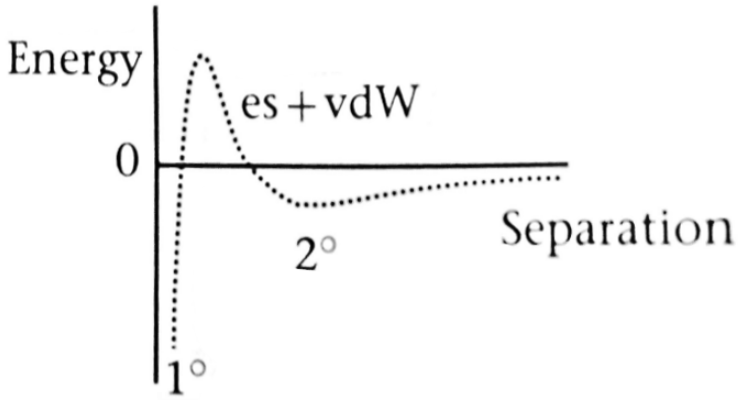

Figure 2.1: DLVO theory. The interaction forces between particles strongly depend on their relative distances. The range and coefficient of the force is interaction specific. Because these are different for Van der Waals and electrostatic forces, the summed curve is not a simple exponential function, but has a local minimum which is the "optimal" distance between two particles (Parsegian, 2005).

2.1.2 The "sandfish effect"

To understand why the sandfish skin has such low friction to sand and is so resilient against abrasion, some basic properties need to be defined and evaluated, which cover all the perspectives in question:

1. Properties which describe the interaction of the sandfish skin's surface with the sand particles of its environment, which include chemical composition and the occurring intermolecular (Van der Waals) forces.

2. Properties which describe skin deformation and recoil behaviour at contact with sand particles, which include material mechanics such as hardness and elasticity.

3. Contact surface - surface topography and the relation between the apparent and the projected surface area, compared to particle size and form.

2.1.3 What we know so far

Since research on the sandfish has been conducted for nearly two decades, many experiments have already been conducted, which help to describe the phenomenon.

Friction angles were measured on the dorsal and ventral side of the skin and on various other materials. The manner in which this was done was as follows: A sample was placed on a plane, which could be inclined while the angle was measured. Through a pipette, sand was applied to the surface and the sample inclination was reduced until the sand stopped flowing on the testing surface. At this point, the inclination was measured, which in this case, was equal to the friction angle of the sample. Different materials, like polished steel, glass, or teflon were measured and compared. The sandfish skin showed very low friction angles (21°), which were substantially lower when compared with the measured technical materials, as shown in Figure 2.2 (Rechenberg et al., 2004; Baumgartner et al., 2007).

AFM (Atomic Force Microscope) measurements. Since the phenomena are related as described before, measuring adhesion, can also reveal some clues about the friction. Adhesion forces between the sandfish epidermis and a silicon nitride (Si_3N_4) tip were measured using an AFM with a contact mode cantilever. While Si_3N_4 is structurally somewhat different from Si_2O_4, which is the main component of sand (Dobkin & Zuraw, 2003), it can still be used to measure adhesion, if comparative measurements of different samples are performed. The surface of sandfish and corn snake (*Pantherophis guttatus*) scales was scanned and force distance curves were measured and compared. Materials with strong adhesion show a large difference between the advancing and receding deflection curve and the difference is very small on materials which show little adhesion to the cantilever. Sample measurements of sandfish dorsal and ventral scales as well as dorsal snake scales can be observed in figure 2.3. In comparison, while the american corn snake exhibits large adhesion, almost none can be observed on the sandfish skin (Baumgartner et al., 2007). Considering that the substrate is chemically quite similar, this is quite surprising.

Wear is the process of material deterioration, which can be the consequence of different origins. We can distinguish different types of wear, such as adhesive wear, abrasion, fatigue and corrosion, each following its own laws, but also affecting others (Rabinowicz, 1995). Adhesive wear occurs

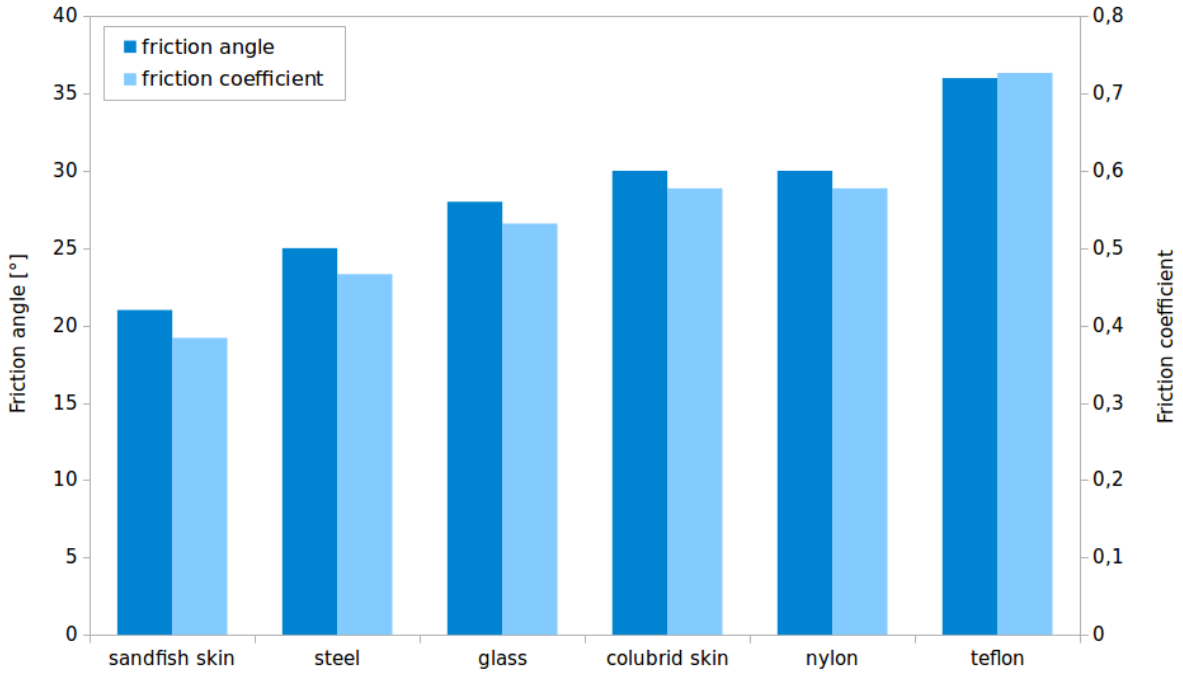

Figure 2.2: Friction angles comparison of sand with sandfish skin and other materials. Data by Rechenberg (2004) and Baumgartner et al. (2007).

at contact of different surfaces, when a part of one surface adheres to the other and is removed at surface separation. This type of wear arises from adhesive forces between atoms which come in close contact. Abrasion is the process where sample material is removed by mechanical scratching of a hard rough surface to a softer material. Adhesive and abrasive wear are sometimes confused, since both can be caused by small hard particles. They can, however, be distinguished, since abrasion typically manifests in deep, sharp scratches with mostly unified direction, while adhesive scratches are shallow and irregular (Rabinowicz, 1995). Fatigue is the result of repeated loading and unloading forces on a material, such as compression, bending, etc. In contrast to the above mentioned forms of wear, corrosion is not caused by mechanical damage, but rather other forms of deterioration, like chemicals or radiation (Rabinowicz, 1995). In previous studies on the sandfish, mostly abrasive and adhesive wear were tested by mild sand blasting. Sand was applied through a pipette to a surface 30cm below and the abrasion created by the sand beam was visually evaluated. Different materials were tested and compared, for example the sandfish skin, polished steel and glass. While both technical materials showed obvious abrasion damage, the sandfish showed no signs of abrasion at all, as seen in figure 2.4 (Rechenberg, 2004).

Artificial ageing by UV exposure was also performed. Sandfish exuviae were exposed to UV radiation, equivalent to the natural solar radiation in a period of 1 year in central Europe. After the treatment, the exuviae were visibly bleached, and the material became very brittle. SEM analysis also showed cracks in the material (Saxe, 2008).

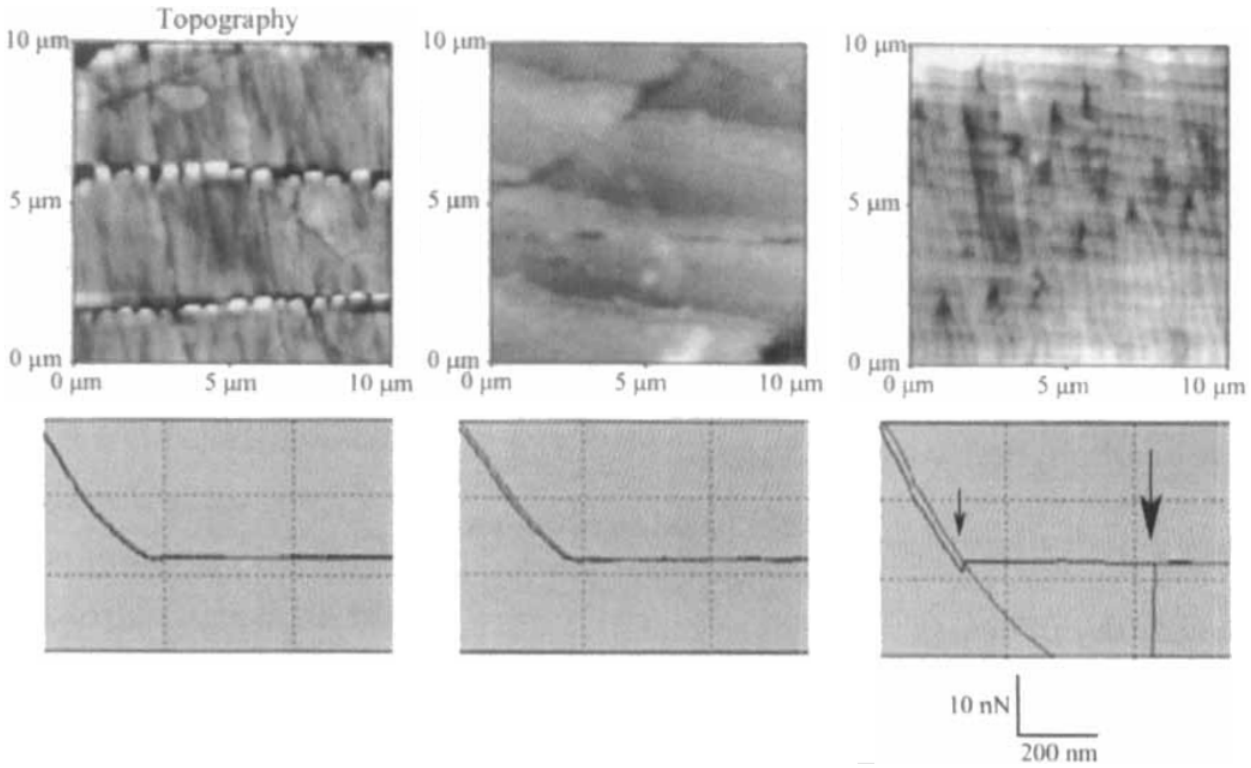

Figure 2.3: AFM measurement comparison of sandfish and corn snake scales. The upper images represent the topography scan, while the lower images show the sample force distance curves. The left column represents dorsal scales of the sandfish, the middle column the ventral scales and the right column the corn snake scales.

SEM (Scanning Electron Microscopy) was conducted on the sandfish and other animals' epidermises to identify any special structures present on the surface. The sandfish skin was compared to that of other sand dwelling reptiles and its relatives living in other habitats. Comb-like micro structures were found on the dorsal scales of many sand swimmers, like the wedge-snouted skink (*Sphenops sp.*), or the sand boa (*Eryx sp.*) and were therefore the reason why these were linked to the low friction properties in early research (Rechenberg 2009). This topic will be further discussed in chapters 3 and 4.

How to proceed Early research has done much to describe the superficial properties of the effect, especially those directly connected to the interaction of the skin with sand, like friction angles, adhesion, abrasion and topography. Also, some investigations were conducted on the biochemical composition of the epidermis which showed the keratin structure and their glycosylation. Still some properties remain to be investigated, before the effect can be thoroughly understood and effectively replicated:

- An in depth chemical and biochemical analysis revealing the glycan structures found on the keratins
- A structural analysis of the epidermis.

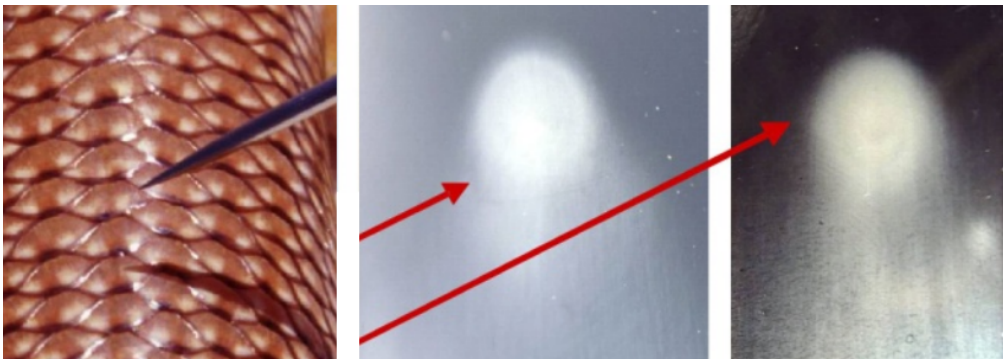

Figure 2.4: Sand blasting comparison of sandfish skin and technical materials. The image on the left shows the sandfish skin after mild sand blasting, compared to steel (middle) and glass (right). The needle, or the red arrows show the point of sand impact (Rechenberg, 2004).

- A mechanical analysis revealing the plasto-elastic properties of the epidermis.
- Further surface analysis revealing the more adhesive properties

2.1.4 Determining the surface energy

In a medium, attractive and repulsive forces occur between the interacting particles (Parsegian, 2005) and the sum of these interactions is called free energy (Israelachvili, 2011). When the surface area (A) of a medium is increased, the change of free energy is referred to as surface energy - γ (Israelachvili, 2011), which correlates to the work (W), which is required to increase the surface area:

$$\gamma = \frac{\partial W}{\partial A} \tag{2.2}$$

When separating a medium, for example into two halves, new surface area is created, one could therefore state, W is the work required to separate two surfaces, i.e. cohesion for a single medium, or adhesion for two different media (Israelachvili, 2011). The surface energy of a material therefore indicates, how this medium will interact with its environment. In liquids, the surface free energy is also equal to surface tension which is defined as the work required to increase the surface of a phase (Krüss). This makes the surface energy of liquids relatively simple to measure on reference surfaces with known properties and vice versa. When a small liquid drop is placed on a solid surface, the size of the interface depends on the solid-liquid interaction which, according to Young's equation, can be determined by measuring the contact angle (Krüss), see equation 2.3 and figure 2.5:

$$\gamma_s = \gamma_{sl} + \gamma_l \cos\theta \tag{2.3}$$

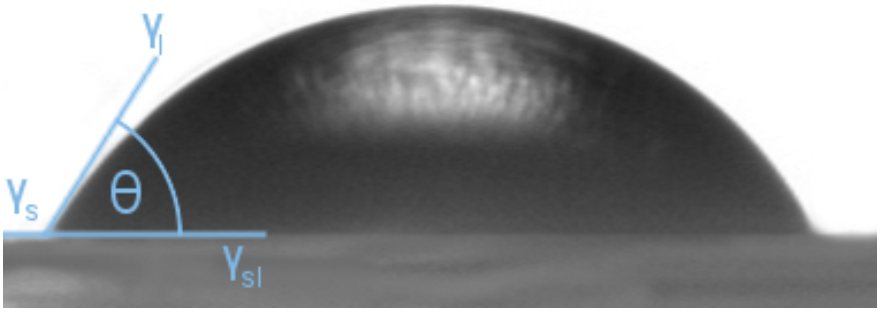

Figure 2.5: Young's equation and contact angle. A drop lying on a flat surface, exhibits a contact angle θ depending on the liquid-solid interaction. If the liquid is water and the solid is hydrophilic, the contact angle is smaller than 90°, as is the case in this example.

2.2 Methods

2.2.1 Epidermis preparation

Sandfish exuviae were thoroughly washed 3 times with tap water by vortexing for 1min, and 2 additional times with dH_2O. The washed scales were then transferred to a petri dish filled with dH_2O. The medial (inner) side of the epidermis is much more hydrophilic than the outer side, the pieces of exuviae therefore unfold spontaneously when floating on a sufficiently large water surface. The skin pieces were carefully placed on a glass slide (inner side of the epidermis facing downwards) and excess water was removed with a paper wipe. Then the epidermis was covered with a lint free kimtech wipe and pressed flat with a second glass slide under a weight. The purpose of this was to flatten the scales as much as possible and therefore create sufficient testing surface for contact angle measurements. The exuviae were dried over night (ON) at room temperature. It would have been interesting to analyse deglycosylated scales for comparison, however, the deglycosylation process includes denaturation and cleavage of the keratin chains, which could change the outcome of the measurements in unpredictable ways. For this reason *E. schneiderii* scales were used and prepared in the same manner.

2.2.2 Contact angle measurement

Contact angles are a means for measuring the wettability of a solid surface by a liquid, which is typically performed with a goniometer. Small drops (0.5-5μl) of a liquid are applied to a flat surface sample and recorded frontally with a digital camera. The drop profile from the image is used for contact angle determination. Various methods are suitable for this purpose, like:

- Drop shape analysis: The parameters of an ellipsoid/polynomial are matched to the optically determined drop arc and the contact angles are determined at the arc - baseline intersection.
- Height-width method: A very simple method which assumes the sessiles drop shape to be

a circular arc. The contact angle is calculated from the width:height ratio of an enclosing rectangle using the equation: $\theta = 2 \cdot \arctan \frac{2h}{d}$

Static contact angles were measured on the flattened, dried sandfish epidermis by applying 0.5μl drops of 7 different liquids, 20 drops each. The contact angles were measured with a goniometer at the Institute of Condensed Matter - RWTH Aachen University. The following liquids with their related surface tensions were used:

Substance	Surface tension (γ_l) [$\frac{mN}{m}$]	γ_P [$\frac{mN}{m}$]	γ_D [$\frac{mN}{m}$]
Diethyl pthalate	39.3	31.4	7.9
Pentadiol	43.3	27.6	15.7
Diethylene glycol	44.8	31.6	13.2
Ethylene glycol	47.5	29.3	18.2
2,2-thiobis-ethanol	53	25	18
Glycerol	65.2	28.3	36.9
dH_2O	72.3	53.6	18.7

Table 2.1: The liquids with their according properties and the equipment were provided at the Institute of Condensed Matter - RWTH. The surface tension, which for liquids is equivalent to surface energy of the liquid-vapour interface - γ_l is shown for each liquid in the second column. The third and fourth columns represent the polar (γ_P) and dispersive (γ_D) parts of the surface tension.

As a rough comparison, *E. schneiderii* scales were measured in the same way, however, only 3 liquids were used, dH_2O, Glycerol and DMSO (Surface tension = 42.9 $\frac{mN}{m}$). 13 drops of each liquid were applied. Since the scales of *E. schneiderii* are slightly larger, the drops were applied with more ease and showed a smaller measurement variation.

2.2.3 Surface energy calculation

The solid-vapour interaction or solid surface energy (γ_{sv}) is a constant under standard conditions, but is not always easy to measure. By measuring the contact angles of different liquids with known surface tensions, the surface energy can be approximated. Different approaches are used for this endeavour, however, the key to all of them is Young's equation. The average contact angle of each liquid was used in the free surface energy calculation for the sandfish and the Berber skinks epidermis. This was done with the help of Christian Effertz (Institute of Condensed Matter - RWTH) who followed a protocol developed at the institute and which is based on the theory of Kwok et al. (1997). For a homogeneous solid surface with a constant γ_{sv}, $\gamma_{lv} \cos\theta$ and γ_{lv} are plotted against each other. γ_{sv} is then determined at the point where $\gamma_{lv} \cos\theta = \gamma_{lv}$, in other words, at the intersection between the cosinus curve and the simetral of both axes.

For comparison, γ_{sv} was also determined with a model suggested by Balkenende et al. (1998). This is useful for predominantly nonpolar liquids, therefore water was excluded from the calcula-

tion. The equation is based on empirical data and uses the constant Φ, which is usually equal 1:

$$\cos\theta = 2\Phi\sqrt{\frac{\gamma_{sv}}{\gamma_{lv}}} - 1 \tag{2.4}$$

Following the protocol of Kaelble (1969), the polar and disperse portions of the epidermis' surface energy were also approximated. The model used is however not very precise and is only suitable for qualitative estimations.

2.3 Results and discussion

The results of the surface energy determination can be observed in figure 2.6. The contact angles for most liquids were relatively high, for dH_2O approximately 90°. The approximated free surface energy of the sandfish epidermis equalled $27.0\frac{mN}{m}$. The calculation of the empirical model for nonpolar liquids resulted in $23.8\pm2.0\frac{mN}{m}$. Both methods show very similar results and both methods indicate that the free surface energy of the sandfish skin is indeed very low when compared to inorganic materials like glass (2000 - 4000 $\frac{mN}{m}$), sapphire (638 $\frac{mN}{m}$) or mica (120 $\frac{mN}{m}$) and is more in the range of low energy surface polymers like teflon (19.1 $\frac{mN}{m}$) or polyethylene (32.4 $\frac{mN}{m}$). Values for the named materials were obtained from TWI-global. The approximated free surface energy of the berber skink is somewhat higher ($34.0\frac{mN}{m}$), but is still in the same order of magnitude. The calculation based on the model of Kaelble (1969) suggests, that the sandfish epidermis has both a dispersive ($21\frac{mN}{m}$) and a polar ($6\frac{mN}{m}$) portion of the free surface energy.

Considering the surface energy, the difference between the sandfish and the berber skink's skin seems small, yet significant. Previous work by Saxe (2008) and Staudt (2012) has shown that in biochemical analysis, sandfish skin is very similar to the skin of the berber skink, the only noticeable difference being that the sandfish has a slightly higher keratin molar mass (molecule size) and a higher glycan density, which is very likely the reason for the measured size difference. It is therefore natural to link differences in characteristics to the glycosylation. Glycans are composed of sugars and therefore contain hydroxylic groups, which should increase the surface energy, at least in the polar portion. It therefore seems surprising, that the surface energy of the sandfish skin with higher glycosylation would be lower than the surface energy of the berber skinks skin. Pure polymeric keratin typically has a contact angle close to 90° (cg2nanocoatings), is thus not considered hydrophilic and should have dominantly dispersive properties. In addition, calculations of the polar-dispersive portions of the surface energy were performed for the sandfish. Despite the fact that these are not precise enough to make assumptions about the quantitative values, it seems evident that the dispersive part of the surface energy is the dominant one, which again seems strange for the reasons mentioned above. The exact glycan structure was not identified to this point, but regardless of the possible modifications (most being potentially on a sialic acid (Varki et al., 2009)), the core structure would exhibit polar and therefore hydrophilic

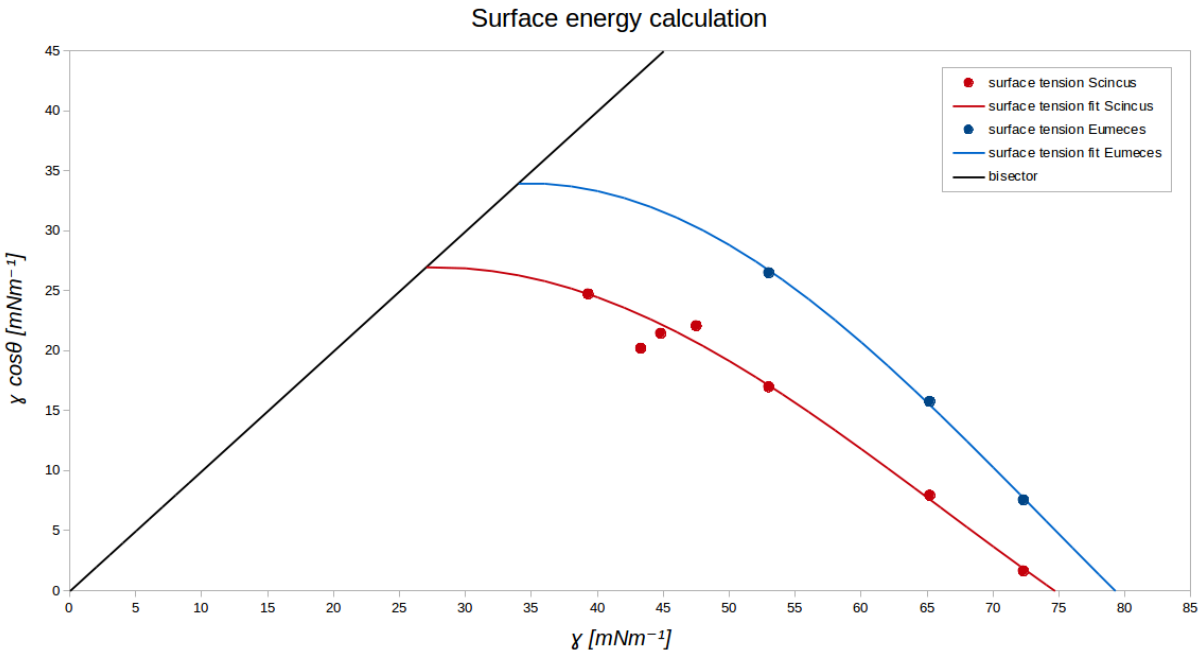

Figure 2.6: Surface energy plot. The blue dots represent the values of $\gamma_{lv} \cos\theta$ on the vertical axis, plotted against γ_{lv} on the horizontal axis. The black line is the plot bisector. Measured data for *S. scincus* (red) and *E. schneiderii* (blue) are plotted as dots and fit with a cosinus curve in the according color. The free surface energy is determined at the intersection of the curve and the bisector where γ_{lv} equals $\gamma_{lv} \cos\theta$.

properties. Typically, glycans have a strong impact on the folding and therefore the tertiary and quaternary structure of proteins (Varki et al., 2009; Shental-Bechor & Levy, 2008). As proteins are composed of a wide variety of amino acids (all with specific properties), their spatial position and orientation is eventually what determines the function and characteristics of the final protein. Even if the glycans are very polar themselves, their influence on the protein folding process might lead to a less hydrophilic end structure. On the other hand, previous studies (Staudt, 2012; Baumgartner et al., 2007) suggest that glycans linked to the sandfish keratins have a direct interaction with the skins environment. A definitive conclusion on their contribution is therefore not possible at this point. Since this seems to be the main difference between the sandfish's and the berber skinks' skin, glycosylation is very likely the main cause of the specific epidermal surface properties of *Scincus scincus*. Though the mechanism is still unclear, it seems to reduce the surface energy of the keratin and thereby adhesion and friction, while increasing abrasion resistance. Reducing surface energy ultimately means reducing the interaction of a surface with its environment (Israelachvili, 2011). There is little reason (however, it cannot be excluded at this point) to propose that this was the result of increased repulsing electrostatic forces. Due to the larger radius of the effect, one would expect the lower surface energy to be the result of weaker (attractive) Van der Waals forces.

Chapter 3 - Surface and ultrastructure of the epidermis

3.1 Introduction

The function of biological materials often as well as their chemistry, depend on their structural architecture. This is therefore one of the fundamental queries which need to be addressed to understand and explain the properties of a material. The main focus of early research on the sandfish skin was set to the surface structure and topography. Rechenberg and colleagues (2004, 2009) rendered extensive research by way of SEM and AFM analyses, which showed repeating patterns of micro structures on the epidermis. The sandfish scales show 200-300 nm high comb-like micro structures, which are positioned approximately in parallels to each other, 5 - 10μm apart. These combs are arranged perpendicular to the body axis with their 'teeth' pointing in the caudal direction (Rechenberg 2009). Other sand swimming animals, like the wedge-snouted skink, or the sand boa also exhibit these same structures, which is why they were connected to the friction reduction and scratch resistance early on (Rechenberg 2004). Figure 3.1 shows a comparison of three sand swimming animals and their skin under magnification.

Figure 3.1: A comparison of sand swimming reptiles and their skin. The sandfish *Scincus scincus* (left), the wedge-snouted skink *Sphenops sp.* (middle) and the sand boa *Eryx sp.* (right). The upper row shows the animals and the lower row shows their scales under the light microscope and SEM. (Rechenberg 2009)

The comb structures can cover the full surface of the scale, additional research has however shown that this strongly depends on the area of the body. As Baumgartner et al. (2007) have found, the lateral and ventral scales may show little or no micro structures at all, while still exhibiting the same friction and abrasion properties. Figure 3.2 shows a topography comparison of dorsal and ventral scales of *S. scincus*, its sand-swimming relative *Scincopus fasciatus*, the non sand-swimming relative *E. schneiderii* and the non related sand swimmer *Meroles anchietae*. Like *S. scincus*, the comb-like micro structure of *S. fasciatus* is found on the dorsal scales, whereas the ventral scales are more or less smooth. Interestingly, the same is true for *E. schneiderii*, which is not a sand swimmer and also has an approximately 5° higher friction angle (Staudt, 2012). On the other hand, *M. anchietae* is a sandswimmer with a similar friction angle as *S. scincus* and has perfectly smooth scales on both, dorsal and ventral side (Staudt, 2012). This does not necessarily exclude the possibility that the micro structure still plays a role, however, it implies a more important role of other factors .

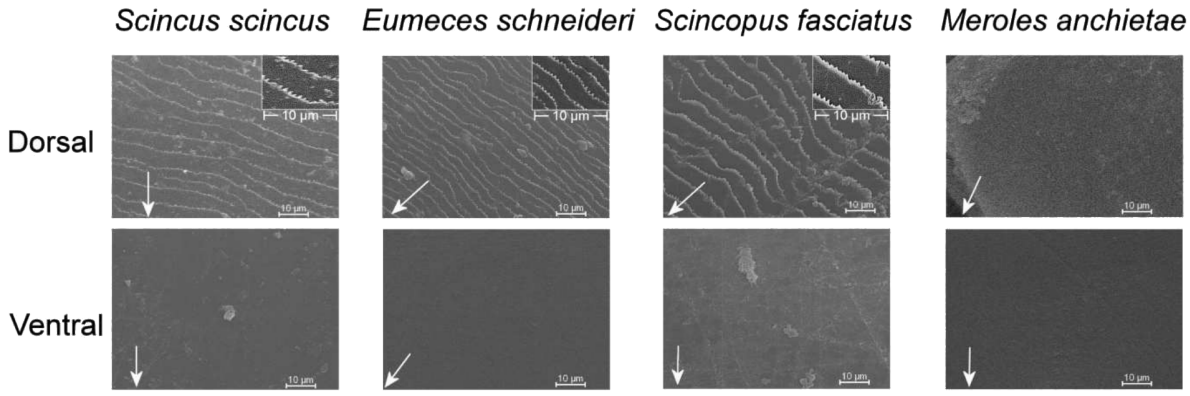

Figure 3.2: A comparison of ventral (bottom) and dorsal (top) scales of four species under SEM. Scales of *S. scincus*, *E. schneiderii*, *Scincopus fasciatus* and *Meroles anchietae* are compared(images from Schmied, 2007 and Staudt, 2012).

While the surface of the sandfish skin was studied thoroughly, an extensive study of the in depth structure of the sandfish is lacking up to date and was therefore performed as a part of this work. In general, the integumentary ultrastructure of reptiles and its development is well known and can be used as a guide for research on the sandfish. As the body's outer boundary, its foremost role is the support and protection of other organs, while permitting movement and growth (Vitt & Caldwell, 2014). Reptilian skin has a fairly general cellular organization which is composed of two basic layers. The external protective epidermis, which lies on top of the internal dermis that contains many functional cells and structures, such as nerves, blood vessels, glands, pigment cells, etc. (Vitt & Caldwell, 2014). The epidermis can additionally have many different layers, depending on the species. In lepidosaurians, such as the sandfish, the architecture can be fairly complex with 6 or more layers, as shown in figure 3.3 (Toni et al., 2007). In general, the innermost layer - stratum germinativum, is composed of living cells which divide continuously to replace the distal layers. During the process, the cells slowly flatten, keratinize and die on their way outward and eventually form a homogeneous, keratinous syncytium - the stratum corneum

(Vitt & Caldwell, 2014). Typically, two different cell types which specialize in a type of keratin they produce, form the later dead keratinous tissue. The proximal cells form an α layer, while the distal cells form the β layer (Vitt & Caldwell, 2014). The two layers are separated by an intermediate mesos layer, composed mainly of lipids which are thought to reduce water loss (Ripamonti et al., 2009). The epidermis of all reptiles is also organized into scales which are replaced in a cyclic process of shedding, called ecdysis, sloughing or moulting (Vitt & Caldwell, 2014). In this process, new skin is produced, and a separation between the old germinative layer and the new β layer occurs (Vitt & Caldwell, 2014).

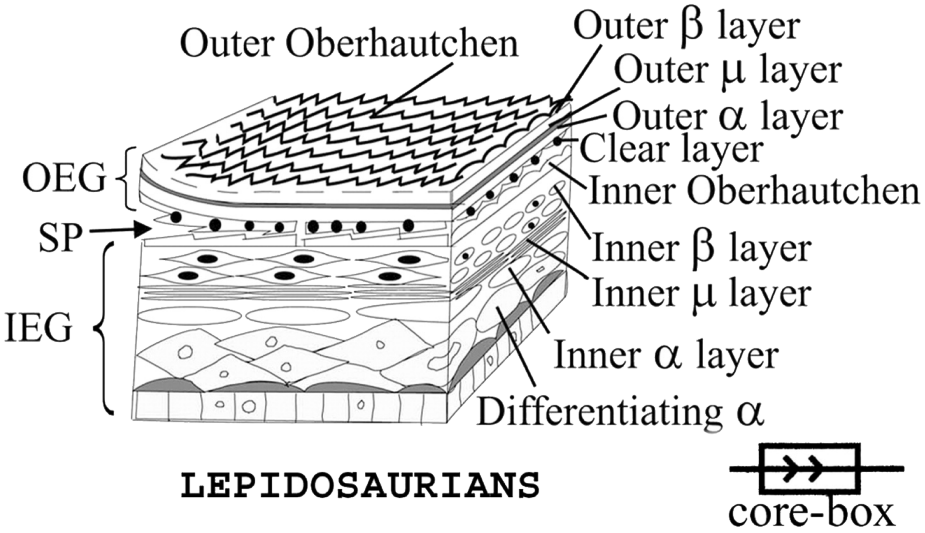

Figure 3.3: The epidermal structure of lizards and its shedding areas. On the left side the outer epidermal generation (OEG), the shedding plane (SP) and the inner epidermal generation (IEG) are marked. Image from Toni et al., 2007.

A good way to examine the structure of a material is to section and observe it in different planes. Compact biological material such as the epidermis often requires additional preparation to reveal specific structures, which would otherwise be invisible. By exploiting the available staining and preparation techniques, including various available microscopic methods, extraordinary magnification and resolution can be achieved. Correct preparation even allows chemical and biochemical analysis of the samples.

3.2 Methods

3.2.1 Polychromatic staining and light microscopy

A sandfish head, which was experimented with in previous projects was used in this method. The sample was prepared for EPON embedding, as described below. EPON is a type of epoxy resin which is, due to its physical properties, suitable for embedding tissue which can be used for semi and ultra thin sectioning and later for light and electron microscopy. Before the embedding

can begin, the to-be-analysed tissue needs to be fixated and dehydrated to secure its structural properties.

Fixation and dehydration protocol

- The tissue was incubated in 0.5ml 25% Glutaraldehyde + 4.5ml 0.2M Cacodylate (in dH_2O) buffer pH 7.2 for 12h at room temperature. In this step, the proteins were fixated by cross-linking with aldehydes.
- The sample was washed 2x15min with the Cacodylate buffer.
- By standard procedure, the next step would be incubation in 0.625ml 4% osmium tetroxide (highly toxic!) + 2.25ml 0.2M Cacodylate buffer for 1h at room temperature, causing fixation and contrasting of lipids by linking with OsO_4. The sandfish head was prepared without the osmium tetroxide.
- The sample was washed 2x15min in dH_2O and then 2x15min in the Cacodylate buffer (0.2M, pH 7.2).
- After the washing, the sample underwent incubation in an ethanol series 2x30%, 40%, 50%, 60% and 70% for 30min at room temperature for each step, to promote tissue dehydration.
- Dehydration was followed by incubation in 2% Uranyl acetate (in 70% ethanol) for 2h at room temperature in darkness (covering and binding electrons from tissue - negative contrasting).
- Afterwards, the sample was washed, 2x15min with 70% ethanol and ON incubation in 70% at room temperature.
- The dehydration continued in the ethanol series, 80%, 90%, 96%, 100% incubation per step for 30min at room temperature.
- The fixated and dehydrated tissue could then be further processed, depending on the embedding material which was for this sample EPON (sandfish head, used for polychromatic staining and light microscopy), but could also be LR white (another type of resin).

EPON Embedding

EPON recipe:

- 6.5g Glycidyl ether 100
- 2.75g DDSA
- 3.75g MNA
- 0.05g DMP-30
- All (toxic) components were mixed vigorously and degassed in a desiccator. The mix was used for direct embedding, but could have been stored for a week at 4°C.

- The fixated material was incubated 2x30min in propylene oxide, which is miscible both with ethanol and EPON.
- Next, the sample was incubated in a 2:1 mix of propylene oxide:EPON ON at room temperature in an open container, so the propylene oxide could slowly evaporate.
- The sample was transferred to fresh EPON and applied to curing forms.
- The curing took place for 48h at 70°C.

EPON embedded samples are difficult to stain with many standard methods, it is, however, possible to create a polychromatic staining as developed by Tolivia et al. in 1994 for epoxy semi thin sections. The sample was cut into 1-5 μm (semi thin) thick sections using a D-type steel blade on a rotatory microtome, stretched on a double distilled water droplet and fixated on a cover slip which was heated to 60°C for 6 hours. Afterwards, the preparation and staining was performed as described by Tolivia et al. (1994), with slight adaptations for the material used in the investigation:

Solution A:

- 2% $KMnO_4$ in dH_2O

Solution B:

- 5% Oxalic acid in dH_2O

Solution C:

- 12.5ml carbol methylene blue
- 12.5ml carbol gentiana violet
- 10.0ml 96% Et-OH
- 12.5ml dH_2O
- 2.5ml pyridine

Solution D:

- 5g pararosaniline powder
- 97ml dH_2O
- 1ml glacial acetic acid
- 2ml 5% phenol

Staining procedure:

1. 30s incubation in solution A
2. 5-10s washing with dH_2O

3. 60s incubation in solution B
4. 60s washing with dH_2O
5. 45s incubation in solution C
6. 45s washing with dH_2O
7. 45s incubation in solution D
8. 30s washing with dH_2O

Since the to-be-analysed material was not contrasted with osmium tetroxide, the sections were only stained with solutions C and D, without previous decontrasting. After staining, the sections were air dried at room temperature for at least 1h. For observation under the light microscope, the stained sections were embedded with a drop of eucalyptol/euparal and the sections were then observed using the bright field light microscopy. According to the authors, the tissue coloration after the staining is as follows:

- Epithelial tissue - blue to violet
- Secretory granules - various coloration from red, magenta, blue to violet
- Connective tissue - pink to red
- Muscle tissue - blue to grey
- Neurons - Blue-violet to dark blue
- Keratin - pink to red

3.2.2 Transmission electron microscopy

Sandfish scales were collected from the terrarium and thoroughly washed, 3x by vortexing in tap water and additional 2x in dH_2O. Afterwards, they were dried in air at room temperature. Single clean scales were extracted and dehydrated, fixated and contrasted as described before. Afterwards, they were embedded into a resin. Both EPON and LR white were tested. LR White is an alternative to EPON embedding, with slightly different physical properties. It is often used for immunohistochemical analysis of TEM samples. EPON embedding was performed as described above, but additionally the scales and resin were transferred to curing forms made from silicone. LR white embedding was performed using the following protocol:

- The fixated material was incubated twice for 30min at room temperature in hexamethyldisilazane (HMDS).
- Afterwards, the material was transferred to LR white and incubated for 1h at room temperature.
- LR white was exchanged with fresh resin and the sample was further incubated ON at 4°C.
- The material and the resin were transferred into curing forms made from polyethylene terephthalate (PET).

- Curing took place under UV light for 48h at 4°C.

Electrons - the radiation used to project the structures of a tissue in TEM are very easily absorbed by any kind of substrate, therefore the samples need to be cut "ultra thinly" (approximately 70 nm) to sustain transmission. The tissue embedded in a resin block (equally for EPON and LR white) was trimmed using a razor knife so that the to-be-cut material had a projected surface of approximately 2x2mm. The block was then implanted into an ultamicrotome's cutting head. Using a glass knife with a water pond, the block was slowly approached while cutting and making sure the water was completely in contact with the knife's edge. When the tissue came into contact with the knife, the section thickness was manually adjusted to 1μm and cut until the section surface was smooth and flat. The glass knife was replaced by a Diatome diamond edge knife and automatic sectioning was enabled. Created sections would remain afloat and could be evaluated if suitable for further evaluation. Sections with a suitable thickness for TEM ($\approx$ 70nm) would have a silver-gold coloration. The sections were flattened by fumigation with chloroform and transferred to formvar coated Ni grids, which were prepared beforehand by the following protocol: A clean glass slide coated with a thin film of unparfumed sodium soap was dipped into a 0.7% formvar solution (dissolved in chloroform), which was then gradually drained. In this way a smooth homogeneous film was created on the slide. After drying (air at room temperature), the film edges were removed with a blade and the coated slide was carefully dipped into dH_2O under a low angle. The formvar film would float on the water and could be transferred to a parafilm sheet. The film was dried and Ni grids were placed upon it with the dim side facing the formvar.

For structures to be visible under TEM, the samples need to be contrasted before microscoping. This increases the absorption of electrons in specific areas of the tissue and decreases the absorption in other areas, thereby improving the image projected on the detector. The process was carried out in the following manner:

- A drop of 2% uranyl acetate in 70% ethanol was placed on a parafilm sheet for every grid.
- A grid with sample was placed on the drop, the dim side (containing the sample) facing downwards, and incubated for 20min at room temperature in darkness.
- 5 beakers with degassed ddH_2O were prepared and every grid was washed by dipping 20-30x in every beaker.
- Excess liquid was drained with filtering paper and the grids were left to dry (optional).
- A drop of 0.2% lead citrate (degassed ddH_2O, 0.1M NaOH) was placed on a fresh parafilm sheet for every grid.
- A grid was placed on the drop and incubated for 7min at room temperature in darkness.
- The grids were washed as described before and extra care was taken to avoid breathing onto the samples.
- Excess liquid was drained and the grids were dried at room temperature for at least 30min.

Immunohistochemical analysis of the sandfish scales in cross section

Since glycans play an important role in the sandfish's skin friction and abrasion properties (Baumgartner et al., 2007), one experimental goal was to determine their distribution in the epidermis. Immunohistochemical analysis for TEM creates the possibility to visualize the occurrence and location of certain molecules in the cell. When prepared for TEM, the immunoincubation needs to be carried out before the contrasting. Due to its chemical properties, LR white does not mask the binding sites in the tissue as much and is more suitable for such endeavours than EPON.[1] The general procedure is performed as follows:

Immuno-labelling

- Blocking (optional)
- Streptavidin gold is added to the working solution [2] (1:60) and incubated for 30min at room temperature while gently stirred.
- A 30μl drop is applied to a slot in the incubation box and a grid is added.
- The incubation box is placed into a wet chamber and incubated for 1h at room temperature.
- The grid is washed 3x5min with the working solution.
- The grid is dried before further preparation (optional).

Blocking To improve the signal to noise ratio, the samples can be blocked before the immunoincubation.

- Incubation in 50mM glycin (sterile PBS) for 15min at room temperature.
- Incubation in 2% BSAc (sterile PBS) for 30min at room temperature.
- Washing 3x5min with sterile PBS.
- Washing 2x5min with sterile dH_2O.

Silver enhancement This method increases the size of gold particles on EM samples, which are then more visible when observed under the microscope. Firstly 1 drop of initiator (Aurion R-Gent) is mixed with 40 drops of activator (Aurion R-Gent), which makes up the developer solution (can be stored for 4 weeks at 4°C). Procedure:

- 20 drops of enhancer (Aurion R-Gent) are mixed with 1 drop of developer
- one 20μl drop per Ni-grid is placed on parafilm

[1] EPON embedded material can be used for immunohistochemical analyses, however, the EPON needs to be etched away beforehand.

[2] 0.15M NaCl, 0.1mM $CaCl_2$,(0.1mM $MnCl_2$), 10mM HEPES pH 7.5, 5-20μg/ml biotinilized lectin like WGA or WFA

- the grids are placed on the drops (sample facing downwards) and incubated for 30 - 60 s at room temperature in darkness
- washing 6x10 s in ddH_2O in darkness
- drying in air at room temperature

Two lectins were used in this experiment, WGA (Wheat Germ Agglutinin) which binds to N-acetyl glucosamine and is a suitable marker for N-linked glycans, and WFA (Wisteria floribunda agglutinin) which binds to N-acetyl galactosamine and is a marker for O-glycans. The protocol was at first performed as described above, and then fine-tuned to obtain the best possible results concerning binding contrast of the gold particles. The adjusted variables were:

- lectin concentration: 5, 7, 10, 20 μg/ml
- streptavidin gold dilution, 1 vs: 30, 60, 90
- the time of washing steps: 5 min, 10 min
- blocking with glycin/BSAc: yes/no

3.3 Results and discussion

Polychromatic staining by Tolivia et al. (1994) is a suitable technique for EPON embedded semi-thin sections, since it gives a coloration to many different tissue types and can even be used for osmated material. Figure 3.4 shows a sagital section of the sandfish skin with dermis and epidermis, which can be divided into at least two layers - the basal germinative layer (violet coloration) and the apical corneous layer (pinkish coloration). As shown in the figure, the corneous layer is partly lacerated into thinner strains. In part this is likely due to the preparation, but mostly to the cutting procedure, since it seems more prominent in one direction. In this example, it is in the anterior - posterior axis. The connective tissue is coloured pink, while the cell nuclei are dark blue. Also seen in the figure is a blood vessel, which has a brownish green coloration. It is noteworthy that the colors in the image captured on the camera do not reflect the exact same coloration as observed with the naked eye.

The epidermis is approximately $5 - 15\mu m$ thick, depending on the region. Its thickness is completely encompassed in the region marked with rectangle A, and can be observed in more detail in figure 3.5. This shows an overview of the sandfish epidermis under TEM. In the basal region (by Vitt & Caldwell, 2014 described as the lacunar layer) of the epidermis, a single flat and elongated keratinocyte is shown. The cells in this layer are approximately 6 - 10 μm long and 0.5 - 1 μm thick. Inside the keratinocyte, keratin clusters can be observed, which are darker than the cytoplasm. Following the tissue in the direction of the arrow, the cells become even flatter and more compact, their thicknesses being reduced to a fraction of the cells in the germinative layer. The tissue is partly lacerated, and some intercellular spaces are therefore visible. The spaces with a light grey coloration probably occurred during the shedding process or the preparation, since

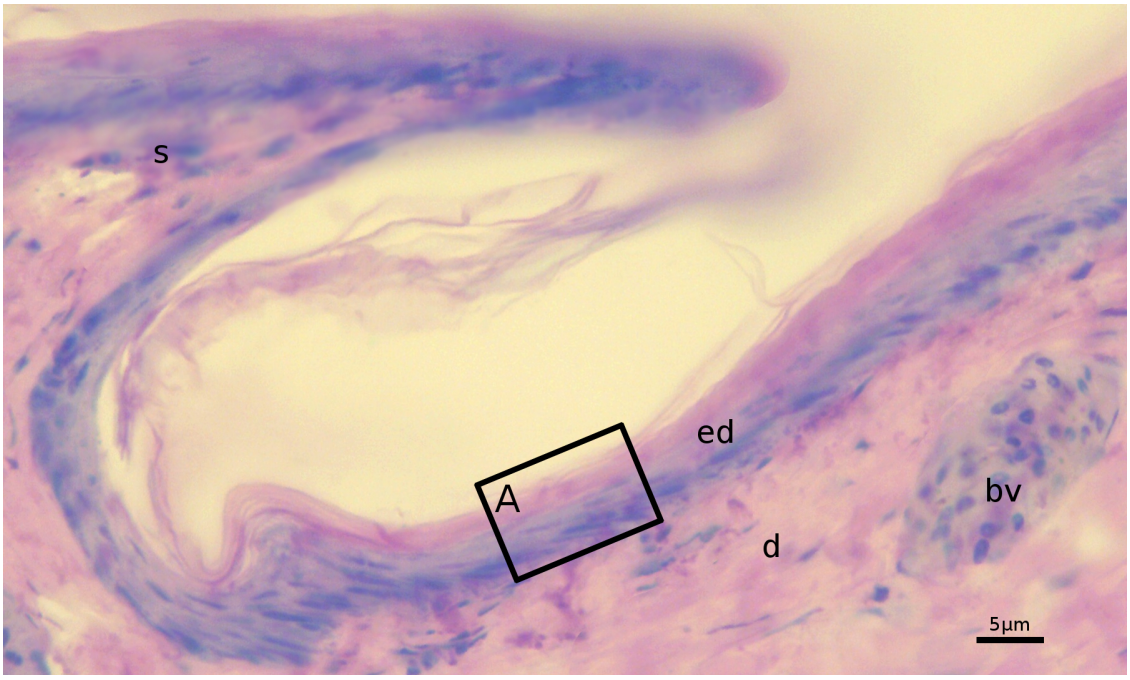

Figure 3.4: A cross section in the sagital plane of the sandfish epidermis is shown. A single scale is marked with s. The epidermis (ed) can be differentiated into the corneous layer - intensive pink and the living germinate layer - violet with separate visible cells. Beneath lies the dermis (d) filled with connective tissue and occasional blood vessels (bv).

they contain embedding material, those being completely white probably came to be during the cutting process, since no other material is present. The epidermis continues into the keratinous layer which is a homogeneous syncytium, filled with keratins and ends in the oberhäutchen. The sandfish has a basic reptilian scale architecture with a basal germinative layer with living cells, a transition layer with dead compacted cells and a dead keratinous stratum corneum (Toni et al., 2007; Vitt & Caldwell, 2014). On the other hand, one would expect the keratinous layer to be differentiated into a separate α and β layer with an intermediate mesos layer (Toni et al., 2007; Vitt & Caldwell, 2014; Ripamonti, 2009). Yet, this was not the case for the sandfish epidermis. Despite the samples being partially lacerated, the stratum corneum appears intact, so we can exclude the possibility that the upper layers were lost in preparation. As is evident from the SDS-PAGE and westernblott analysis (Baumgartner et al., 2007; also see chapter 6), both keratin types are present in the sandfish skin, however, it was not possible to pinpoint these in the ultrastructural analysis. This is difficult to confirm at present, however, the stratum corneum of *S. scincus* might just be a homogeneous layer of evenly distributed α and β keratins.

Immunohistochemical analysis of the sandfish scales in cross section

As described previously, the optimum conditions were tested for maximum gold particle labelling on the glycans, but with minimum unspecific binding to the resin material. The best conditions, as found in this experiment, were 5μg/ml of WGA, with a gold particle dilution of 1:60. Standard 5 min washing steps were followed and no additional blocking was done before the labelling. Further

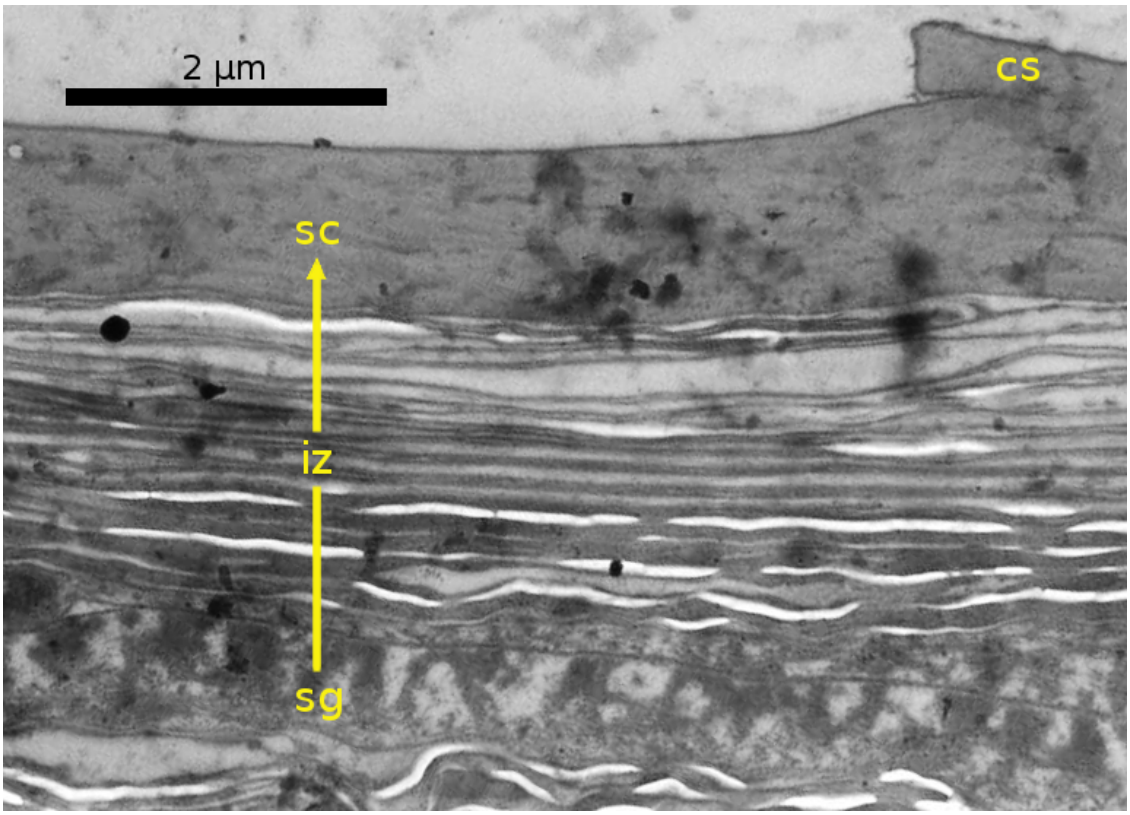

Figure 3.5: Shows a TEM image of a sandfish scale in cross section. Three main zones can be observed. The germinative layer or stratum germinativum (sg), the corneous layer or stratum corneum (sc), ending as the oberhäutchen and the intermediate zone. Comb structures (cs) can also be observed in the apical part of the oberhäutchen.

refinement is still possible, since some gold particles were found on the LR white resin. Figure 3.6 shows a TEM image of an LR white embedded sandfish scale in cross section labelled with WGA (lectin with N-linked glycan affinity) and streptavidin gold. An overview is shown together with a zoomed area marked in yellow. The oberhäutchen was missing in this sample, and was probably lost in the sectioning process, other than that, all typical structures were present. The gold particle distribution was very even throughout the sample and no "hot spots" could be identified. This can be explained by an equal distribution of N-linked glycans throughout the epidermis, which is not surprising, considering epidermis' growth. For the WFA (lectin with O-linked glycan affinity) samples, the gold particles would either bind to both sample and resin equally or wouldn't bind at all (less gold, longer washing steps). The reason for this could be the concentration of O-linked glycans, which could be too low to improve the signal to noise ratio.

Structural analysis on the skin of squamates has been performed extensively over the past years. Ripamonti et al. (2009) performed epidermal research on the tiger snake (*Notechis scutatus*) and the gabon viper (*Bitis gabonica*) using various methods, including Raman spectroscopy. These species exhibit typical epidermis composition with separate α and β layers, which can indeed be differentiated. Neither TEM nor later Raman analysis on the sandfish(see chapter 6) could help identify separate keratin compartments, despite the fact, that both types of keratins

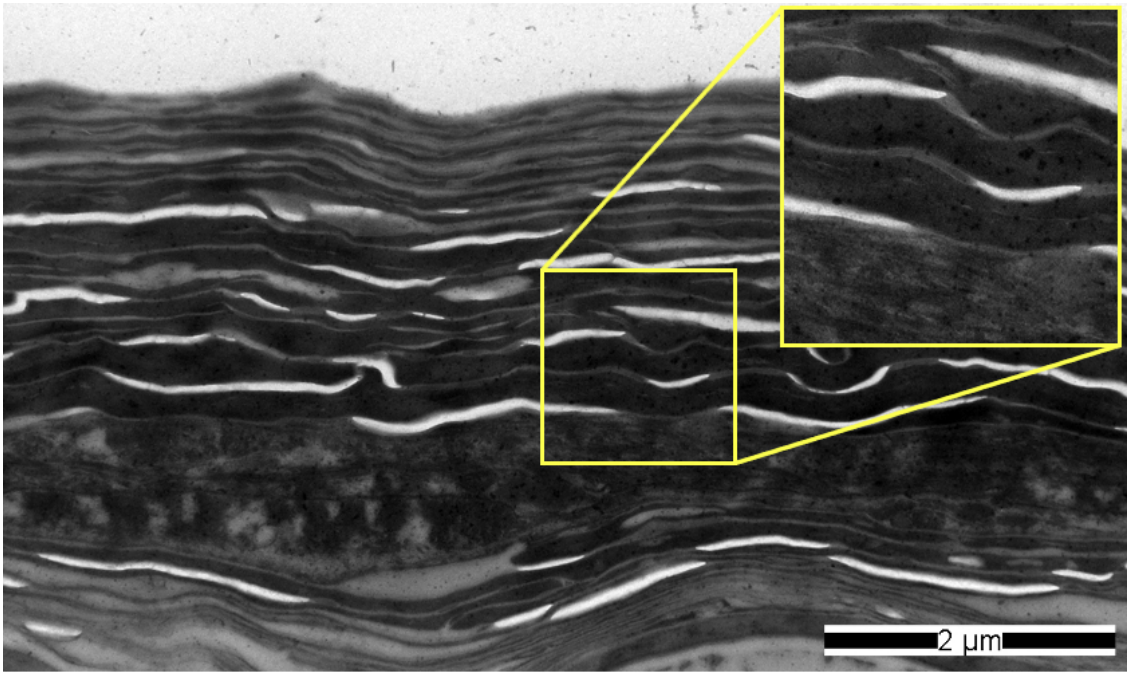

Figure 3.6: A TEM image of a sandfish scale in cross section, labelled with WGA-Strepatividin gold. The magnified area marked in yellow shows a more detailed image where the gold particles are clearly visible.

were found by westernblotting. While the sandfish epidermis does have a complete structural transition from whole keratinocytes to the oberhäutchen and the intermediate zone with compacted, flattened cells, it seems chemically homogeneous. This is, indeed, very intriguing and could have an impact on the scale mechanics.

Chapter 4 - Optical properties

4.1 Introduction

One of the interesting feats of the sandfish skin is the micro structure on the dorsal scales. As already described in chapters 2 and 3, the micro structures have a comb-like form and are placed like 200 - 300nm high roof tiles in transverse lanes across the dorsal skin, approximately 5 - 10μm apart. Previous studies on the sandfish epidermis suggested that they play an important role in the friction reduction (Rechenberg, 2004; Rechenberg, 2009). It is, however, curious that these structures are mostly concentrated on the dorsal side of the body, whereas a significant difference in friction angle, in comparison to other body sides, could not be measured. In addition, these structures can also be found on dorsal scales of the nonswimming relative of *S. scincus*, *E. schneiderii*, which exhibits higher friction angles (Saxe, 2008; Staudt, 2012). While the structure might still have an impact on the real measured friction, the exact purpose of the comb structures is not entirely clear. It is possible it remains as a remnant of the sandfish's evolutionary past and was not affected by the pressure of selection. It is also possible that it serves another purpose. One aspect is provided by the research performed on the oriental hornet (*Vespa orientalis*), which has shown that "microcombs" found on the epicuticule can function as light trapping (harvesting) structures (Plotkin et al., 2010). The effect of increasing light absorption by adjusting the geometry of a surface has been known for quite a while now (Deckman et al., 1983), and it is possible, a specific form has the optimum absorption for a specific wavelength (Zhu et al., 2010). While the hornet combs differ from the ones found on the sandfish, this may be an adaptation to a different wavelength. As noted before, the sandfish stays buried in the ground most of the day and usually only shows up for feeding and reproduction (Hartmann, 1989). Its successful hunting and evasion from predators is improved vastly with fast locomotion, which in terrestrial animals often correlates with body temperature (Paladino, 1985). It would therefore be advantageous for a poikilothermic animal like the sandfish, to sufficiently heat its body as quickly as possible. In this respect, solar radiation seems as a viable source of heat, if it is harvested appropriately, and the right diffraction grating on the epidermal surface might facilitate just that.

4.2 Methods

4.2.1 Creating keratin thin films

Thin film production from purified keratins is becoming increasingly interesting for industrial applications, for example, in food conservation or biomedical applications (Khosa & Ullah, 2013). In this work, thin film production was used solely for the analysis of the keratins, as a homogeneous layer facilitates measurements of contact angle and optical properties. A controlled keratin polymerization in vitro is, however, not trivial, therefore different set-ups were tested to create a homogeneous and transparent thin film.

On top of a glass slide, a simple chamber was built from acrylic glass, with dialysis tubing separating the chamber in the middle. The lower compartment was filled with skin lysate, which was obtained as described in the skin lysis section, see chapter 6. In the upper compartment, a series of urea solutions in water (9M:dH_2O = 4:1, 3:1, 2:1, 1:1, 1:2, 1:4, 1:6, 1:8) was slowly exchanged and after the last step, the glass slide was washed with dH_2O and left to dry. 20, 40 and 60 min solvent exchange times were tested. It was possible to create a thin keratin film with this procedure, however, none of the exchange times produced the wished result. In the end, all the films were milky and rough on the surface.

The second protocol was devised for chicken feather keratins as described by Fujii & Li (2008). 40mM solutions of NaCl, KCl and $CaCl_2$ were prepared and inert silicone wells were created on clean microscope slides. 500μl of each solution was placed in a well and 100μl of sandfish skin lysate was pipetted on the bottom, where the keratins would polymerise. There were some differences in film transparency, depending on the salt used in the solution. All probes were milky to some extent, however, noteworthy was the excellent adhesion of all films to the glass surface.

Alternatively, two additional protocols were devised, based on the observations made during biochemical analysis of the sandfish skin (chapter 6). Instead of diluting the solution and thereby forcing precipitation, the medium was removed by evaporation:

Mercaptoethanol method Sandfish epidermis lysate was dialysed (as described in chapter 6) in dH_2O, causing keratin precipitation. Water was changed 3 times per every 20min. The dialysate was collected and transferred to fresh containers. To 1 ml of solution, 10μl of 2-mercaptoethanol were added, to dissolve the now finely particulate keratin the second time. The mixture was thoroughly vortexed for 1min. The solution was then filtered through a membrane with 0.4μm wide pores and pipetted into a silicone well, placed on a glass slide. The sample was left to evaporate for 48h at room temperature, while the mercaptoethanol would evaporate jointly with the water. With this method it was possible to create fully transparent films, though the yield was relatively low.

Iodoacetamide method 50mg of iodoacetamide per 300μl solution were added to sandfish epidermis lysate (chapter 6), vortexed and incubated further for another hour. Afterwards, the

solution was dialysed in dH_2O. The water was changed three times, once every hour. The remaining sample was collected, filtered and left to dry for 48h at room temperature. This method prevents dissulfide bond creation, therefore the polymerization is relatively slow. With this procedure, it was possible to create transparent films, however, it is likely that blocking the dissulfide bridge formation distorts the polymerization and therefore the optical properties of the film.

4.2.2 Refractive index

The refractive index is a coefficient which describes how electromagnetic waves propagate through an optical medium (Hecht, 2002) and is therefore crucial for determining the light trapping properties of surfaces. It can be measured by various methods, the one suitable for surfaces and thin films, is by measuring the angle of polarization or Brewster's angle which is the angle of polarization, created when a wave is reflected off a homogeneous material:

$$\theta_B = arctan\left(\frac{n_2}{n_1}\right) \tag{4.1}$$

where θ_B is the polarization angle, n_1 is the medium through which the wave travels and n_2 is the medium from which the wave is reflected. Clean sandfish scales as well as a glass slide with a keratin thin film, created from the exuviae were used in the measurement. The samples were irradiated by polarized monochromatic light with a wavelength of 532nm, while slowly rotated. Simultaneously, the angle of the scales and the intensity of the reflected light were measured. When Brewster's angle was reached, the double polarization resulted in wave extinction and the light intensity dropped to zero. The refractive index of the sandfish scales was then determined by using the above equation.

4.2.3 Scale diffraction

To test if any diffraction had taken place on the grating of the dorsal scales, a focused beam of monochromatic light was emitted on a scale and projected on a sheet of squared paper. The formation of interference modes was observed at a defined distance, the gap between the modes was measured and the procedure was repeated. Two sources of light were used, a green (532nm) and a red (680nm) laser. 6 measurements were performed for each color and with both sandfish and *E. schneiderii* scales. The distance between the scale and projection screen was 8 cm.

4.2.4 Light transmission

Light harvesting for heating or other uses requires the material to absorb the appropriate wavelengths. Therefore, the light transmission of the sandfish scales was measured for a wide spectrum of solar radiation, with special emphasis on heat radiation - infrared (IR) light. The transmitted light is equal to the intensity difference between the source and detector, which occurs due to intensity loss on the sample. The intensity difference should be the result of absorption, reflection

and refraction. This set of measurements was carried out in cooperation with prof. Johannes Heitz at the Institute of Applied Physics (JKU Linz). Two samples of each kind were measured for the whole range of light between UV and IR in 3 different positions per sample. The exuvie were thoroughly washed by 3x1min vortexing in dH_2O, excess water was removed with a clean kimtech tissue and then pressed between 2 glass slides, covered with a fresh tissue and left to dry over night, so that the exuviae were clean, dry and flat after the treatment. The measurements were performed in two steps, with two spectrometers: the Cary 500 spectrometer with an UV/VIS (ultraviolet, visible light) to NIR (near infrared) and the Bruker Equinox in the NIR and MIR (mid infrared) spectral range, the full spectrum ranging from 200 - 16000nm. In addition, other materials were measured for comparison, such as glass, epoxy resin, scotch tape and scotch tape with sand.

4.2.5 Heat absorption

Epoxy resin replicas of the ventral and dorsal side of the sandfish were created, following the protocol of Koch et al. (2013) using dental silicone. Identical casting forms were used for the silicone to ensure identical projected surface area. For curing with epoxy, two identical forms were used, and the epoxy was weighed to ensure identical mass of the finished replicas. A third sample was created, but with a smooth surface. To test the thermal behaviour, the samples were placed under a terrarium daylight bulb, all within the same distance to the light source, and over time, the temperature progression was measured using an IR thermometer, which was installed to a rail, ensuring that the samples were measured from the same distance and angle. In addition to measuring the heating behaviour of the replicas under a light bulb, the samples were also exposed to direct sunlight and tested for comparison. As observed in the transmission experiments, glass absorbs IR radiation after a certain wavelength (data not shown). Therefore the experiment was performed outdoors. The second set-up immediately showed difficulties, because even the smallest air movement in the vicinity had a radical impact on the temperature of the samples. These were apparently to small for light absorption to be the dominant factor in temperature change and the results were therefore irreproducible.

4.2.6 Simulations of light trapping behaviour

To test whether the micro structure found on the dorsal scales could facilitate light trapping at least in theory, simulations of the diffraction grating and possible light trapping were performed. This methods section was performed at the Institute of Applied Physics (JKU Linz) by Prof. Dr. Johannes Heitz and Dr. Nikita Arnold. The refractive index, determined from the polarization angle, and an approximated average scale geometry were used. The scale thickness was set to 12μm and the comb structures were set at a height of 200nm, the space between them being 10μm.

4.3 Results

4.3.1 Refraction and diffraction

The precision of determining the refraction index by calculating it from the polarization angle is limited to a window of 1 - 5 degrees, therefore the value of the refraction index could only be approximated to one decimal position. For sandfish scales and keratin thinfilms, this value was somewhat above the value of glass, a little above 1.5. In literature refractive index values of keratins are found at approximately 1.56 (Land, 1972; Osorio & Ham, 2002; Leertouwer et al., 2011). Diffraction of monochromatic light was observed in both, sandfish and berber skink's scales, but to somewhat different extent. A sample image of a diffraction measurement is shown in figure 4.1.

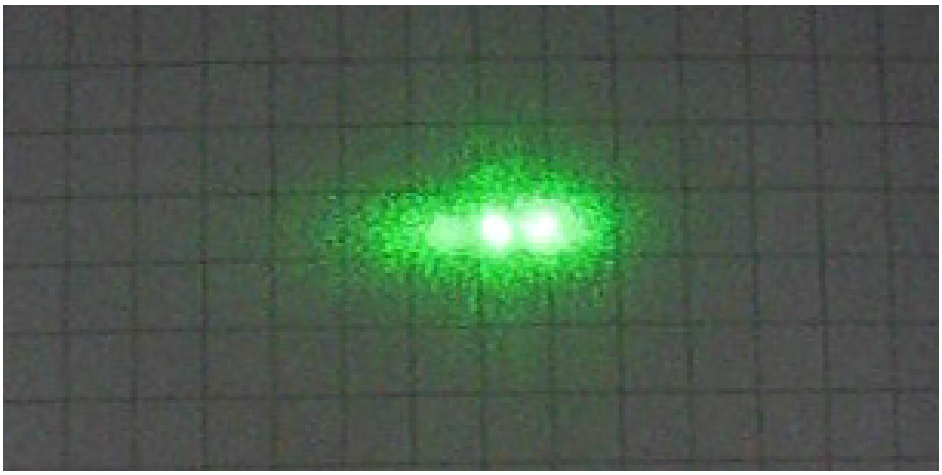

Figure 4.1: A sample measurement of light diffraction on a sandfish scale. green monochromatic light at 532nm was projected through a scale and the diffraction was recorded by means of a video camera. The first modal maxima have an uneven intensity, which could be the result of asymmetry of the micro structure.

Only the first modular peak, in addition to the main (zero) peak, could be observed for all samples, with differences in distance between the 0. and 1. peak (d), depending on the sample and wavelength. The results of the measurements are shown in figure 4.2. The smallest differences were measured for green light (532nm), where d was between 3.5 and 4mm. With increasing wavelength, d increased as well, to approximately 5mm for the sandfish and 7mm for the Berber skink. The angle of diffraction for the first mode would for the sandfish be $\approx 2.5^\circ$ at 532nm and $\approx 3.6^\circ$ at 680nm. In other words, an increase in wavelength of approximately 150nm would result in an increase of 1.1° diffraction angle for the first mode. The critical angle for total reflection is calculated from the quotient of the two media, light passes through:

$$sin\theta_c = \frac{n_{air}}{n_{epidermis}} \tag{4.2}$$

With a refraction index of 1.56 and under the presumption that the wavelength-diffraction

relation continued linearly, a total reflection and thereby "trapping" of the first mode would occur at $\approx 40°$, which would match infrared light at $\approx$ 5500nm. Due to limitations of optical diffraction (Riedl, 2001), such a linear progression is unlikely and more precise calculations are required to determine light trapping behaviour, which was done in the simulations.

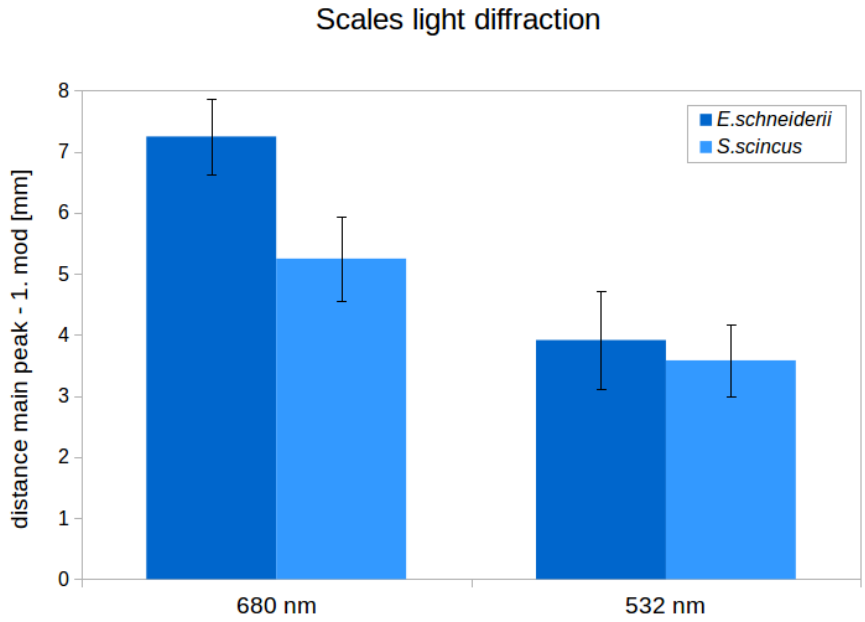

Figure 4.2: Diffraction of monochromatic light on sandfish and Berber skink's scales.

4.3.2 IR transmission

The results of IR transmission measurements are shown in figure 4.3. While complete spectra were measured for the same samples, the measurements were performed in sections with different spectrometers due to their range limits. The average values therefore do not show a smooth line throughout the full spectrum. This is especially evident for the dorsal scales. The form of both types of scales is very similar. In the near UV spectrum (200nm) no transmission is observed, probably due to high absorption in this range. Afterwards, the transmission rises in a logarithmic manner, approximately for 20% between 350 and 3000nm and then drops rapidly to almost zero. In this part of the spectrum, the deviation between samples of the same type is greater, than the difference of the averaged curves of dorsal and ventral scales. In the next part of the spectrum the difference becomes greater, up to 20%. At approximately 3200nm, the transmission rapidly rises again and remains high until 6400nm when it drops once more. The transmission peak in this region is at approximately 40% for the dorsal and up to 60% for the ventral scales. After 6400nm, the signals are very variable, with rapid rises and drops, peaking at approximately 10000nm, with a transmission of up to 30% for the dorsal and 40% for the ventral scales. Partially high signal variations were measured between different positions of the same sample, especially in the VIS-NIR spectrum. While the curve progression may qualitatively reflect reality, additional repeated measurements would be necessary to acquire reliable absolute transmission values. Occurrence

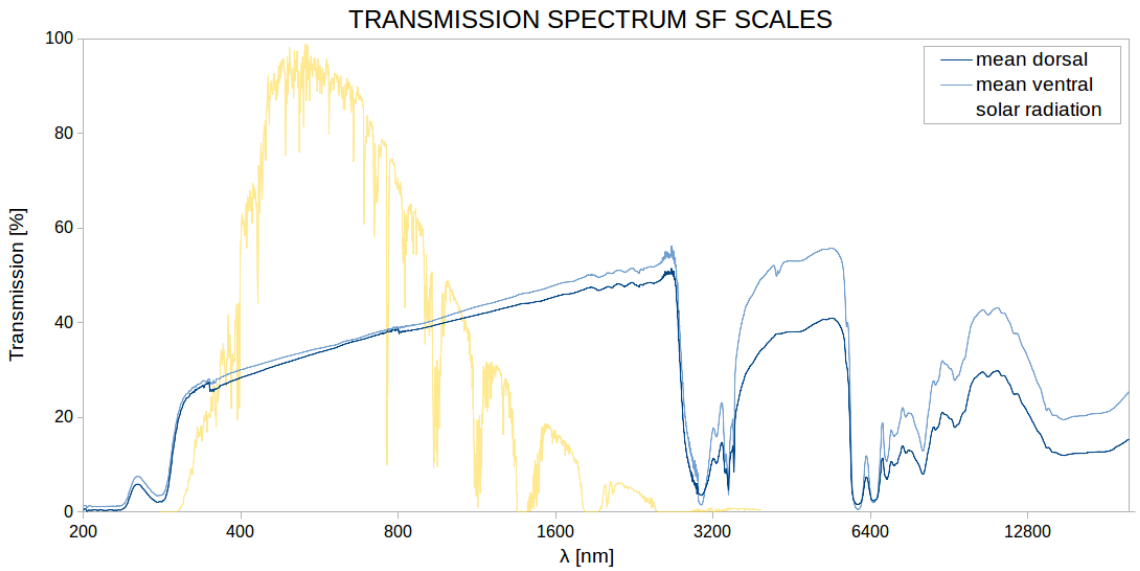

Figure 4.3: Light transmission of dorsal and ventral sandfish scales. The average dorsal scales spectrum is labelled in dark, the ventral in light blue. For comparison the measured transmission of solar radiation (Renewable Resource Data Center, accessed April 2014) is shown in yellow.

and position of absorption bands may be assessed, on the other hand, without the samples being smooth and homogeneous, the absolute intensities cannot. In this regard, measurements with a wider light beam from the source would average over many positions and could provide better results.

Nonetheless, the results in the MIR spectrum suggest significant transmission differences between dorsal and ventral scales. On average, the dorsal scales transmit up to 20% less light and while no difference in chemistry of dorsal and ventral exuviae was recorded up to date, this could lead to the conclusion that the transmission difference is the result of diffraction on the micro structure. Interestingly enough, this spectrum much coincides with atmospheric thermal radiation, which is shown in figure 4.4. If the dorsal scales of the sandfish could indeed "trap" this spectrum of radiation, their body could potentially temperate faster to a temperature suitable for locomotion, reducing the time of hunting and thereby their exposure to possible predators.

4.3.3 Heat absorption

Cylindrical, approximately 5mm high replicas with a diameter of 15mm were placed within the same distance of a terrarium light bulb and the progression of their change in temperature was measured, the results of a sample measurement are shown in figure 4.5. All measurement curves had the same progression with a steep linear beginning and an asymptotic approach towards the maximum temperature, which depended on the distance to the light source. Despite the different surface micro structure, no significant variation in heating under identical conditions could be measured whatsoever. The samples were relatively small in diameter, but thick in comparison with the sandfish epidermis, which is 12μm thick, yet covers a surface of a few square cm.

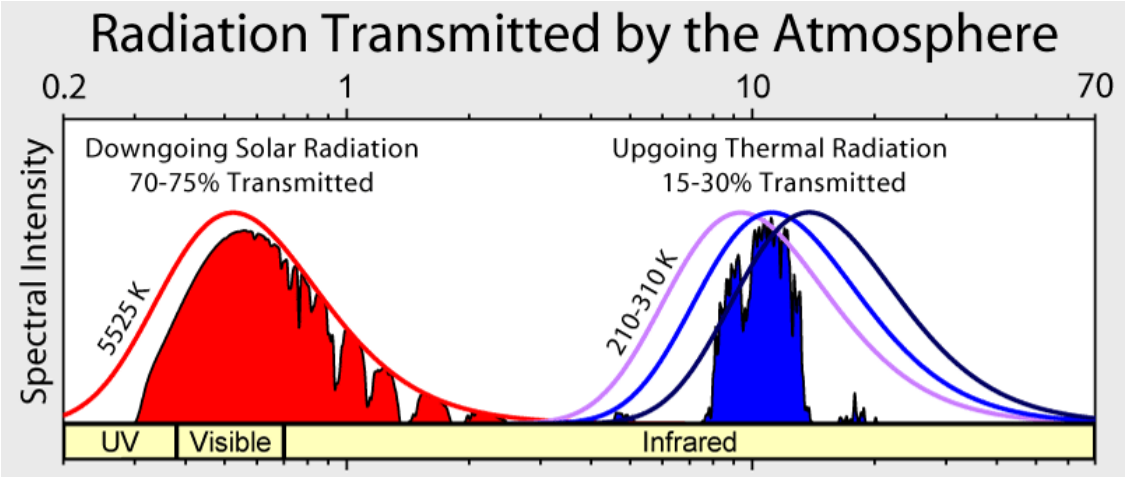

Figure 4.4: Atmospheric transmission of EM radiation in the spectrum from UV to IR. Prepared by Rhode (2007) on data from HITRAN database (Rothman et al., 2004). The downgoing solar (red) and the upgoing thermal (blue) transmissions and their normal curves are shown.

Because of this significantly different relation between volume and surface area, it is possible that the heating and dissipation overpowered the effect of light trapping on the surface, due to the material properties, such as heat capacity. It is difficult to comment on the results at this moment, since thinner samples with a larger surface area could not be produced at this point. However, the possibility of light trapping remains.

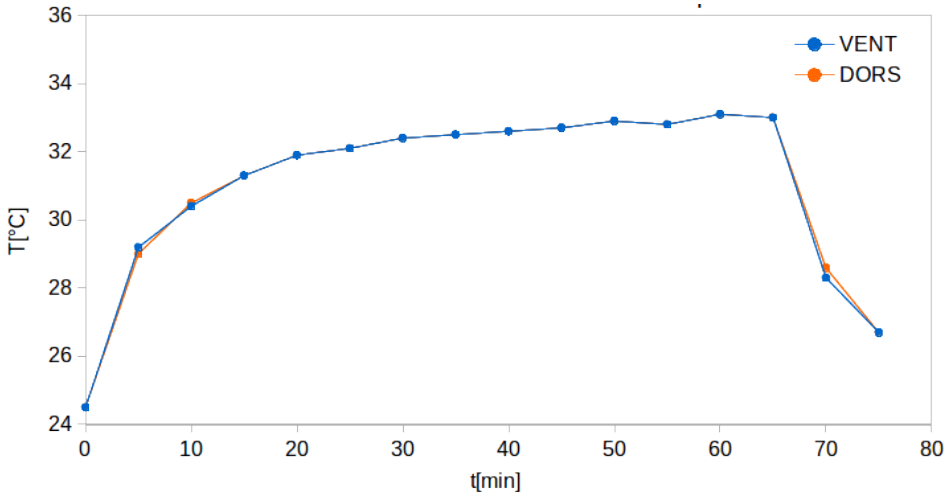

Figure 4.5: Greenhouse effect of the sandfish scales. A sample measurement of the greenhouse effect of the sandfish scales is shown. Being irradiated by the same light source from equal distance, the temperature of a replica made from the dorsal scales (orange) and from the ventral scales (blue) was measured. The curve shows an extremely high overlap.

4.3.4 Simulations

Since light trapping could not be directly confirmed by temperature measurements, simulations were performed to test whether the micro structure on the dorsal sandfish epidermis could at least theoretically facilitate light trapping and thereby improve harvesting of solar and containing thermal radiation. Diffraction was simulated over a near and mid IR bandwidth. Rayleigh points, where light trapping would actually occur existed at a wavelengths 2000nm, 4000nm and 6000nm, the strongest being at 4000nm. The spectrum of diffraction simulation is shown in figure 4.6. While light diffraction may occur at these wavelengths, the simulation has also shown that the absorption of the scale without the diffraction grating is not significantly lower. As of now, it is therefore likely that most of the absorption is caused by optical properties of the material itself rather than regular diffraction effects.

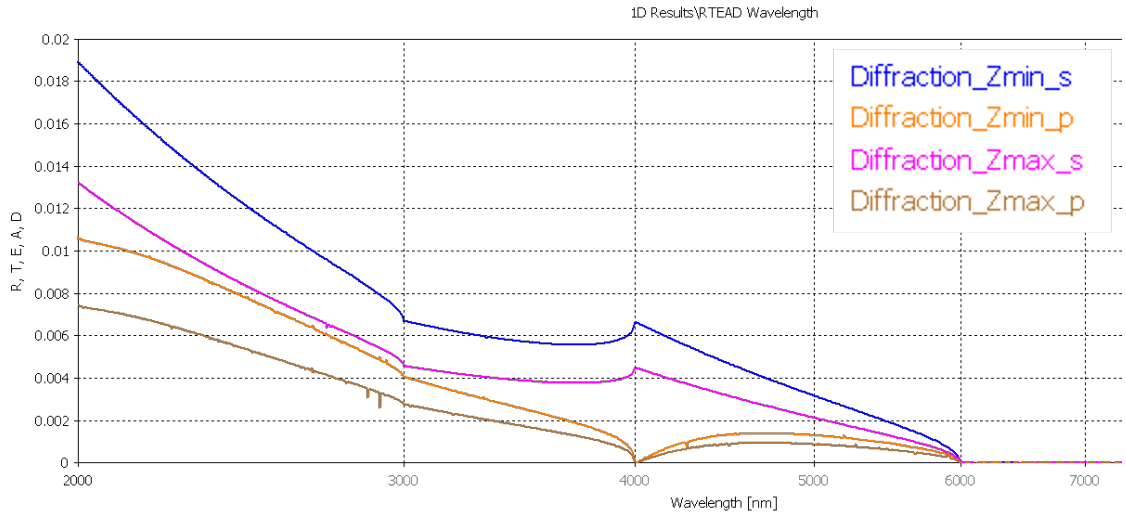

Figure 4.6: Rayleigh points on the simulated sandfish scale occur at 4000nm, which could be the wavelength of light being trapped by the micro structure. Light projection was simulated from above (Zmax), or from below (Zmin), with a P and S polarization from both sides.

In retrospect, the micro structure found on the dorsal scales of the sandfish can indeed function as a diffraction grating, suitable for light trapping (preferably IR light, at approximately 4000nm) and therefore faster heating of the body. However, its effect on body temperature seems insignificant when compared to the absorption properties of the material itself. For this reason, the issue of the micro structures purpose and function remains unsolved at this point. The fact that they can be found on other scincid lizards may imply a broader spectrum of possibilities. For example, instead of accelerating the heating of the lizard's body, the micro structure could promote dispersion of certain wavelengths of light, thereby making the animal less visible for predators from above. Another option which also has to be taken into account is, that the micro structure is a remnant of scincid's evolution, which has not been eradicated by selection.

Chapter 5 - Mechanical properties

5.1 Introduction

When trying to discover how friction and wear are reduced in the sandfish skin, the aim of the research needs to be directed into understanding of their underlying principles. For wear and friction, it is the mechanical properties, especially the plasto-elastic strength parameters which are ultimately based on the atomic compounds of the material, more precisely the bonds between them (Rabinowicz, 1995). A well known example is diamond and graphite, which are both minerals composed solely of carbon, yet they have very different properties. Compounds which have strong bonds, as a consequence also have a large resistance to deformation and thermic effects and a high surface energy (Rabinowicz, 1995). In general, this means that soft metals with a high melting point or hard metals with a low surface energy cannot exist (Rabinowicz, 1995). Such obstructions may, however, be surmounted by composite materials. By combining components with different properties in a correct manner, the components act together and give rise to new materials with possibly the best properties of all the components (Jones, 1999). Thus, many material properties, such as strength, wear resistance, weight, conductivity, etc. can be improved, though usually not all at the same time (Jones, 1999).

Keratin, the structural protein found in vertebrates is also considered a composite material, being a short fibre reinforced polymer (McKittrick et al., 2012). The basic forms of keratin are either α-helices or β-sheets. Both are found in most structures, however, there is a clear dominance of one, depending on the structure and function (McKittrick et al., 2012). Depending on the type, keratins can have many residual cysteins, which can form strong dissulfide bonds, thereby linking the chains and the matrix. Depending on the composition, keratin structures can have very variable mechanical properties. The stratum corneum alone can have an elastic deformation resistance (Young's modulus), ranging from 10MPa to 9 GPa, which is highly dependent on relative humidity and temperature (McKittrick et al., 2012).

To shed some more light on the reduced friction and wear of the sandfish epidermis, the mechanical properties or, more precisely, the plasto-elastic strength, needs to be measured. The two main parameters for this measurement are the resistance of elastic deformation or Young's modulus (also elastic, or E modulus, often only referred to as E) and the resistance to plastic (permanent) deformation or hardness (Askeland & Phulé, 2006). For hardness, there are different values and scales with the according measurements, like scratch hardness (Mohs scale) or indentation hardness (Rockwells, Vickers' scale, etc.), which are correlated (Wredenberg & Lars-

son, 2009). The Young's modulus, on the other hand, is a standard parameter and while it can have different values for macro and microscopic measurements, its connotation remains the same (Askeland & Phulé, 2006). Typically, it is measured by tensile testing. A sample with a constant cross section is stretched at a slow steady pace to the breaking point. At the same time, force (F) and distance (l) are measured in the stretching direction, thereby creating a force-distance curve. Also considering the cross section (A_0) and the starting distance (l_0), the stress (σ) and strain (ϵ) can be calculated. Stress is defined as the force applied to the initial cross sectional area, and strain as the length change in relation to the starting length. A typical stress-strain curve is shown in figure 5.1.

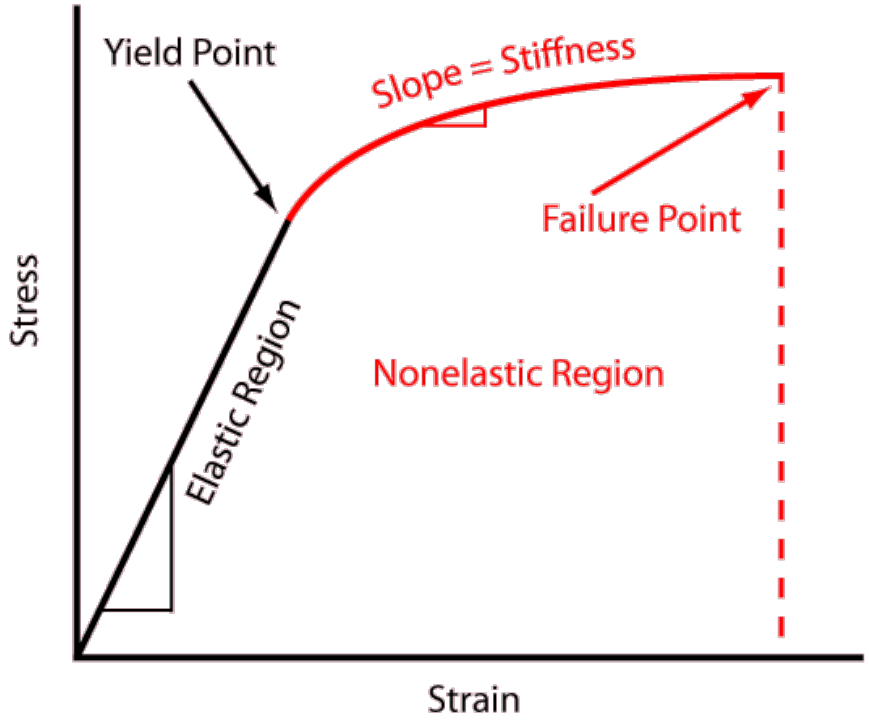

Figure 5.1: A stress-strain (σ-ϵ) curve. The linear section of the curve is in the elastic region. When material is stretched up to the yielding point, it can rebound back to its natural state. The red non-linear part of the curve is in the plastic region. Strain beyond this point is permanent. (Kinesiology course - UTA)

The curve has two characteristic regions, the initial linear one, known as the elastic region. When force load is stopped at any point in this region, the material returns to its original state. The slope of the elastic part of the stress-strain curve is also equal to Young's modulus of the material. Beyond the yield point (end of elastic region) lies the plastic region in which strain remains permanent. The failure or rupture point equals the maximum strain, the material can absorb before breaking (Rabinowicz, 1995). On the microscale, the elastic modulus can differ from the one measured on the macro scale. The means of measuring Young's modulus at the microscale is nanoindentation with an atomic force microscope. Instead of stretching the sample, a cantilever tip is pressed into the sample and the load (P)-displacement (h) curve is measured.

The elastic modulus can then be calculated from the slope, as described by Oliver and Pharr (2003).

5.2 Methods

5.2.1 Tensile testing

Preparation of single scales

Larger single scales were isolated from dorsal sided exuviae. The preparation was performed by gently removing the scales from larger pieces of epidermis, using tweezers. Special care was taken to handle only the lateral ends of the scales, without damaging the main scale body. The scales were cleaned by a stream of pressurized nitrogen, which was channelled through a Pasteur pipette. The scales were not washed, since they easily absorb water and the wetting-drying procedure may have an impact on the mechanical properties of the epidermis. The width and thickness of every scale was measured, then the scale was secured on the backside of a sticky note. Berber skink epidermis was prepared in the same way for comparison.

Scale holder construction

Standard tensile testing equipment used in this experiment is adapted for a few cm long samples. To effectively measure the Young's modulus of a single sandfish scale, a holder which would hold the small scales in place and allow standardized measurements, had to be constructed. The holder had two separate clamps, each immobilizing one side of a sandfish scale, and a connecting plate, which could be removed for measurement. This would allow installing the clamps into the testing equipment without putting strain on the scales, while enabling normal testing. A sketch of the holder construction is shown in figure 5.2, and its photograph is shown in figure 5.3. Each "clamp" was constructed from two 30x20x2mm aluminium plates. The two plates were screwed together with 2 3mm screws, which could be loosened to install the scale. At the positions where the scales were to be secured, the inner side of the plates was covered with a thin rubber membrane to prevent slipping of the scale during the test and thereby impact on the measurement. To ensure the scale was not damaged during the mounting process, the aluminium composites were secured on a plexiglass plate with 4 metallic rods 3mm in diameter to hold the composites in place, 1mm apart. 1mm thus being the "zero measurement length" of the scale (l_0).

Measurement

The measurements were done in cooperation with Umut Cakmak at the Institute for Polymer Product Engineering (IPPE), at JKU Linz. A scale was mounted on the holder, the lateral ends being secured in between the aluminium plates "clamp". The construction was installed to the tensile tester and the aluminium clamps were placed in the predetermined sample holders. Prior

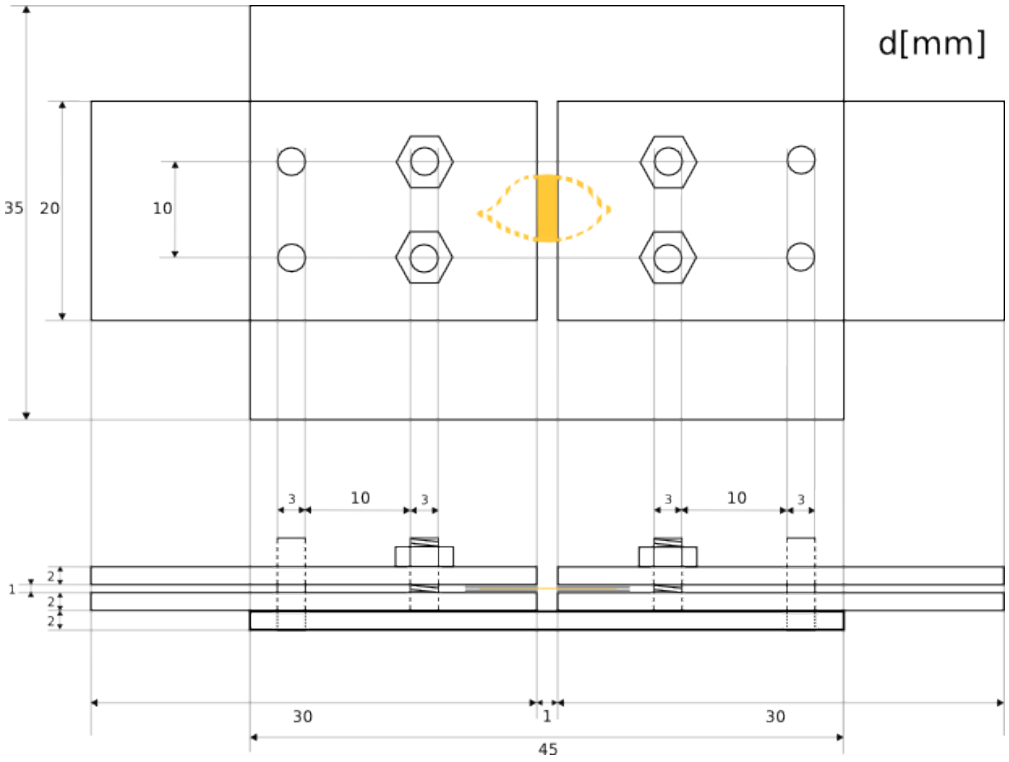

Figure 5.2: A draft showing the scale holder construction from a top-down (upper sketch) and lateral (lower sketch) perspective. The object marked with yellow is a representation of a single sandfish scale, the construction itself is in black. All shown distances are in milimeters.

to measurements the plexiglass plate was removed, liberating the aluminium clamps and the scale. The scale was stretched with a constant speed of $0.1\frac{mm}{s}$, while the force (F) and the change of distance (Δl) were measured and recorded on a computer until the rupture point of the scale was reached. The force - distance curves ($F(l)$) were recalculated to stress - strain curves ($\sigma(\epsilon)$) according to the following equations:

$$\sigma = \frac{F}{A_0} \qquad \epsilon = \frac{\Delta l}{l_0} \tag{5.1}$$

Young's modulus (E) was then calculated from the slope of the elastic part of the curve. A measurement was deemed successful, if the scale remained in its original position and the rupture occurred in the middle. The scales of both sandfish and berber skink were measured, 20 for each species, only 6 of which were successfully measured for the sandfish.

5.2.2 Nanoindentation

Scale preparation

Like for the preparation for the tensile testing, scales were cleaned under a stream of pressurized nitrogen using a Pasteur pipette. Afterwards, the scales were attached to a glass slide using a fine layer of super glue gel. As the raman spectroscopy analysis has shown (chapter 6), the glue does not penetrate the sample material and should therefore not have a strong impact on the

Figure 5.3: A photograph showing the scale holder construction from a top-down perspective.

measurement. As the glue was still wet, the scales were covered with a paper wipe and flattened with a second glass slide, which was forcefully pressed on the scales. This position was secured until the glue was completely dry and the scales immobilized on the glass surface.

Measurement

The nanoindentation measurements were performed with a nanoindenting AFM in cooperation with Lisa Maria Uiberlacker from the Institute of Polymer Science (IPS) at JKU Linz. The analysis was performed using a pure silicon cantilever with a cylindrical tip, with a 5μm radius. Before the measurement, the samples were inspected. Local air bubbles beneath the scale were observed, which, if measured, substantially distort the results. Therefore sample areas of 20x20 μm were selected, which showed full adhesion to the glass substrate. Every area was divided into 100 subregions for which the average Young's modulus values were determined. The cantilever was pressed into the material, while load-displacement curves were recorded. The approaching and retracting curves were measured, from which the mechanical properties of the materials could then be calculated. Young's modulus was determined using an algorithm developed at IPS, as well as the slope of the approaching curve in its primary linear part. Normally, every measured 20x20 μm area would show typical results, with the exception of the comblike micro structures, which had a large measurement variability due to their versatile topography and possible cantilever slipping during indentation. Preferable areas between the comb structures were therefore selected for the measurement. Altogether 9 scales were measured, 2-3 20x20 μm areas per scale and 15-20 measurements for every area.

5.3 Results and discussion

5.3.1 Tensile testing

As long as the aluminium clamps were interlocked with the PMMA fastener, the system was rigid. Thus, when installing it to the measurement device, even the slightest difference in holder

angles would lead to a tension on the actuator. In addition, the actuator was installed under the sample, so after a scale broke, the weight of half the construction would pose stress on the device. Prior to each measurement, the force value on the actuator was set to zero, however, with regard to the mentioned reasons, it was not expected the value would return to the tare zero value, but rather to the natural zero point which would deviate from it slightly. The tensile measurements showed a very similar progression, a sample measurement is shown in figure 5.4. After a short linear section, the curve continued logarithmically, followed by an exponential rise, another linear and another short logarithmic section. The curve ended at the rupture point which was then followed by a damped oscillation which would settle approximately at the level between the first logarithmic and the exponential section. This curve form was observed for both sandfish and berber skink's scales.

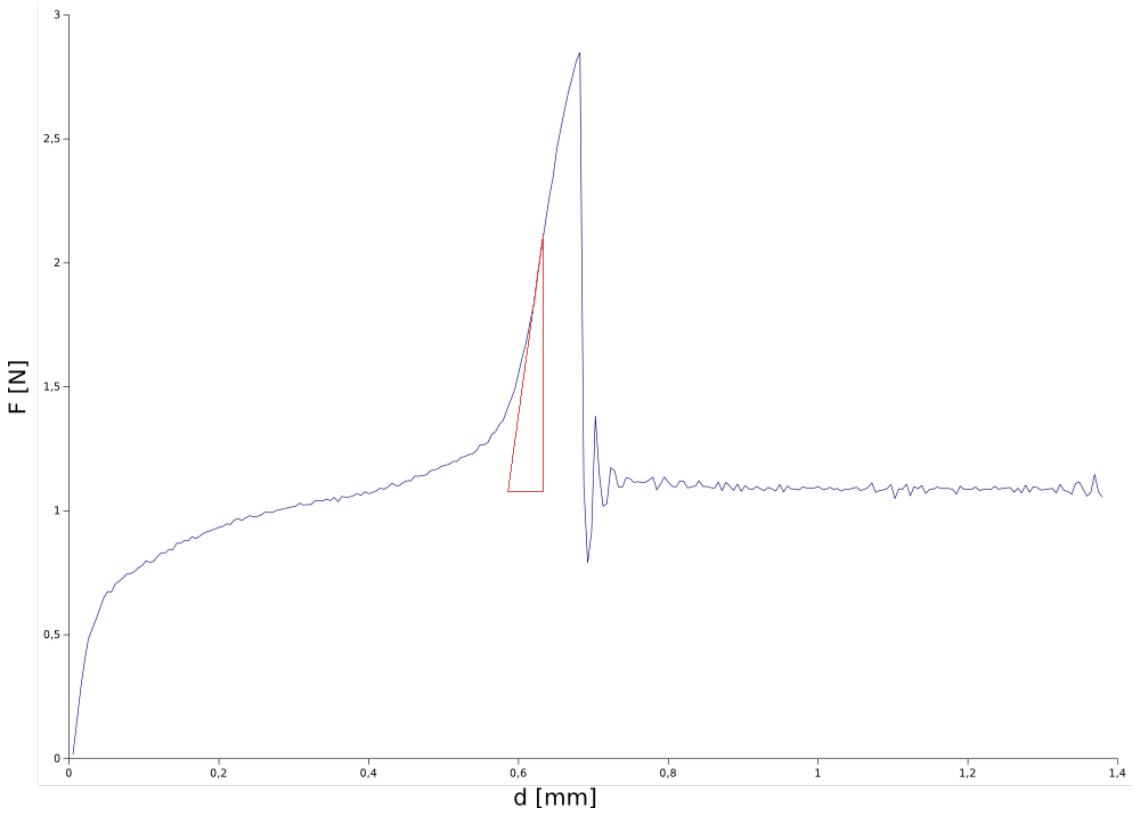

Figure 5.4: Force-distance curve measurement of a dorsal sandfish scale sample. Stretching distance (in mm) is plotted on the x and the measured force (in N) is plotted on the y axis. The curve progression changes often, two linear regions seem to appear, the second is marked in red. After rupture, the actuator measures a damped oscillation around the point of relaxation, which deviates from the zero point.

Two possibilities arise from these results. Either the measurement was distorted by the construction or this is indeed the real tensile profile of the sandfish scales. Stress-strain curves of materials can take various forms (Askeland et al., 2010), as shown in figure 5.5.

Elastomers in particular can have very similar tensile profiles, like those observed in the tensile experiment for the sandfish. A large portion of elastomer deformation is non-linear (Askeland et

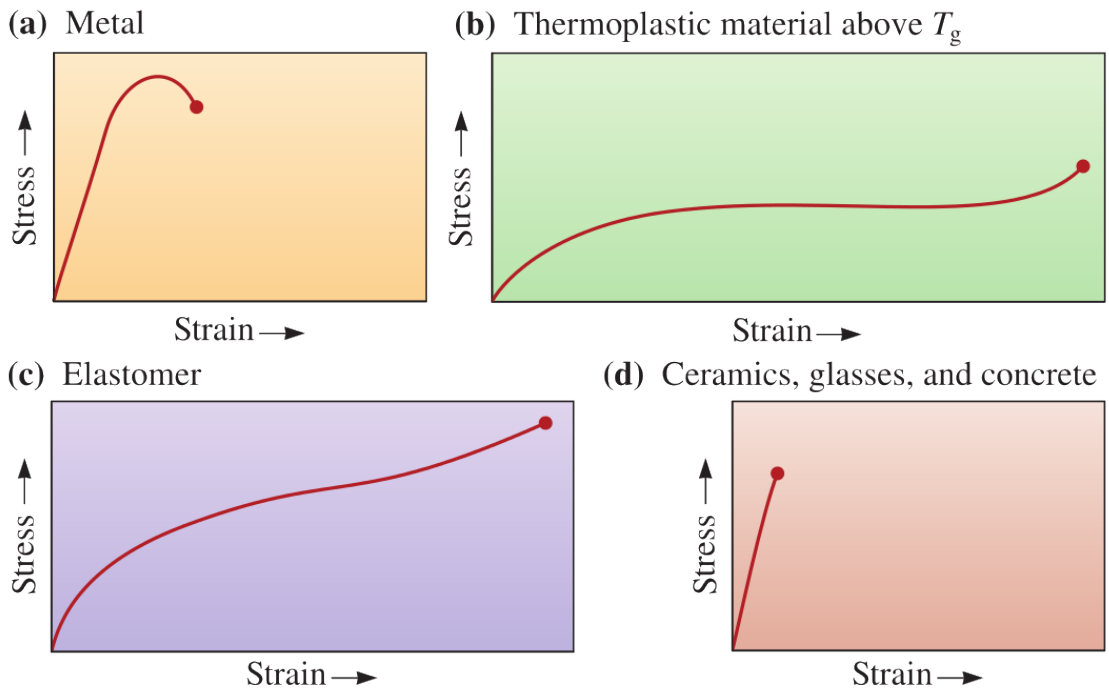

Figure 5.5: A comparison of stress-strain (σ-ϵ) curves of some materials. The values are qualitative and the magnitudes should not be compared. The data for thermoplastics are shown for a temperature above the glass-transition (T_g). Data by Askeland et al., 2010.

al., 2010). A brief elastic section is followed by a logarithmic one which gradually progresses into a slight exponential rise and ends with a linear section. Naturally occurring materials such as hair, spider silk, etc. also show various forms of tensile behaviour (Ko & Jovicic, 2004; Beyak & Meyer, 1968). From this point of view, the measured profile of the sandfish skin seems realistic. However, there seems to be a problem with the resting force value, which stabilizes after scale rupture. The stress created by the weight of the holder would put pressure on the actuator, which should shift the value below zero (since it works in the opposite direction as the stretching). The only stress which could explain the difference between the zero and the "after-rupture" value is the tension of the holder, created while securing the construction. However, this puts into question the reliability of the measurement below this level of stress, since it also incorporates the holder relaxation. Moreover the scales could have slightly slipped from the holders, additionally distorting the result. While the maximum stress and strain, measured at the point of rupture, would remain equal in both scenarios, the determination of the Young's modulus would change dramatically. If one were to presume the material behaved as a plastic material, the stretching initiated after the holder relaxation (above the "after-rupture" value), its modulus of elasticity would be determined from the linear section in this part of the curve, by incorporating the spatial factors of the material (A_0 and l_0). Young's modulus is, however, not a constant value for elastomers (Askeland et al., 2010). If it were therefore presumed that the scale behaved as such a material, the relation of stress (σ) and strain (ϵ) would replace it as a varying quantity (Askeland et al., 2010). For the sandfish, this value would vary from 0 (minimum σ-ϵ coefficient) to 1050

MPa (maximum σ-ϵ coefficient).

Young's moduli were determined on the premise of plastic behaviour for both *S. scincus* and *E. schneiderii* and visualized with the according box - whisker plots (fig. 5.6). Due to its larger scales, berber skink's skin was easier to measure, which is reflected in significantly smaller standard deviations from the average value. Still, both skin types seem to share similar Young's modulus values, which are in range of some thermoplastic elastomers, between 300 and 400MPa (Dominghaus, 1998). At rupture, the average strain for the sandfish scales was 67.3% $\pm$ 9.4%, while the average stress was 60MPa $\pm$ 30Mpa, with a maximum of 111.7 MPa.

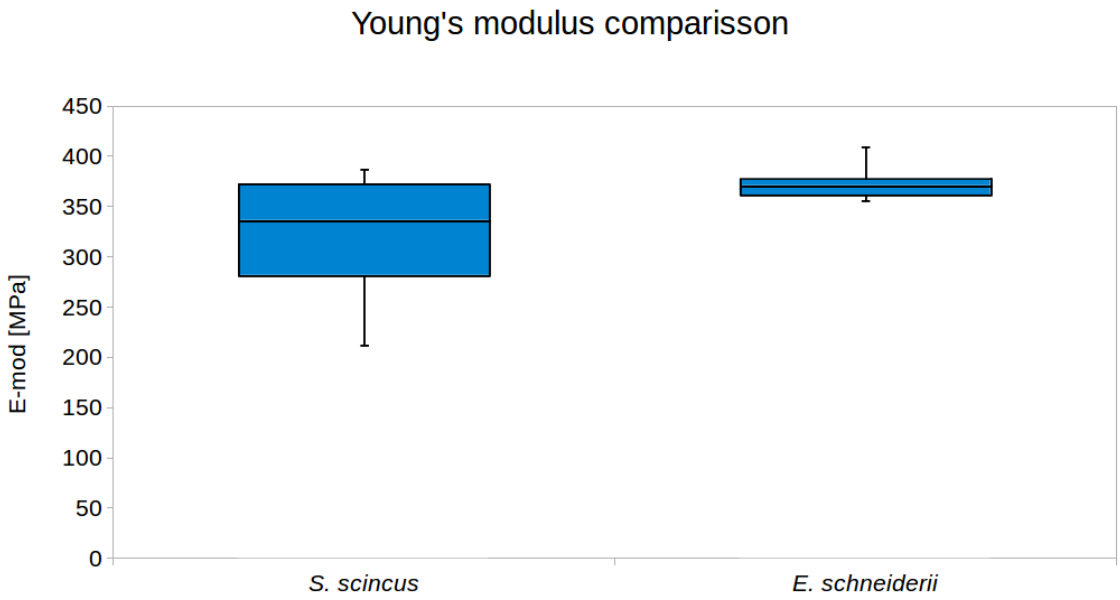

Figure 5.6: Young's modulus for *S. scincus* and *E. schneiderii*. Young's moduli were measured by tensile testing and 10 successful measurements (measurements where the scale ruptured before the measurement were not used) for each species were used for data visualization in box-whisker plots.

After deformation, perfectly elastic materials return to its original state, while plastics stay deformed to some extent. To determine whether the sandfish scales behave as plastics or nearly perfect elastomers, a cyclical stress-strain measurement would be required. Due to their small size and the (un)available equipment, this was not possible. However, there are other means of evaluation for mechanical properties, which can shed more light on the subject, one of which is nanoindentation.

5.3.2 Nanoindentation

Sandfish scales, fixated on glass were scanned with an AFM, and nanoindentation measurements were performed. Advancing and receding curves were sampled, which measured the force (F) on the y axis and the indentation depth (h) on the x axis, as shown in figure 5.7. (a) shows a single

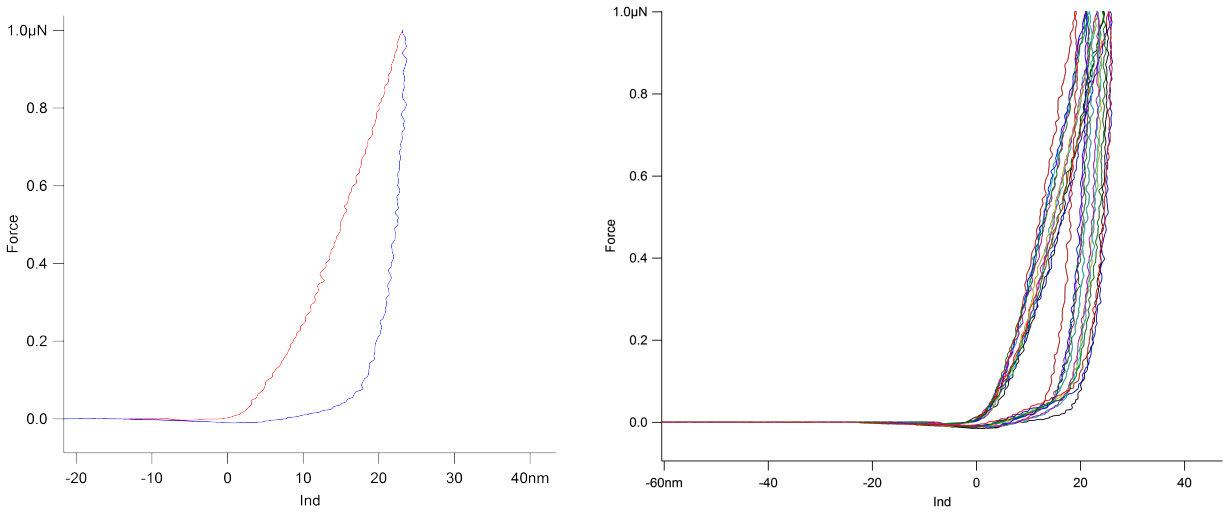

(a) (b)

Figure 5.7: Sample force indentation curves for *S. scincus*. Nanoindentation was conducted on prepared dorsal sandfish scales using a silicon cantilever with a cylindrical needle with a 5μm radius. (a) shows a single measurement. The red curve represents the needle approach, and the blue curve the retraction. (b) shows 12 measurements on a sample area. Most indentations reach a depth of 10-20nm.

measurement with the advancing (red) and receding (blue) curve. (b) on the other hand, shows a comparison of 12 measured curves on a sample area.

The receding curves show minimal negative force when approaching zero value, which suggests the adhesion is also very small. This is not very surprising and confirms previous studies (Rechenberg 2004; Baumgartner et al., 2007; Staudt et al., 2012). The complete extension curve is created by pressing the cantilever tip into the substrate with a force of 1 μN. While all measurements exhibit the same behaviour, there is a certain versatility in indentation depth, which varies from 10 to 20nm. The distribution of the curves is surprisingly even over the indentation depth bandwidth, not displaying a typical gaussian behaviour. This is also reflected in the Young's modulus values, most of which are found between 0.7 to 1.7GPa, with both the average and the median of approximately 1.3GPa. Young's modulus values calculated from the nanoindentation measurements are shown in figure 5.8.

Due to a different measurement procedure, a slight deviation between the nanoindentation and tensile testing results was expected. As discussed above, the Young's modulus value determined by the tensile testing would only be valid if the scales behaved as a plastic material. The measured difference between the average values is, however, approximately a factor of 5 higher. This difference seems quite high and cannot be easily explained. As a result of the scales geometry, the stress distribution in the tensile experiments was not completely even, causing a sample to break at the point of the maximum strain. The results of the tensile testing may therefore somewhat underestimate the real value. The scale geometry may also contribute to the variation of the nanoindentive measurements, therefore these were performed so as to reduce such variations to

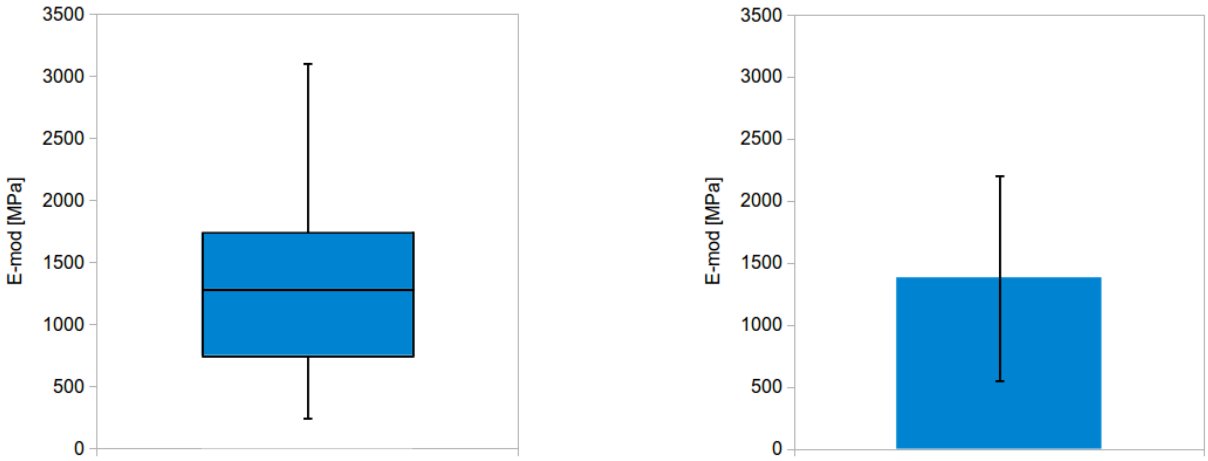

(a) (b)

Figure 5.8: Sample force indentation curves for *S. scincus*. Nanoindentation was conducted on the prepared dorsal sandfish scales using a silicon cantilever with a cylindrical needle with a 5μm radius. (a) shows one sample measurement. The curve has two parts, an advancing (red) and a receding (blue) one. (b) shows 12 measurements of a sample. The curves exhibit the same shape, however with somewhat different slopes.

a minimum (avoiding comb structures themselves). The scale thickness lies at approximately 12μm. At an indentation depth of 20nm maximum, the substantially stiffer glass substrate (50-90 GPa according to the engineering toolbox) should not impact the measurement significantly. On the other hand, another option, which arose from the tensile experiments, was that the scales behave elastically. If this were true, the material would lack a constant Young's modulus, and the stress and strain relationship would be indeed very variable (Askeland et al., 2010), which seems evident from the measured results of both experiments. In their book, Askeland et al. (2010) state that in nanoindentation, the deformation upon loading is both plastic and elastic, while being mainly elastic during unloading. As shown in figure 5.7 (b), the highest variability can be observed in the loading curve, which results in the variable indentation depth. While the variable stress-strain behaviour of the epidermis could be explained by elastic properties, this is somewhat in contradiction with the variability difference between the loading and unloading curves of the nanoindentation. What is presumably safe to state at this point is that the modulus of elasticity for the sandfish scales lies somewhere between 0.3 and 1.7 GPa, which would, according to Domininghaus (1998), fall into the category of many synthetic polymers such as elastomers and thermoplastics. Whether the scales truly behave as elastomers, remains to be confirmed. It is difficult to propose the impact, the gathered data have on the abrasion resistance of the sandfish skin. Its tensile strength of 60MPa (possibly underestimated as discussed above) is in the range of Nylon (Engineeringtoolbox), but it has and a wider range of elastic recoil, which could facilitate improved abrasion resistance. An improved set-up for tensile testing with cyclic measurements could possibly reveal more on the subject.

Chapter 6 - Biochemical composition and properties

6.1 Introduction

To understand any kind of matter, it is vital to study of which elements it is comprised and how these interact, in other words, the chemistry. Biological materials are composed of four basic types of macromolecules: nucleic acids, proteins, carbohydrates and lipids, all of which are created from smaller subunits which connect into chains, thereby giving the large molecules their properties (Alberts et al., 2003). The most diverse group, also responsible for the majority of processes in the living cell are the proteins. Proteins are composed from so called amino acids. The latter can have different functional groups, which create the form and function of the larger polymers when interacting with their neighbouring molecules (Alberts et al., 2003).

The skin's outermost layer (at least, of most terrestrial animals) - the epidermis is densely packed with proteins, so-called keratins. Two types of keratin can be found in the skin of lizards, the so called α-keratins, which have an α-helical form and the β-keratins (β-sheet form). α-keratins are usually larger in size, from 40 to 70kDa, are soft and elastic, they promote epidermal stretching and prevent water loss (Toni et al., 2007). β-keratins, on the other hand, are somewhat smaller (10-20kDa) and bundle to dense 3-4nm thick filaments, which can form aggregations with α-keratin helices, or compose compact and stiff packets. These are used to create hard structures like claws, scales, or beak and feathers in birds (Toni et al., 2007). Ultimately, the combination of both determines the chemical and physical properties of the structure they compose. Keratins are rich in cysteins (Cys), which facilitates the formation of stable dissulfide bonds between single structures, promoting polymerization. A schematic display of the keratin organization is shown in figure 6.1.

In their research, Baumgartner et al. (2007) have found both types of keratins in the sandfish's epidermis. α-keratins at approximately 35kDa and β-keratins at approximately 15kDa. Additional bands of larger proteins at approximately 55kDa were found. In addition, molecular studies were performed to identify the DNA sequence, coding the β-keratins (Staudt et al., 2012). What is peculiar about the sandfish skin, however, is not the keratin composition itself, but the fact, that the keratins are highly glycosylated - have attached glycans (Baumgartner et al., 2007; Saxe, 2008; Staudt, 2012). Glycans are oligosaccharides which are linked to proteins. These

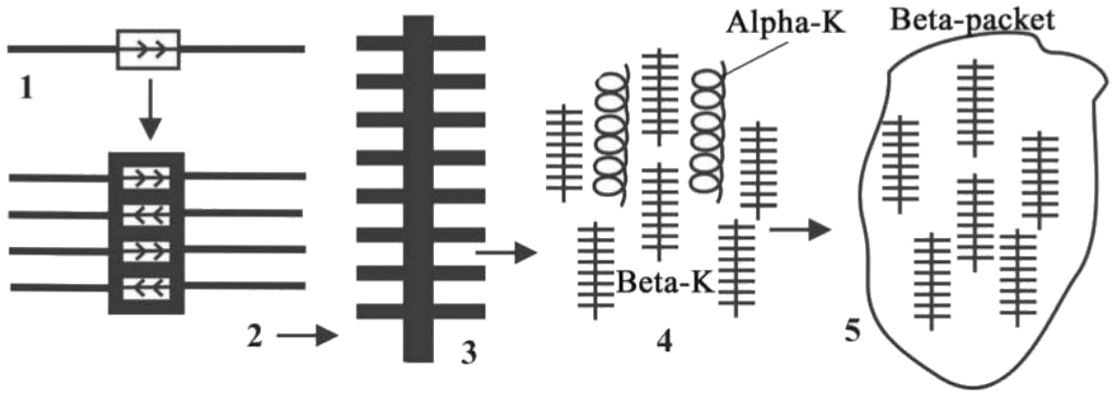

Figure 6.1: Molecular organization of keratins. β-keratin monomers (1) form the framework by antiparallel polymerization to cores (2) which construct β-keratin filaments (3). (4) shows an aggregation of β and α-keratin filaments, and (5) pure β-packets (Toni et al., 2007).

oligosaccharides, in most cases, bind to the protein via a nitrogen atom, referred to as N-linked glycans, or via an oxygen atom - O-linked glycans (Varki et al., 2009).

N-linked glycans have a typical pentasaccharidic core structure, composed of 2 N-acetyl glucosamines (GlcNAc), followed by a mannose (Man) which binds two additional Man (Varki et al., 2009). Many sugars can continue the chain from the core structure, however, we distinguish three categories of N-glycans based on their composition. High-mannose N-glycans only carry additional Man (Varki et al., 2009), but the two terminal mannoses in the core structure can also bind additional GlcNAcs. These are normally followed by a galactose (Gal) and can end with a sialic acid (Sia), which, if present, is always terminal (Varki et al., 2009). Such structures are called complex type N-glycans. Structures which have features of complex and high mannose glycans are referred to as hybrid type glycans (Varki et al., 2009). Figure 6.2 shows a schematic representation of N-glycan structures. The synthesis and coupling of N-linked glycans begins in the endoplasmatic reticulum where the core structure binds to an asparagine (Asn), linked to either a serine (Ser) or threonine (Thr) and the synthesis is typically completed in the Golgi apparatus (Varki et al., 2009). The modification process varies between different Golgi compartments, preparing the glycoproteins for their specified functions. In the trans-Golgi compartment for example, GlcNAcs, Gals and Sias can be added to cytoplasmic proteins (Varki et al., 2009). By understanding these processes as well as the function and final destination of a protein, the glycosylation pattern can be anticipated to some extent.

O-linked glycans are usually found in mucins and mucin-like proteins, but can also bind to other protein types (Varki et al., 2009). A N-acetly galactosamine (GalNAc) binds to a Ser or Thr, but from there on, many sequence patterns are possible (Varki et al., 2009). In contrast to N-glycans, the complete process of O-glycan coupling and synthesis occurs in the Golgi apparatus (Varki et al., 2009).

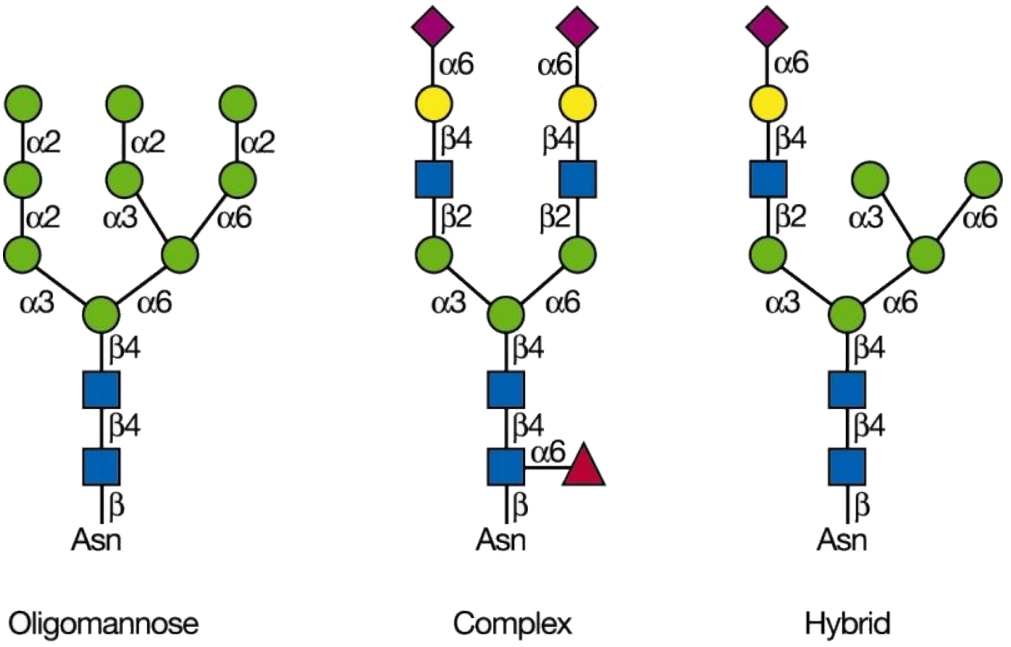

Figure 6.2: A schematic of N-linked glycans. Blue squares represent GlcNAc or GalNAc, Man is represented by green circles, Gal by yellow circles and Sia by violet spades (Varki et al., 2009).

Many proteins have attached glycans, which alter the folding during protein synthesis and can thereby change the protein functionality (Varki et al., 2009). Staudt (2012) has shown that if whole exuviae are deglycosylated, the epidermis loses its low friction properties. Normally, it is difficult to cleave glycans from a polymerized structure, because the binding sites are not accessible to the cleaving enzymes. The substrate therefore needs to be denaturated to some extent and it is unlikely that the material would return to its original state after the procedure. However, isolated glycans reduce the friction on a technical material when linked to it covalently (Staudt et al., 2012). Further research on the glycans would thus be vital for understanding the underlined principles. Some glycan analysis has already been conducted by Saxe (2008) who used specific lectins. Namely these are proteins which bind specifically to certain sugars, and if labelled, can be used to identify the carbohydrates. The following lectins were used in the analysis:

- GNA (*Galanthus nivalis* agglutinin) - binds exclusively to Mannose
- SNA (*Sambucus nigra* agglutinin) - binds to Galactose and Sialic acid
- MAA (*Maackia amurensis* agglutinin) - binds to Sialic acid
- PNA (Peanut agglutinin) - binds to Galactose and N-Acetyl Galactosamin
- DSA (*Datura stramonium* agglutinin) - binds to N-Acetyl Glucosamin, Galactose and N-Acetyl Galactosamin

The results of the lectin analysis are shown in table 6.1. The *S. scincus* lysate was positive for all lectins, which confirms that the glycans definitely contain Man and Sia, possibly Gal, GalNAc and GlcNAc. If the glycans are N-linked, both Man and GlcNAc must be present, because of the

typical core structure. If they also contain Sia, they are either complex or hybrid structures and will also contain Gal and GalNAc. If the glycans are O-linked, they will certainly contain GalNAc, however, many other options are possible. Since no structures could be conclusively identified, further research was required in this area.

Characterization of the glycosylation of β-keratins

	MAA	SNA	GNA	DSA	PNA
Scincus scincus	+	+	+	+	+
Boa constrictor	+	+	+	+	/
Fetuin (PC for MAA, SNA, DSA	+	+	-	+	-
BSA (NC)	-	-	-	-	-

Table 6.1: Lectin analysis of *S. scincus* skin lysate. The sandfish epidermis was positive for all tested lectins, while all the control samples showed the expected results. Hence, Man and Sia are definitely present, possibly Gal, GalNAc and GlcNAc (Saxe, 2008).

The keratins, the DNA that codes for them, and the keratin glycosylation was discovered, which, according to previous research, is the key to understanding the reduced friction properties of the sandfish epidermis. To gain a better understanding of the principle, a more in depth investigation of the glycans needs to be carried out. Continuing the previous methodology, the types of glycans can be determined by deglycosylation and lectin blotting. Molecular characterization and identification is often performed by various methods of chromatography - the process of separating different components by exploiting their properties. Usually, the components are distributed between a stationary and a mobile phase, moving in a certain direction (Ettre, 1993). Depending on their specific characteristics, the components interact with both phases, thereby being transported by the mobile phase with different velocities. By knowing the properties of both phases and using appropriate detection methods, the components can be identified and characterized. The standard method for protein separation is SDS-PAGE (sodium dodecyl sulphate polyacrylamide gel electrophoresis) in which the proteins are transported through a polyacrylamide gel by an electrolyte under an electric current (Laemmli, 1970). After separation, the proteins can be transferred to a membrane and analysed by labelling with dyed molecules which bind to specific parts (antigens) of either the protein itself (western blotting) or a glycan (lectin blotting).

In contrast to proteins, the glycans are not that easy to analyse. Although previous studies have shown a relatively high glycosylation of the sandfish keratins, when compared to epidermises of other reptile species, the glycans are not easily accessible and can be collected only in small amounts. After isolation, the glycans need to be separated and detected. The latter often proves very difficult, since the detectors are either very stable, yet not very sensitive (for example refractive index (RI) detection (Scott, 1986)), or very sensitive, but also very susceptible to impurities, such as salts in the sample (like evaporative light scattering detection - ELSD, or mass spectroscopy - MS (Scott, 1986)). Techniques which show high sensitivity and stability at the same time, often require additional preparation of the glycans by labelling (UV/Vis detection with fluorescent markers (Scott, 1986)). In accordance with the detection technique, a suitable

separation method is also required. There are a few techniques which facilitate successful glycan separation once they were cleaved from the target proteins. A broad spectrum of methods are HPLC (high performance liquid chromatography) techniques, which exploit different aspects of the molecule and their adsorption to a solid or liquid phase, depending on the set-up. Also another method, which can be used for glycan separation is CE (capillary electrophoresis), which exploits electrokinetic properties of particles for their separation (Kemp, 1998) and is therefore mainly suitable for glycans which lack charged groups like Sia.

In addition to biochemical analysis, which results in identification of known reference structures, other analytical methods can be used for identifying the composition of biological structures. Raman spectroscopy for example, is a technique used to analyse the low frequency spectrums of materials, such as vibrational, rotational and other low frequency emissions, aroused by intensive monochromatic light. The photons of a laser interact with the molecules of an irradiated surface and thereby receive an energy shift. Since the scattering is bond-specific, the chemical composition of a material can be determined (Gardiner & Graves, 1989).

6.2 Methods

6.2.1 Skin lysis and transfer to a watery medium

As mentioned before, keratins are a type of proteins which polymerise with each other and can form very strong and stable structures. For biochemical analysis, they need to be dissolved in a watery medium, which requires extreme conditions with high osmolarity and pH values. For this work, exuviae were the main source of keratins for analysis. To prevent as much pollution of the sample as possible, the exuviae were cleaned beforehand. The scales were vortexed twice for 1min with tap water and twice for 1min with dH_2O. Excess water was removed with a lint-free kimtech wipe and the material was dried in air at room temperature. 5mg of the material was used for further preparation. A lysis buffer was prepared following the recipe of Alibardi (2006):

- 267μl 9M Urea (dH_2O)
- 20μl 1.5M Tris/HCl pH 7.6
- 5.2μl PMSF (Et-OH)
- 2.1μl Mercaptoethanol
- 5.7μl dH_2O

The exuviae were incubated in the lysis buffer ON at room temperature in total darkness while slowly stirred. The next day the undissolved material was removed and the solution was used for further analysis.

6.2.2 SDS-PAGE

The dissolved keratins were separated by SDS polyacrylamide gel electrophoresis. Gel electrophoresis is a set of techniques used in biochemistry to separate macromolecules according to their mobility through the gel. SDS-PAGE specifically, is designed to separate proteins according to their size. SDS binds to the proteins, thereby unfolding and giving them a negative charge. In an electric field, they can be transported through the gel from the cathode to the anode with different speeds. The transport medium (gel) needs to be homogeneous and evenly long and thick in the transport direction to ensure a steady protein movement.

Two clean glass plates with equal width and thickness were prepared, one approximately 1cm higher than the other. Two equal clean plastic spacers were placed in between the plates on the outer edges, and the appliance was fastened to remain in the same position. Afterwards, a gel was prepared and used to fill the space between the plates. The exact composition can be adapted for different sizes of proteins (denser gel is used for smaller proteins).

Gel recipe:	7.5%	10%	12%	15%
dH_2O	9.8ml	8.1ml	6.8ml	4.8ml
30% Acrylamide	5ml	6.7ml	8ml	10ml
1.5M Tris (pH 8.8)	5ml	5ml	5ml	5ml
10%SDS	0.2ml	0.2ml	0.2ml	0.2ml
10%APS	60μl	60μl	60μl	60μl
TEMED	30μl	30μl	30μl	30μl

For the keratin solution, a 15% gel was prepared. The ingredients were mixed swiftly and applied between the glass plates approximately 1cm below the edge of the smaller plate. dH_2O was carefully pipetted on top, at the same time avoiding mixing with the gel, to ensure a smooth horizontal edge of the gel. After the gel had polymerised, the water was removed and a stacking gel was added, with a teflon comb inserted into the top, to create the voids for later protein application.

Stacking gel recipe:

dH_2O	6.2ml
30% Acrylamide	1.2ml
0.5M Tris (pH 6.8)	2.5ml
10%SDS	0.1ml
10%APS	30μl
TEMED	15μl

After polymerization, the comb was removed and the glass plates containing the gel were inserted into a gel electrophoresis chamber (higher plate to the outside). An electrophoresis

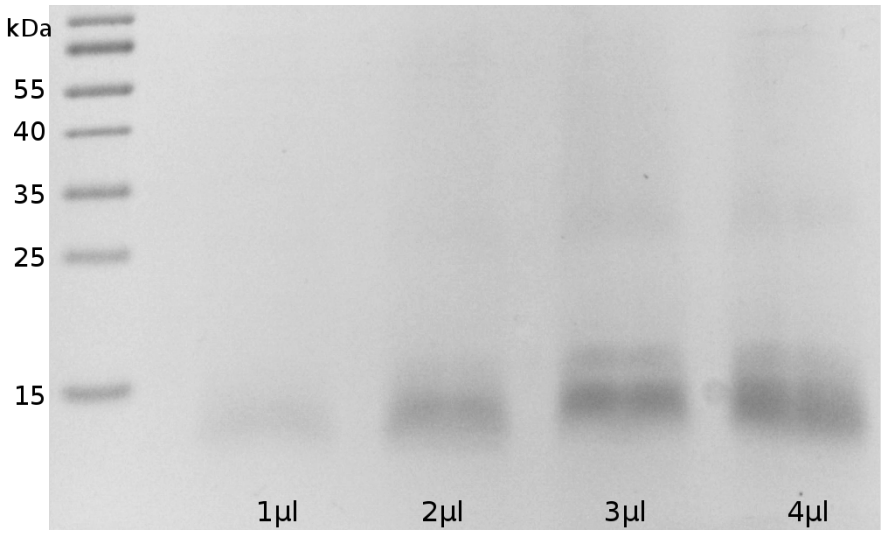

Figure 6.3: Sandfish lysate series in an SDS-PAGE. The lane numbers equal to the amount of lysate used in the analysis. 2μl are sufficient to see the expected protein bands.

buffer[1] was added to the extent, it completely covered the gel. Proteins were mixed with a sample buffer [2] and incubated for 5min at 96°C. Different amounts of lysate with sample buffer were used in the first analysis to determine the optimum amounts for keratin separation. 1+19, 2+18, 3+17, 4+16μl of keratin solution + sample buffer were used. The samples were inserted into the voids left by the comb, in a series side by side. A protein ladder was used for comparison, to mark reference protein sizes. 80V were applied to the system until the samples reached the separation gel, then the voltage was increased to maximum 150V. After the sample buffer left the gel, the voltage was stopped and the gel extracted. The first gels were dyed by Coomassie's blue staining protocol to visualize the protein bands:

Coomassie's blue staining: The gel was incubated in Coomassie's staining solution [3] for 30min-1h at room temperature. Afterwards, the dye was removed, the gel washed with tap water and incubated in the destaining solution [4] for 1h at room temperature. After that, the gel was washed again and incubated in tap water ON at room temperature. In the end, the gel was washed and incubated twice in dH_2O for 1h at room temperature. The finished gel could then be pressed between two semi-permeable membranes, dried and stored.

The protein bands were analysed and compared to the known data. 2 to 3 μl were sufficient to create clearly visible protein bands, see figure 6.3. When analysed with other samples, additional sample buffer was added to the lysate to secure an equal sample volume and protein travel speed across the analysed lanes.

Under the harsh conditions of the lysis buffer, which are necessary to denaturize and dissolve

[1] 10g SDS, 144g Glycin, 30g Tris, ad 2l dH_2O - diluted 1:5 with dH_2O before use
[2] 3x concentrated: 0.454g tris, 1.2g SDS, 7.56g glycin, 400μl bromphenol blue (2mg/ml), ad. 20ml dH_2O
[3] 2.5g Serva Blau G250, 454ml 2-Propanol, 454 dH_2O, 92ml glacial acetic acid
[4] 50ml glacial acetic acid, 75ml Ethanol, ad. 1l dH_2O.

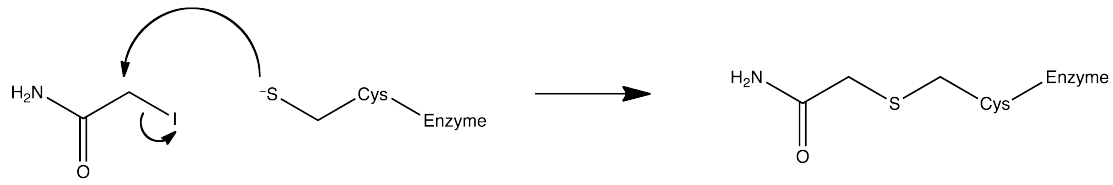

Figure 6.4: Dissulfide bridge prevention by Iodoacetamide. The mechanism of irreversible conjugation of iodoacetamide with a Cys thiol group, as proposed by Smythe (1936).

the keratin polymers, enzymes would denaturize as well, making the enzymatic experimentation very difficult, if not impossible. However, the keratins can be transferred to a more physiological environment before further research. The problem with the latter is that keratins repolymerize when transferred to physiological conditions (personal observation), obstructing biochemical analysis. To prevent this, iodoacetamide was added to the buffer and the solution was dialysed after incubation. Iodoacetamide forms an irreversible bond with the thiol group of the amino acid cysteine, thereby preventing the assembly of dissulfide bridges between proteins (Smythe, 1936). The proposed mechanism of Cys inhibition is shown in figure 6.4. The correct amount of iodoacetamide for optimum keratin solubility in PBS (phosphate buffered saline) [5] was tested, by adding varying amounts of it (Iodoacetamide) during different stages of the lysis. 50 to 100mg were added in 10mg steps, depending on the sample, before or after the incubation, with an additional incubation for 1h. Next, the solution underwent dialysis. Optimum conditions were determined to be 80mg of iodoacetamide per 300μl of keratin solution added after the overnight incubation, followed by short vortexing and further incubation for 1 hour.

To transfer the dissolved proteins from the lysis buffer, to another solution like PBS or water, dialysis was performed. For this purpose, dialysis tubing was prepared as follows:

- A knife peak of EDTA (Ethylenediaminetetraacetic acid) was added to a 500ml glass beaker and filled with dH_2O until half full.
- A 4cm long piece of dialysis tubing with the appropriate pore size (MWCO 3500 for keratins) was carefully cut onto the solution.
- The beaker was heated in a microwave and removed just before boiling.
- The tubing was transferred to fresh dH_2O and heated again. This step was repeated twice.
- In the end, the tubing was transferred to fresh dH_2O and either used directly, or stored at 4°C.

For the actual dialysis, the sample was transferred to the prepared tubing. One open ending of the dialysis tube was closed with a freezer clamp. The to-be-dialysed solution (exuviae lysate) was transferred to the tubing while the other end was closed with a freezer clamp. The Filled tubing was carefully transferred to a dialysis solution, either PBS or dH_2O. The dialysis solution was stirred and substituted every hour with fresh solution. The complete process was sustained

[5] 137mM NaCl, 2.68mM KCl, 9.58mM $Na_2HPO_4x2H_2O$, 1.47mM KH_2PO_4

for at least 3h. Afterwards, the tubing was removed and the content transferred to a fresh container. Some clearly visible precipitate formed due to the lower solubility of the keratins in the new solution. To remove the larger particles, the sample was centrifugated at 5000g for 30 seconds and the supernatant was transferred to a fresh container. The remaining sample was used for further analysis and was compared to the lysate in SDS-PAGE analysis, western and lectin blotting (further discussed below). In addition the protein content was measured, using the Bradford method. This method can be used to determine the amount of protein in an aqueous solution in mg/ml and follows this protocol:

- A series of dissolved reference protein (for example BSA) in steps of 0, 0.1, 0.25, 0.5, 0.75 including 1mg/ml in a solution (dH_2O or PBS) was created.
- 10μl of each sample (test and series) solution was added to 1ml of Bradford reagent (Roti quand (Roth) diluted 1:5 with dH_2O).
- The samples were incubated for 15min at room temperature.
- Sample absorption was measured in a Spectrophotometer at 578nm.

Not all samples would yield the same result, as they were largely dependent on the dialysis and the solubility of the keratins. The optimum incubation protocol for transferring the keratins to a physiological solution with added 80mg of iodoacetamide, yielded approximately 0.3 mg of keratins per 1ml of solution. Side-by-side SDS-PAGE analysis of lysate and dialysate (2μl of lysate mixed with 28μl of sample buffer and 15μl of dialysate mixed with 15μl of sample buffer) showed approximately the same band strength after Coomassie's blue staining. The amount and variety of proteins in a living cell can be immense and it is possible for different proteins to have the same size. This means that even if the observed bands in the gel represent proteins, which are the same size as keratins, it is not guaranteed that they are. To prove that the found proteins were indeed keratins, the lysate and dialysate were also tested by western blotting.

6.2.3 Western blotting

Western blotting is used for visualizing specific proteins by immunohistochemistry. Proteins are "recognized" by antibodies which bind specifically, and can be made visible by means of labelling. Blotting, however, does not take place directly on the polyacrylamide gel, instead, the proteins need to be transferred to a suitable material, like a nitrocellulose membrane (NC). This was carried out as follows: Two packs of 3 pieces of feltcloth were soaked in a transfer buffer [6]. A nitrocellulose membrane and the unstained PAGE gel were placed in between the two soaked packs and transferred to a semi-dry blotting device. Voltage was applied to the appliance and the current was set to 43mA for 90min. The NC membrane, now containing the proteins, was stained with Panceau red (the membrane was also blocked in this step) and washed with dH_2O. At this point, the protein bands became visible. The membrane was completely destained by washing with PBS and was ready for further procedure steps.

[6] 3.03g tris, 14.41g glycine, 10g SDS, 200ml methanol, 800ml dH_2O

To obtain meaningful results, the SDS-PAGE gel had to be prepared Accordingly: The protein ladder marker was applied to a lane in the middle of the gel and the samples (lysate and dialysate) were applied once on each side of the marker. After the transfer to the NC membrane, the membrane was cut through the marker in the middle, so that one side could be used as a test, and the other as a negative control. Next, the procedure went as follows:

- Blocking of both pieces in a 5% milk solution (5g skimmed milk powder, 100ml PBS tween (0.05%)) for 30min at room temperature.
- Incubation of test membrane with primary antibody (AB): (milk solution, 1:2000 Rabbit-Anti-ß-Keratin antibody[7]) ON at 4°C (negative control membrane was incubated under the same conditions without the primary AB).
- 3x5min washing of both membranes with PBS tween (0.05%).
- Incubation of both membranes with a secondary antibody (milk solution, 1:3000 Goat-Anti-Rabbit-Peroxidase AB) for 1h at room temperature.
- 3x5min washing of both membranes with PBS tween (0.05%)
- Transferring both membranes to PBS

If the binding was successful, the anticipated proteins would be made visible by chemiluminescence. This was accomplished by oxidizing luminol with the peroxidase in the secondary AB (horseradish peroxidase or HRP), using peroxide as the oxidizing agent. The activated luminol (Dicarboxylat-Dianion) emits light, which can then be captured by a photographic film. Procedure (in a darkroom):

- ECL1[8] and ECL2[9] solutions were mixed (8ml each), transferred to a petri dish and the NC membranes were bathed in the solution for 1min.
- The membranes were laid flat on a plate and covered with transparent saran foil.
- Photographic film was placed over the membranes and the protein ladder was marked with a pen, then the film was covered with another plate to hold everything in place and protect the film from light.
- The film was briefly washed in the developer, next in tap water, then fixative and finally again in tap water.
- If the procedure was successful, specific protein bands could be observed on both lanes of the test film, but none on the negative control.

[7] kindly provided by prof. Lorenzo Alibardi from the University of Bologna

[8] 1ml 250mM Luminol(DMSO), 0.44ml 90mM p-Cumaric acid(DMSO), 10ml 1M Tris pH8.5, ad 100ml H_2O

[9] 64μl 30% H_2O_2, 10ml 1M Tris pH 8.5, ad 100ml H_2O

6.2.4 Lectin blotting

Lectin blotting is used for visualization of glycoproteins which were separated by gel electrophoresis. Lectins are proteins which bind to specific monosaccharides and can therefore be used for sugar identification. Concanavalin A, for example, binds preferably to Man and Glc, which are present in most glycans, and can therefore mark a wide spectrum of glycans. As already mentioned, two types of glycans are most common in biological tissues, N- and O-linked glycans. Along with their glycoproteins, they form specific sites which can be recognised by specific proteins and either labelled (if the antibody is a lectin) or cleaved off the protein, if the protein is an enzyme. PNGase F, also known as N-glycosidase, cleaves N-glycans, while O-glycosidase cleaves (certain) O-glycans. If a protein sample is treated with a glycosidase, according glycans (if present) should be removed. If the sample is then separated by SDS-PAGE and tested for glycans in comparison to an untreated sample, one can determine if a certain type of glycans is present in a sample or not. However before the procedure can be executed, certain conditions have to be met for the enzymes to work properly. The medium needs to have the correct composition and pH, also O-glycosidase can, for example, only cleave O-glycans without a linked sialic acid. Since the composition of the keratin glycans was unknown, the proteins had to be pretreated by a Sialidase (an enzyme which cleaves sialic acids). Glycosidases work with a specific activity (can cleave n structures per unit of time in certain conditions). 1 unit (U) of PNGase F from *Flavobacterium meningosepticum*, for example, can hydrolyse 1 nmol dabsyl fibrin glycopeptide or 0.2 nmol dansyl fetuin glycoprotein within 1 minute at 37°C and pH 7.8 (Roche). To ensure all the glycans are removed before testing, the amount of glycan binding proteins has to be known. The PBS keratin samples were therefore analysed with the Bradford test. The typical protein concentration was approximately 0.2-0.3 mg/ml. 40μl keratin dialysate samples were made and 2μl of glycosidase stock solution were added to ensure total deglycosilation within 30-60 min at 37°C. Before the addition of sample buffer and the application on the SDS gel, the samples were cooled to room temperature, and centrifugated, to ensure that all condensation droplets returned to the main sample body. Glycosidases were added to the samples in different combinations to precisely determine the presence of different types of glycans. The following samples were prepared:

***** - native PBS keratin sample

***N** - PBS keratin + N-glycosidase (should cleave all N-glycans, only O-glycans would remain)

***O** - PBS keratin + O-glycosidase (should cleave all O-glycans not containing Sialic acid)

***OS** - PBS keratin + O-glycosidase + Sialidase (should cleave all O-glycans, only N-glycans would remain)

***NOS** - PBS keratin + N-glycosidase + O-glycosidase + Sialidase (should cleave all glycans)

Unglycosylated BSA (bovine serum albumin) was used as the negative control sample in this experiment and glycosylated fetuin was used as the positive control. After SDS-PAGE

separation and blotting to a nitrocellulose membrane (as in Western blotting), the lectin analysis was performed in accordance with the following procedure:

- The NC membrane was blocked in a 2% PBS tween solution for 2min.
- Secondary blocking was performed with a 1:10 diluted Roti block solution in which the membrane was soaked ON at 4°C.
- The membrane was then incubated in a ConcanavalinA solution (1-5μg/ml ConA-HRP, 1mM $CaCl_2$, 1mM $MgCl_2$, 1mM $MnCl_2$ in PBS tween (0.05%)) for 1h at room temperature in darkness.
- This was followed by 2x5min washing with PBS tween (0.05%).
- Finally, the membrane was transferred to PBS and the glycoproteins were visualized using luminol (as in Western blotting).

6.2.5 Capillary electrophoresis

This set of experiments was done in cooperation with Dennis Hirtz at the Helmholtz-Institute for Biomedical Engineering, RWTH Aachen. Before the analysis, the glycans had to be released from the keratins and purified accordingly. The exuviae were dissolved and dialysed in PBS, as described above. Firstly, N-linked glycan analysis was performed, and the glycans were then enzymatically cleaved off the proteins. PNGase F works more efficiently if the proteins are denaturated, therefore 45μl of the keratin PBS solution ($\approx$ 0.3mg/ml) was extracted and 1μl of 5% SDS and 1.5μl 1.67M 2-mercaptoethanol (like iodoacetamide, mercaptoethanol also interacts with free thiol groups of cysteins) were added. The mixture was shortly vortexed and incubated for 20 min at 37°C. 5μl Nonidet NP40 (protects enzymes from denaturation) and 4μl PNGase F were added to the sample which was then incubated ON at 37°C.

After being extracted from the keratins, the glycans were purified from the solution. Proteins are not soluble in organic solvents, SDS is not soluble at low temperatures and the mercaptoethanol is highly volatile. Therefore 150μl of ice cold, 100% ethanol were added to the PNGase F treated keratin sample and incubated at 0°C for 20 min, while gently stirred. The proteins and the SDS precipitated during this process, and formed an insoluble pellet after centrifugation at 12000g for 5min. The supernatant containing the glycans and mercaptoethanol was transferred to a fresh container and dried by means of vacuum rotation, thereby removing the mercaptoethanol. The separation of the glycans took place in a capillary electrophoresis system at the Helmholtz-Institute for Biomedical Engineering. The glycan detection was done with a fluorescent light sensor.

Glycans alone would be invisible in this case, therefore they were labelled with the fluorescent dye APTS (8-Aminopyrene-1,3,6-Trisulfonate). In a reductive amination reaction, the primary amine from an APTS molecule reacts with the reducing -OH group of a GlcNAc (part of an N-linked glycan), thereby forming a C-N-C bond. To trigger the reaction, a reducing agent is required. Sodium cyanoborohydride ($NaBH_3CN$) was used in this experiment, which is activated

under acidic conditions. Caution is advised during the procedure, since HCN is released! 3μl of a maltose (Mal) standard was added to the dried glycans. In addition, a second sample with a glucose G1 - G18 ladder and Mal was made (and used) for comparison. The samples were dried using vacuum rotation for 2 - 3h. 2μl of 1M $NaBH_3CN$ and 2μl APTS (in 1M citric acid) were added to both samples. The samples were incubated for either 90 min at 60°C or ON at 37°C. In the subsequent labelling procedure, the samples were partially predigested with sialidase. Due to its polar nature, sialic acid, if present, can change the travel speed of a glycan structure in the capillary. It is however not very stable and is peeled off the structure at 60°C.

After the incubation, the reaction was stopped by adding 195μl of ddH_2O and was ready for analysis. Separation was accomplished on a fused-silica capillary with a 50mM $Na_2B_4O_7$ x $10H_2O$, 64mM borate buffer, at pH 8.9. Migration was promoted at 25kV (23mA) at 25°C. and UV detection was performed at 254nm. O-glycan analysis was to be carried out in a similar manner after a successful N-glycan analysis.

6.2.6 Mass spectrometry

Mass spectrometric analysis was done in cooperation with prof. Franz-Georg Hanisch from the department of Molecular Glycobiology, Center for Biochemistry, University of Köln. The extraction of N- and O-linked glycans was performed in a different manner and will be described separately.

N-glycans

Exuviae were dissolved and dialysed in dH_2O as described before. 200μl of the dialysate ($\approx$ 0.3mg/ml) were transferred to a fresh eppendorf tube (epi). 200μl of a 100mM NH_4CO_3 solution, 0.4μl of 1M $CaCl_2$ and 1μl of trypsin were added and the mix was incubated for 2h at 37°C. Trypsin cuts proteins at the carboxyterminal ends of lysine (Lys) and arginine (Arg), creating peptide fragments, and making the peptide-glycan linking sites more accessible for cleavage by the PNGase F. After incubation, the trypsin was inactivated by incubation for 30min at 60°C. The sample was cooled and dried in a speed vac (vacuum rotation). NH_4CO_3 evaporates along with the water, which makes it a suitable incubation buffer salt for analyses, where such can agitate the detection even in small concentrations.

The glycan - protein mix was resuspended in 50μl of fresh 50mM NH_4CO_3 and 1μl of PNGase F solution was added, then the sample was incubated ON at 37°C. The PNGase F stock solution contains glycerol, which is a disturbing agent in Mass spectrometry (MS), therefore small amounts were used (0.5-1μl).

The sample was dried in a speed-vac and sent to prof. Hanisch for labelling and MALDI (Matrix-assisted laser desorption/ionization) TOF (Time of Flight) MS analysis, as described in detail by Breloy et al. (2012). MALDI is a gentle ionization technique and allows the analysis of fragile molecules. The isolated glycans were purified from the peptide rich sample on a C18 column (solid phase extraction column Agilent Technologies, Waldbronn, Germany) in liquid

chromatography (LC) system. The sample was dried and methylated in 100μl DMSO containing NaOH in two incubation steps for 30min at room temperature. Before the second incubation, 50μl of methyliodide were added. After the methylation labelling, 300μl of chloroform were added and the glycans were repeatedly extracted with 200μl of dH_2O. The chloroform phase was dried in a nitrogen atmosphere and the sample was dissolved in 20μl methanol. The analysis itself was performed on an UltrafleXtreme instrument (Bruker Daltonics).

Permethylated glycans in methanol were applied to a steel target by mixing 0.5μl of the sample and 1μl of matrix solution (saturated 2,5-dihydroxy benzoic acid in ACN:0.1% TFA = 1:2). Alternatively, 0.75μl of the sample were mixed with 0.75μl α-cyano-4-hydroxycinnamic acid matrix solution. TOF analysis was performed by positive ion detection in reflectron mode. Ionization was induced with approximately 5000 shots of a pulsed "Smart-beam" laser and the ions were accelerated in a field of 20kV and reflected at 23kV.

O-glycans

O-glycans, if containing sialic acid, cannot be cleaved by glycosidases, therefore enzymatical deglycosylation protocols are seldom used in analytical procedures. Instead, a chemical deglycosilation strategy was used. Exuviae were dissolved and dialysed in dH_2O. 200μl of the probe were transferred to a new epi and 200μl of a 100mM NaOH/2M $NaBH_4$ solution was added. The mix was incubated ON at 60°C. During this procedure, O-glycans are released by β-elimination of the keratins. To prevent peeling of the carbohydrates, the reaction took place in the presence of a reducing agent ($NaBH_4$). The sample was dried in a speed-vac, labelled and analysed by prof. Hanisch, using MALDI TOF MS (as described above for the N-glycans).

6.2.7 Raman spectroscopy

The substance specific Raman scattering facilitates the detection of structures which are chemically different, even if they optically form a homogeneous structure. For basic spectral analysis, a piece of sandfish exuviae was cleaned by vortexing 2x1 min in H_2O and subsequently 2x1 min in dH_2O. A single scale, which was still wet and soft, was then extracted and placed flat on a glass slide, the distal side facing upwards. Excess water was removed with a lint-free kimtech wipe. The scale was covered with a dry piece of the wipe and pressed flat with a second glass slide on top and dried at room temperature for 2h. The dry scale was then analysed in a Raman spectroscope (Witec, Ulm, Germany) with a green light laser by Christian Reisecker at the Institute of Polymer Science, JKU Linz. For comparison, the same procedure was performed on a berber skink scale.

In addition, keratin dialysate and purified glycans were also measured. A 30μl drop of each sample was applied to a polished and cleaned silicon wafer, which has a narrow band of peaks in the Raman spectrum and can be subtracted from the spectrum. The sample was protected from dust and dried at room temperature. The measured spectra were then compared with the available data for keratinous structures found in literature.

For an in depth analysis of the material, the sandfish exuviae were also analysed in cross section. The exuviae were washed by vortexing for 2x1 min in H_2O and 2x1 min in dH_2O, followed by the extraction of a single scale, which was dried in air and protected from dust. The scale was firmly mounted on a plastic ultramicrotome holder, using super glue (cyan acrylate) gel, and left out to dry. The scale was cut in the frontal plane using an ultramicrotome, while being observed under a stereo microscope. After a suitable spot was found in the substrate, the section advancing speed was gradually reduced until 20μm per cut were reached (polishing). 5 additional sections were performed to secure a very smooth surface. The scale was then analysed in cross section with the Raman spectrometer. A sample spectrum was measured again (same settings as before). Then, the cross section was measured in 0° and 90° polarity. This was done to test whether the material was homogeneous or any lamellar structures could be observed, as they might have an impact on the mechanical properties in different directions.

6.3 Results and discussion

6.3.1 SDS-PAGE

The skin lysate, which was separated in the SDS-PAGE and stained with coomassie blue staining, showed typical bands between 10 and 20, around 15 kDa and a band at 35kDa. If the sufficient amount of protein was applied to the SDS gel, another band could be observed at 55kDa. It was otherwise significantly weaker in comparison with the other two. A sample coomassie stained gel with 10μl sandfish epidermis lysate is shown in figure 6.5 (a). Subfigure (b) shows a coomassie stained gel with the applied lysate (2μl) and dialysate (15μl). Interestingly, if the lysate was not separated the day after the lysis and the substrate was exposed to the lysis buffer for a longer period, the protein bands (especially those between 15 and 20kDa) began to shift towards the 10kDa mark.

Since the lysis buffer has a high pH and salt concentration, it is possible prolonged incubation leads to molecular peeling and chemical deglycosylation (Sigma; Aminoff et al., 1980). The band shift can therefore be explained in two possible ways. Either the glycans or the keratins are being peeled, thus slowly reducing the size of the glycoprotein. This is also the reason why the dialysis of the sample is important, especially if the samples are to be stored for longer periods. Concerning dialysis effectivity, (in theory) it would be possible to bind most of the keratins to the iodoacetamide molecules and thereby increase the soluble keratin yield. This would, however, also increase the incubation time, which would potentially result in several keratin/glycan molecules being damaged by the buffer.

Because the peeling process takes time, both glycosylised, deglycosylised and intermediate structures should be present in the solution. As a result, the proteins would be visible as clearly separated bands in the gel, with the separation difference equivalent to the size lost due to peeling. Such bands were observed in the majority of stained SDS gels (and western blots later on). These might also appear as a consequence of different keratins which exhibit a small difference in size.

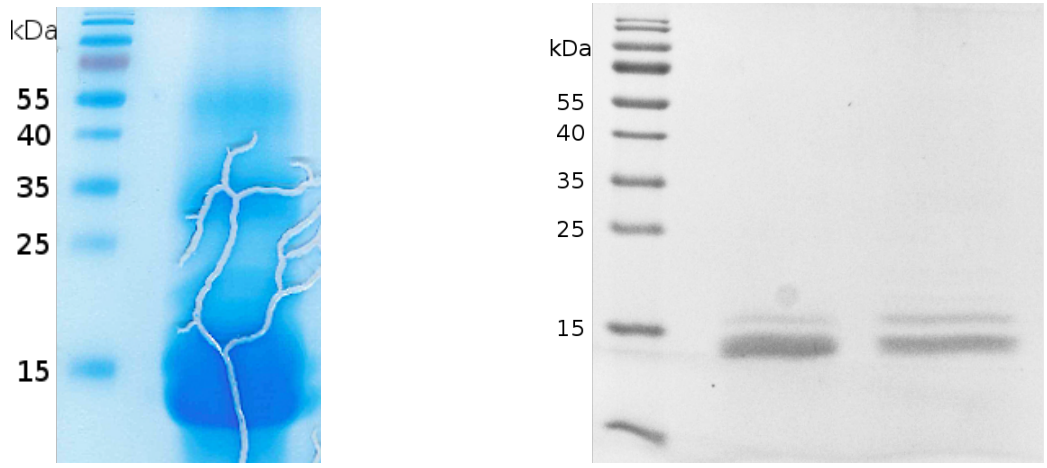

(a) SDS-gel lysate (b) SDS-gel lysate vs dialysate

Figure 6.5: *S. scincus* skin lysate coomassie. A coomassie blue stained SDS gel, with the analysed sandfish skin lysate and dialysate. (a) shows a coomassie stained gel of only the lysate, which was applied in high doses, showing bands at 15kDa, 35kDa, as well as at 55kDa. (b) shows a greyscale image of a coomassie stained gel with lysate (left) and dialysate (right).

However if this was the case, identical bands should be observed in all gels, yet there was a slight variation, especially well observed in western blotting (discussed below).

6.3.2 Western blotting

A photograph of a western blot sample for lysate and dialysate is shown in figure 6.6. The dialysed sample showed significantly weaker signals than the pure lysate, very likely due to the precipitation during dialysis, as previously discussed. The bands that could be observed were between 10-25kDa, at 35kDa, and a very weak signal was also observed at the 55kDa mark. The negative control showed no bands whatsoever, which means that the secondary antibody (HRP) did not bind to the keratins, since the primary antibody was missing. The experiment shows that the proteins extracted from the skin were indeed keratins and that it is possible to transfer them to a physiological buffer, while keeping them soluble to some extent. This step facilitates the enzymatic digestion of the keratins and therefore further analysis.

The lysate shows substantially stronger bands in comparison to the dialysate, especially between the 15 and 25kDa mark. Despite using iodoacetamide, many keratins still precipitated to a large extent during dialysis. Therefore some bands are completely missing in the dialysate lane in the western blot. Two possibilities arise: the bands missing in the dialysate sample belong to different β keratins with somewhat higher molecular weight or these bands are a part of the same keratin, containing glycans, which were peeled during the lysis/dialysis process. This consequently resulted in different positions in the gel. The latter would also imply that the more glycosylised β keratins are substantially less soluble in a moderate medium such as PBS or dH_2O. While this is not conclusive, it would be in agreement with the surface energy experiments which showed that the glycosylated keratins have a higher contact angle for water in comparison to less

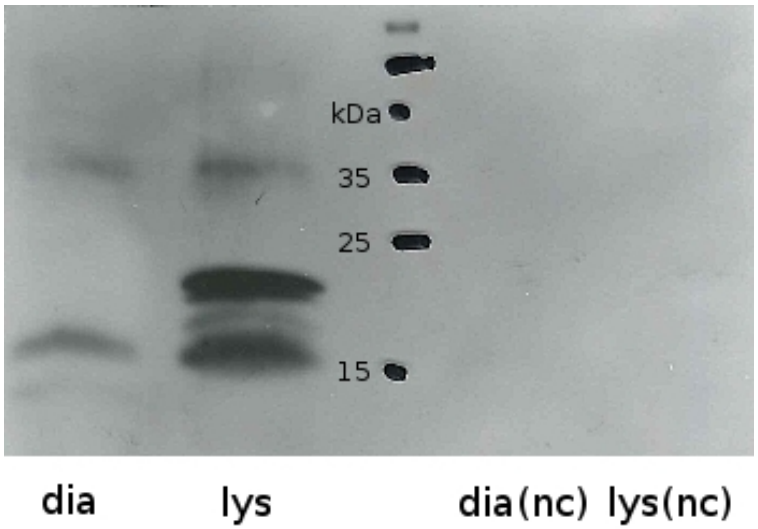

Figure 6.6: *S. scincus* skin lysate western blot. A western blot of the sandfish skin lysate and dialysate is shown. The membrane containing the proteins was treated with Rabbit-Anti-β-Keratin (1. antibody) and Goat-Anti-Rabbit-Peroxidase (2. antibody). The testing samples are shown on the left side of the marker and the negative controls on the right side.

glycosylated keratins.

6.3.3 Lectin blotting

To determine which types of glycans are present on the sandfish keratins, the dialysed keratins were predigested with deglycosylation enzymes in different combinations before chromatography and blotting. The blotting was performed with Concanavalin A, which binds strongest to glucose and mannose and is therefore suitable to mark most glycans. Figure 6.7 shows a lectin blot of deglycosylated sandfish keratins.

The native glycan sample showed glycan signals at all bands, including 15-20kDa and 35kDa, yet the strongest signal appeared at the 55kDa mark. This is surprising since these bands showed the weakest signal in gel staining and western blotting. It further implies that the proteins at this band either have a very high glycan concentration, the glycans are more accessible, or contain more Glc and Man to which Concanavalin A binds the most. As the signal at this height was weakest in the coomassie stained gel, we can assume, that this band has the least amount of proteins. What is more important is that the proteins digested with PNGase F (N-glycosidase) had significantly weaker bands when compared to the untreated sample. The band around 35kDa disappeared completely, which suggests that the α keratins bind only N-linked glycans. The remaining bands showed a slight shift in molecular weight, which is also a sign of deglycosylation. When treated with O-glycosidase or O-glycosidase and Sialidase, no significant change in comparison with the native sample could be observed. This is possibly due to the strong signal from the N-glycans which masked the O-glycan change. Moreover if O-linked glycans were present, they should appear relatively small in size, otherwise their removal would manifest as a shift in band position.

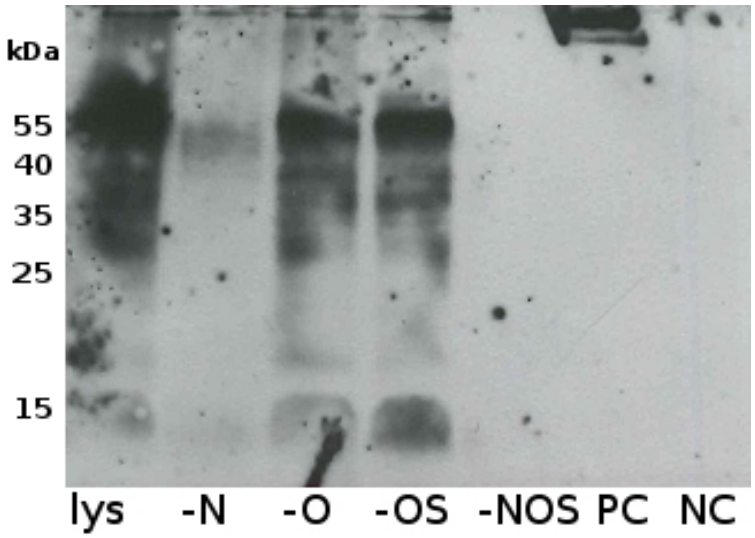

Figure 6.7: *S. scincus* skin lysate lectin blot. The different lanes mark the differently prepared samples. The standard control sample of the lysate (lys), predigested with PNGase F (-N), predigested with O-glycosidase (-O), sialidaze and O-glycosidase (-OS) and with all three enzymes (-NOS). The positive control with Fetuin (PC) and the negative control with BSA (NC) are on the right side of the blot.

After being treated with all three enzymes, all bands disappeared completely, which is a strong indication that O-linked glycans are linked to the tested proteins. Positive and negative controls appeared as expected.

While the O-glycans appear to be present, the N-glycan concentration is substantially higher. It is possible the latter appear stronger due to better affinity to Concanavalin A, however the band shift for O-glycans is also insignificant, which suggests they are present in lower amounts. Lectin blotting is a viable method for glycan identification (N- or O-linked) on separated proteins, however, it does neither facilitate quantitative analysis nor the identification of the monosaccharide components. For such analysis other methods are more suitable.

6.3.4 Capillary electrophoresis

As discussed in the introduction of this chapter, various monosaccharides were plausible candidates for composing the keratin glycans, one group being sialic acids. This is a family of approximately 30 derivatives of N-acetyl or N-glycolyl neuraminic acids (Mandal & Mandal, 1990). The 9-C monosaccharide chain has a charged state created by the carboxylic group at C1 (Varki et al., 2009) and can change the travelling speed of a complete glycan during capillary electrophoresis. Thus, if glycans are detected, they cannot be allocated on the size scale in the same way as neutral structures. For this reason, the glycan labelling protocol for CE analysis took place at 60°C in an acidic milieu, which should have resulted in hydrolysis of present sialic acids (Hirtz & Elling protocol; Jayo et al., 2014; Varki et al., 2009). As these are always terminal monosaccharides in N-glycans, the size of the complete structure can still be approximated if they are missing. The

labelling was also repeated at 37°C and the glycans were partially predigested with sialidase for comparison.

The signals of the CE analysis were extremely weak, and it was difficult to differentiate the peaks from background noise. A measurement of the glc standard ladder and a sample measurement, with the labelling carried out at 37°C, is shown in figure 6.8. Under standard conditions (labelling at 60°C without predigestion), the CE showed 5 different structures which when compared to the glucose ladder, had the following sizes: 3Glc, 4Glc, 6Glc and 9-10Glc (Glc only being a measure of size). If any of these structures contained sialic acid in the native form, their size would be adequately larger. The core structure of N-glycans consists of 2GlcNAc and 3Man, resulting in a minimum size of 5Glc. One can thus assume the 3 and 4Glc structures were the products of peeling.

When labelled at 37°C, the peaks at 6 and 9-10Glc disappeared, further suggesting these structures had an incorporated Sia which accelerated the travelling of the structure through the capillary. To prove this, the peaks should reapear under the same labelling conditions, but with glycans predigested with a sialidase. Indeed, the 6 and 9-10Glc peaks reappeared in the pretreated samples, which confirms the premise. On the other hand, the 3 and 4Glc structures were missing in this last measurement. The reason behind this is not clear. The 3 and 4Glc structures, observed after the harsh labelling, could have been peeling products of larger structures, which were then contained in the larger 6 and 9-10Glc structures. However, if this was true, they would be also missing after the labelling at 37°C without pretreatment with sialidase.

The results suggest that the skin contains at least two N-glycan structures, one the size of 6Glc with additional Sia and the other the size of 9-10Glc with additional Sia. According to known data, if Sia is present in N-glycans, it is terminal and follows a Gal, which can also follow only a GlcNAc or GalNAc (Varki et al., 2009). Since the core structure is approximately 5Glc large, it is relatively easy to calculate the structure of the 9-10Glc structure. If it was a complex glycan, it would have 2 additional GlcNAcs, one for each free Man. Each GlcNAc would then bind a Gal, creating a 9Glc structure. The complete glycan with terminal sialic acids would in this case have an end size of approximately 11-12Glc. If the structure was a hybrid glycan, one chain would be composed in the same way as in complex type structures and the other would bind additional mannoses. It is more difficult to predict the structure for the 6Glc structure, since at least 2 additional monosaccharides are required on the core structure for a Sia to bind. Another possibility is, that the glycans are complex, but do not have a terminal Sia. It is also possible that the structures were damaged by the peeling effects and therefore have a reduced size. Overall, additional research was required to identify the (occurring) glycans in the sandfish epidermis. Since O-glycans, if present (at all), presumably appear in even smaller amounts, CE analysis was not performed for this type of oligosaccharides.

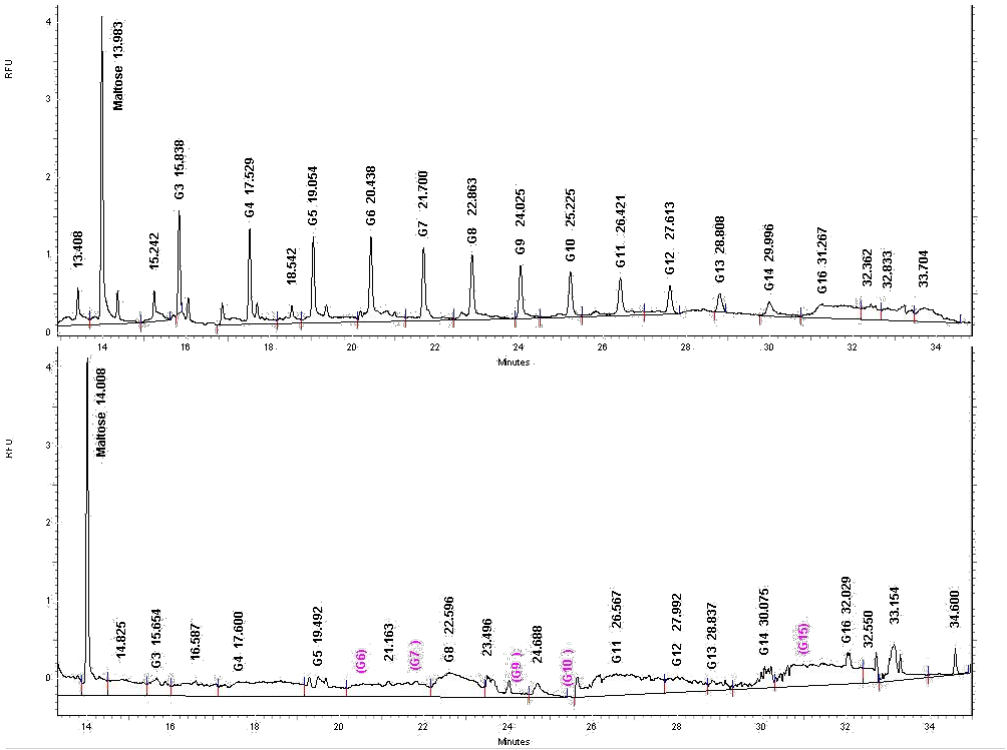

Figure 6.8: CE measurements of *S. scincus* skin lysate N-glycans. The upper image shows the Glc standard ladder measurement, and the lower image shows the sample measured after labelling at 37°C. The signal is extremely weak and is hardly distinguishable from the noise.

6.3.5 Mass spectroscopy

N-glycans

Figure 6.9 shows a Mass spectrogram of the N-glycan analysis. Each peak represents the signal of a molecule with specific mass. The mass increment between two peaks with the difference of 204 m/z (mass to charge ratio) would correspond to a molecular weight difference of one labelled hexose. The mass increments which comply with hexoses (H), like Glc or Man and hexosamines (N) like GlcNAc, are marked accordingly. An N-glycan core structure, which comprises of 2 hexosamines (GlcNAc) and 3 hexoses (Man) would using this simple nomenclature, starting with the terminal structure be described as H3N2. In contrast to the CE measurements, the MALDI-TOF analysis showed only high Man glycans. Double MS analysis showed 5 different high mannose structures, ranging from M5 (5 Man + 2 GlcNAc) with 1580 m/z to M9 with 2396 m/z. M5 and M9 showed the strongest signals (>25% of the base peak intensity), M6-M8 had slightly weaker, yet still significant signals (5-25% of the base peak intensity). The proposed (but not yet confirmed) structures can be observed in figure 6.10. In addition to the glycans, a polyhexose structure was observed. Since it contained no GlcNAc, it could not have been cleaved off a keratin by the PNGase F. It is not likely to be a part of the deglycosylised structures, however, its occurrence could be a sign of impurities in the sample. Whatever the case, the structure cannot be accurately classified at this point.

Considering the results from SDS-PAGE and western blotting, which indicate glycan peeling during the lysis/dialysis, it is possible that the smaller structures were a side product of larger glycans. In the western blot, the bands between 15 and 25kDa were clearly separated, which supports a potential loss of equally sized "chunks" one at a time, which are roughly the size of 1-2 kDa. A typical hexose (Glc, Man,...) has a molecular weight of 180Da, so the weight loss could only coincide with the position difference (of the keratin bands), if every keratin had multiple glycosylation sites. Staudt (2012) has found 4 potential glycosylation sites in a keratin gene fragment, of which all were however O-glycan and none was N-glycan specific. However, the complete gene was not analysed, and it is possible that multiple N-glycan sites are present as well. Potentially this could mean that all high mannose structures originate from one N-glycan which was peeled to different extent. In this scenario the original structure would definitely be the largest one, however, it is uncertain whether this would be the M9 or some even larger structure.

It is unclear whether the found glycans perfectly resemble those linked to keratins in their native form. It can, however, be concluded that high mannose N-glycans can be found in the keratin lysate, the largest being M9 and the smallest M5 with all intermediary structures, which may or may not be products of peeling.

O-glycans

MALDI-TOF analysis was also performed for O-linked glycans. Two signals could be observed in the spectrum (data not shown), which might represent known O-glycan-aldite structures - S1H1N1 with 895 m/z and S2H1N1 with 1256 m/z, however, due to the missing signals which should have also occurred in the presence of these structures, this is not conclusive. Even double MS analysis could not confirm the presence of O-glycans in the sample. It is possible that the observed signals were the consequence of some digested or peeled N-glycans. The Sia signals, however, remain mysterious, especially since they were observed in the CE analysis (and were even confirmed in previous studies by Saxe, 2010), but were missing in the MS analysis for N-glycans.

6.3.6 Raman spectroscopy

In addition to the biochemical analysis, Raman spectra of the sandfish epidermis were measured and analysed. As mentioned before, the sandfish, as well as the berber skink exhibit comb-like micro structures on the dorsal scales. The shading patterns observed in the Raman scans coincided with these structures and were probably the result of elevation and not different composition. When comparing the spectra of different positions, these are not distinguishable. Figure 6.11 shows the scan of a sample sandfish epidermis measurement. The average spectrum of a sample scale is shown in figure 6.12. Figure 6.13 shows a sample scan of the berber skink's epidermis. Its average spectrum is shown in figure 6.14. The average spectrum of the dorsal scale for the sandfish as well as the berber skink, had a high overlap, both showing typical keratin peaks (Paquin & Colomban, 2007). All measured vibrations and the corresponding bonds for the sandfish are

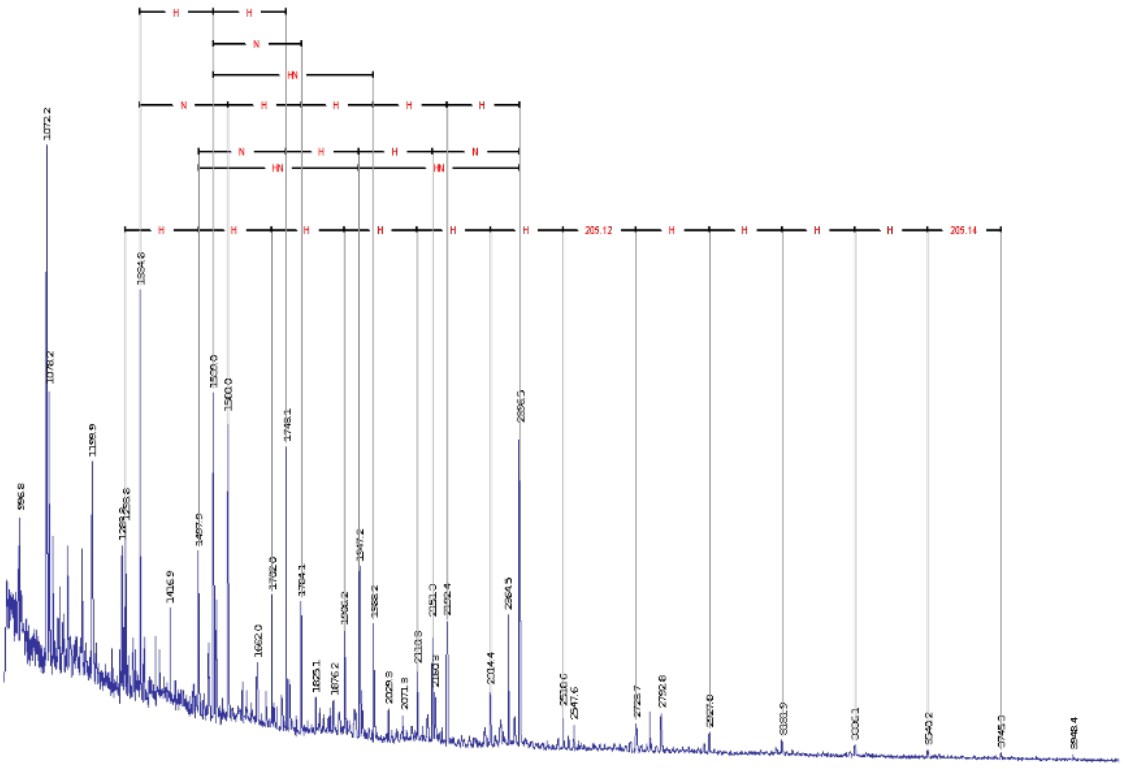

Figure 6.9: *S. scincus* skin lysate N-glycan MALDI-TOF. Mass increments which accord to hexoses (204 m/z) are marked with H, those related to hexosamines (280 m/z) with N.

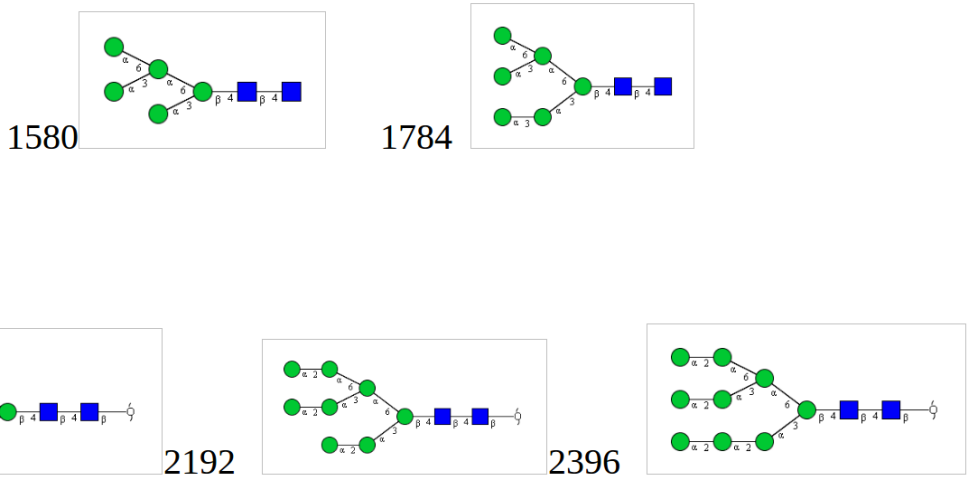

Figure 6.10: Proposed N-glycan structures for *S.scincus*. Based on the measurements and known data, the shown structures were proposed by prof. Hanisch, at the University of Cologne.

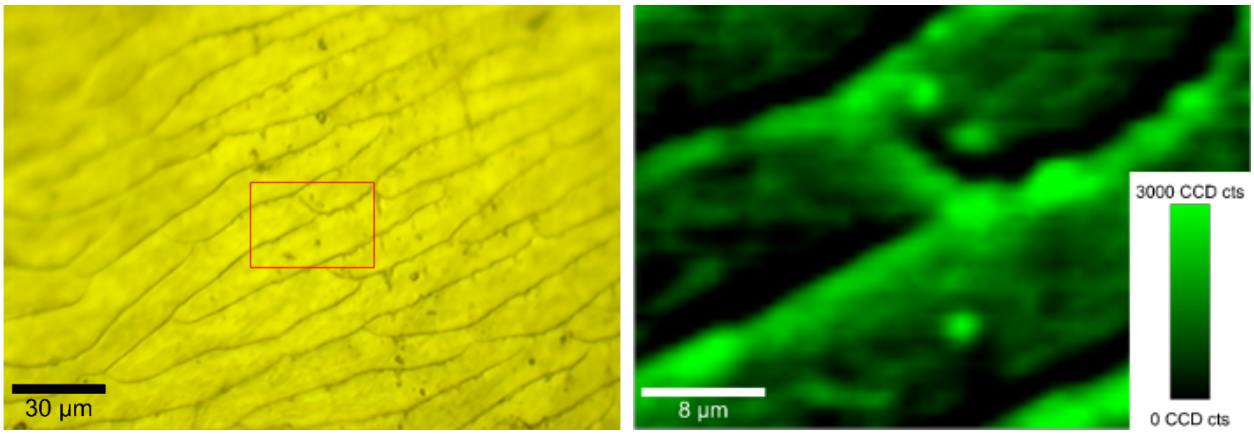

(a) slika (b) graf

Figure 6.11: An overview of a*Scincus scincus* dorsal scale captured with a light microscope (a) and in detail, scanned with a Raman spectrometer (b). The comb structures of the dorsal scale create an intensity artefact, however the surface is chemically homogeneous.

listed in table 6.2.

In contrast to the spectra themselves, the behaviour of the sandfish and berber skink scale samples was not entirely equal during the measurement. The sandfish skin could withstand scanning with the preadjusted settings without suffering observable damage to the surface. In contrast, the berber skink scales were scorched under the same settings, therefore the laser intensity had to be reduced. Pigment cells (or chromatophores) of reptilian skin are found in the dermis (Cooper & Greenberg, 1992). Except for the dark dorsal stripes, which also show coloured edges in the epidermal layers of the scales, the sandfish exuviae show no coloration. In a side by side comparison, the berber skink scales seem slightly darker to the naked eye. It is therefore possible that these scales absorb more light and are more susceptible to damage.

Isolated keratins showed a complete overlap in the Raman spectrum when compared to the epidermis. This was expected, since the outer epidermal layer - the oberhäutchen mostly consists of keratins. The isolated glycan spectrum also showed many peaks of the typical epidermis or keratin spectrum, although some were missing. This includes the olifinic C-C and the amidic C-O bonds between 1600 and 1700 cm^{-1} and at 3062 cm^{-1} and all the peaks associated with sulphur. It is noteworthy though, that many of these are found between 400 and 800 cm^{-1} - also a region with a strong silicon signal, which was due to the wafer present in the glycan sample. The glycan spectrum is shown in figure 6.15.

A polished cross section of a sandfish scale was also analysed in the Raman spectrometer. Figure 6.16 shows the sample in overview under a light microscope (a) and its average spectra in 0° and 90° (b). In (a) the material seems fairly homogeneous as expected, since the sample was not stained as in the experiments performed before (polychromatic staining, TEM analysis). The average spectra in (b) do not have a full overlap, however, all of the spectral peaks are in the same position. Both spectra are in agreement with the basic spectrum measured on the scale surface, further suggesting that the material is chemically homogeneous.

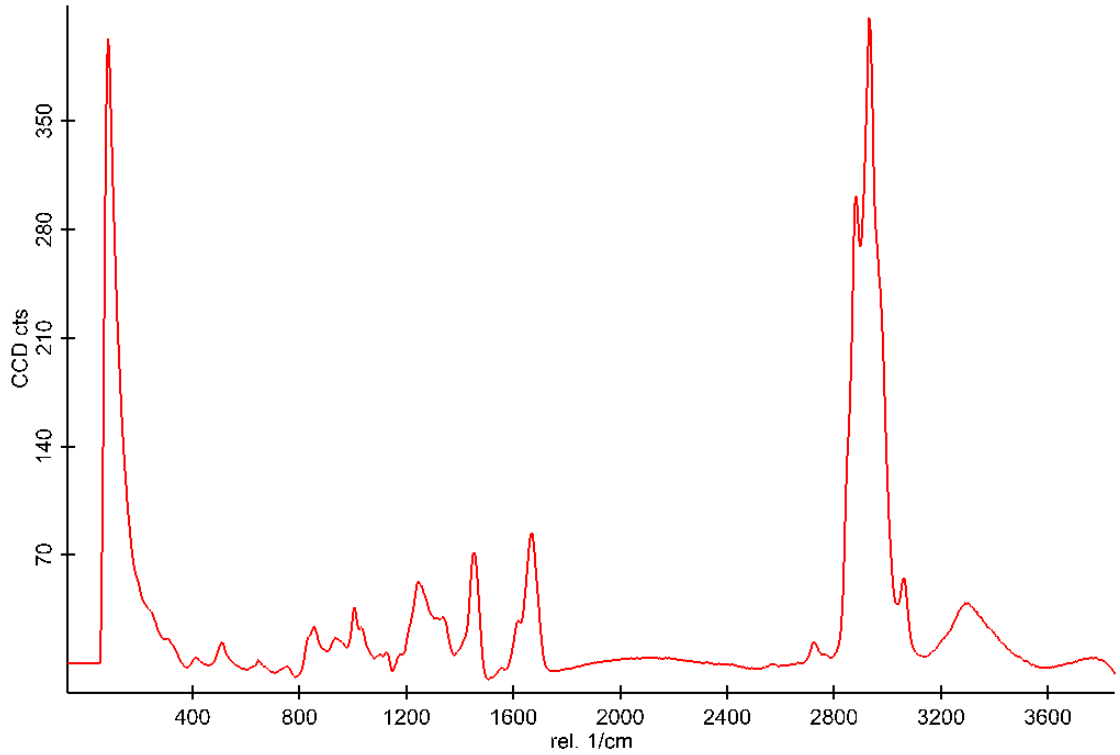

Figure 6.12: An average Raman spectrum of a *S. scincus* dorsal scale as observed in Figure 6.11. The material specific spectrum begins at 400 cm^{-1}. The observed spectral peaks coincide with those typical for keratins. Most peaks represent carbon, which bonds mostly with hydrogen, but also with nitrogen, oxygen and sulphur. The N-H bond has its typical peak above 3200 cm^{-1}. Typical for β-keratins, disulphide bonds oscillate at approximately 510 cm^{-1}.

As seen in the TEM analysed samples, the epidermis has distinct regions in the tissue structure, however, there is no significant deviation on a purely chemical level. Therefore detailed polar measurements were conducted for vibrational energies of the C-H and the C-O bonds. The results are shown in figure 6.17. The upper images (a,b) show the measurements for the C-H bond (green), while the lower two images (c,d) show the measurements of the C-O bond (cyan). The images on the left (a,c) represent the results of 0° polarity and the images on the right (b,d) the results of the 90° polarity measurements. Despite the noise present in all of the measurements, no outstanding features between the bond or polarity specific results could be identified. Same as in the TEM analysis no differences between layers was observed, concerning keratin composition, endorsing the hypothesis of a homogeneous composite of both α- and β- keratins.

The brightness of a pixel in each polarity image equals the intensity of the Raman scattering in this position. Figure 6.18 shows the average intensity over the cross section in the samples measured for the C-H bond in 0° (a) and 90° (b) polarity. The curves show a fine overlap. A small indentation in the curve can be observed in the 90° (blue) polar measurement in-between 9 and 11μm, however, it does not indicate any specific structure.

In conclusion, the biochemical composition of the sandfish was analysed, with the focus on the keratins and the glycans. For the analysis, the epidermis was partially dissolved in a

WN $[cm^{-1}]$	assignments	WN $[cm^{-1}]$	assignments
418	δ (CCC)	1179	ν (CC)
513	ν (SS)	1212	ν (CC)
624	ν (CS)	1248	δ (CH_2), ν (CN)
647	ν (CS)	1319	δ (CH_2)
753	ρ (CH_2)	1345	δ (CH_2)
831	δ (CCH) aliphatic	1419	δ (CH_3)
856	δ (CCH) aromatic	1453	ν (CH_2)
902	ρ (CH_2)	1554	δ (NH), ν (CN)
936	ρ (CCH_3), ν (CC) α helix	1619	ν (CC) olifinic
961	ρ (CH_3), δ (CC) α helix	1669	ν (CO) amide β sheet
1005	ν (CC) aromatic	2563	ν (SH)
1034	ν (CC)	2725	ν (CH) aliphatic
1064	ν (CC)	2882	ν (CH_2) asymmetric
1105	ν (CC)	2933	ν (CH_3) asymmetric
1130	ν (CC)	3062	ν (CH) olifinic
1158	ν (CC), δ (OH)	3294	ν (NH)

Table 6.2: A table showing the peaks measured in the Raman spectrum and the corresponding vibrations for *S. scincus* scales.

buffer with high osmolarity and pH. Peeling of glycans is common in a such milieu, if it is not suppressed by a reducing agent (Patel & Parekh, 1994). The protocol used for keratin lysis was designed to be mild and non-destructive (Alibardi et al., 2006), however, some peeling might have nonetheless taken place. Only the presence of high mannose structures could be confirmed to this point, although the experiments (and previous studies) also hint towards the presence of other structures, possibly complex or hybrid structures containing sialic acids. The confirmed structures were high mannose glycans, ranging from M5 to M9, whereas the shorter structures could also be the result of peeling and not be present in the native keratins.

Despite being hydrophilic structures, the glycans seemingly reduce the solubility of the keratins in watery media. The lysate sample in the western blot had 3 clear bands more than the dialysate in the β keratin region, which could explain the correlation between decreased solubility of glycosylized keratins as well as the peeling of larger high mannose glycans. If peeling does occur, it could also explain the difference between the results of CE and MS analysis. Due to the differences in the sample preparation, the results may vary substantially, especially considering the delicacy of the structures. The basic Raman spectra showed no observable differences between the sandfish and the less glycosylated berber skink's skin, which is not very surprising. The two species are genetically close, and all intermolecular bonds found in the glycans are also present in keratins and would mask the glycan spectrum if they were present. It is, however, strange that the samples with such similarity in keratin composition behave differently during the measurement.

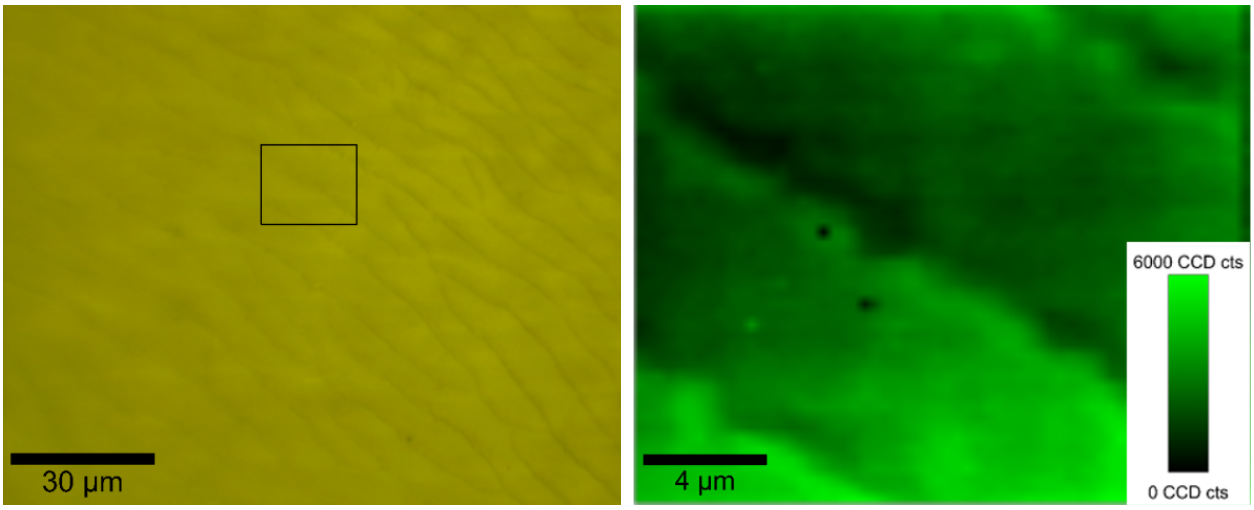

(a) slika (b) graf

Figure 6.13: An *E. schneiderii* dorsal scale in overview captured with a light microscope (a) and detail, scanned with a Raman spectroscope (b). The intensity of the laser needed to be decreased for the *E. schneiderii* sample, not to burn the surface. The typical dorsal comb structures can be observed, the surface is however chemically homogeneous.

The berber skink's skin was much more sensitive towards the Raman laser and had to be measured at a lower intensity. As discussed above, this is likely the result of somewhat darker coloration. However, one cannot exclude the possibility, that some of the light is absorbed by the glycans, which could increase the stability of the skin. Raman spectroscopy measurements, which were performed in scale cross section, have shown a perfectly homogeneous material without special layers such as the separate α and β keratin layers, which are typically found in the epidermis of lizards (Vitt & Caldwell, 2014). Although unusual, it confirms the TEM analysis and might even be an adaptation for improved skin mechanics.

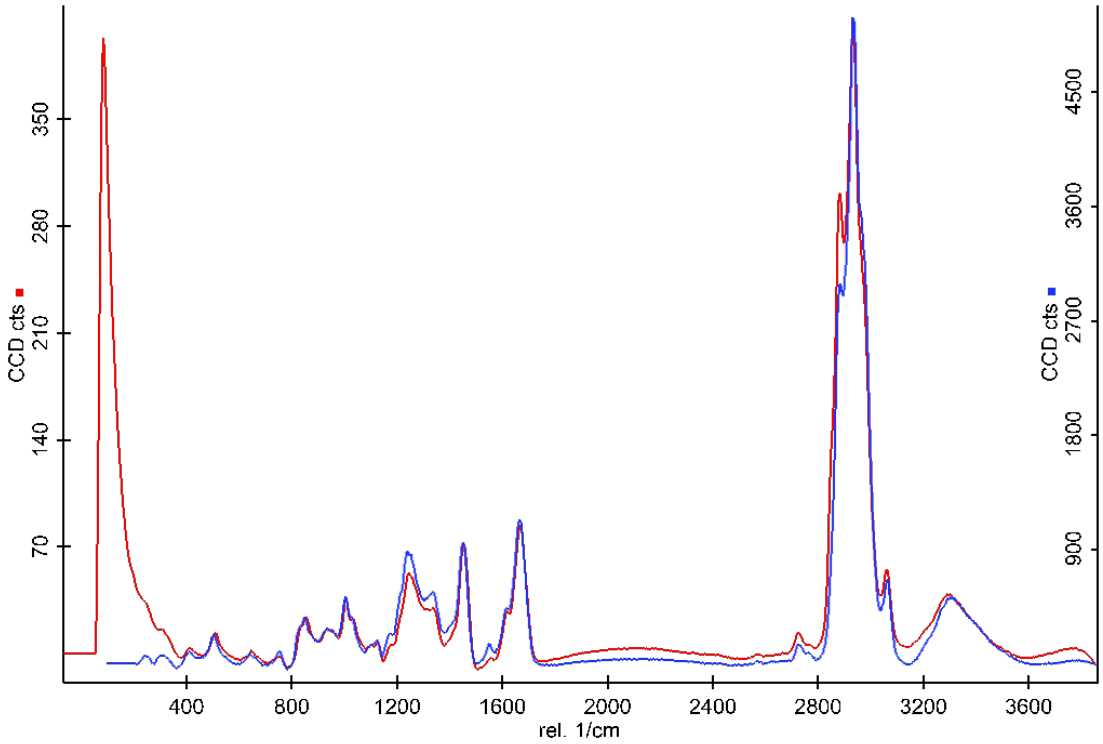

Figure 6.14: *Eumeces schneiderii* average Raman spectrum compared to that of *S. scincus*. Although there is a clear difference in intensity gain between the sandfish (red, left y axis) and the berber skink (blue, right y axis), the vibrations show a full overlap considering peak positions. Except for some C-H corresponding peaks between 1179-1453cm^{-1} and the peak at 2882cm^{-1}, which slightly deviate in relative y position, the spectra undoubtedly show the same basic chemical composition.

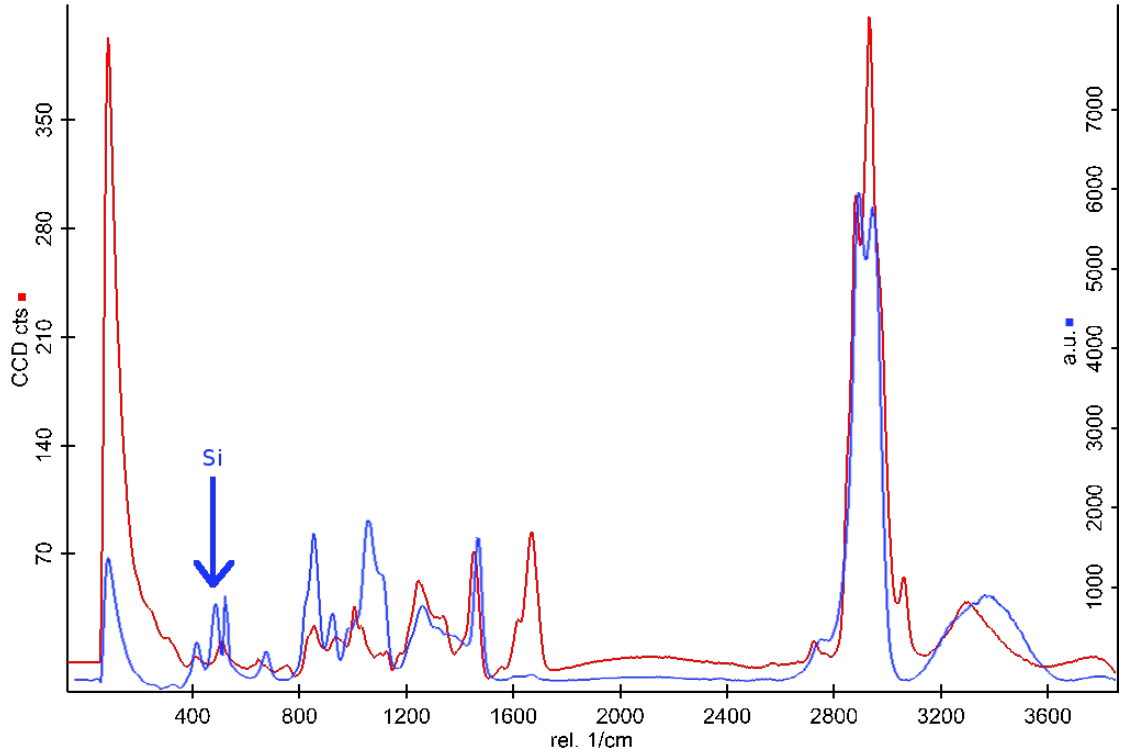

Figure 6.15: *Scincus scincus* glycans (blue, right y axis) compared to the basic spectrum (red, left y axis). The region between 400 and 600 cm^{-1}, also marked with a blue arrow showed a strong silicon signal. This has been removed by calculation, some unidentifiable peaks have however remained. Many peaks observed at the basic sandfish keratin spectrum are still present, all of which correspond to either C-C, C-H, C-N or N-H bonds, all of which would be expected in typical glycan structures. The relative y positions differ substantially more, than we saw in the *S. scincus* -*E. schneiderii* comparison. The reason for that may be the fact, that vibrations of some bonds overlap with vibrations of other bonds, making up a different cumulative peak.

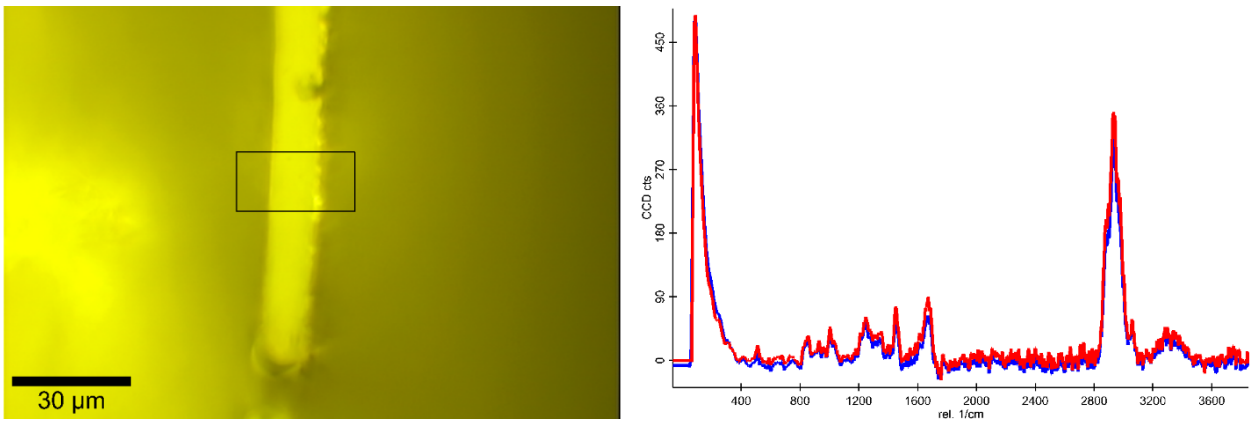

(a) (b)

Figure 6.16: The cross section of a *S. scincus* dorsal scale was analysed. An overview of the cut and polished scale can be seen in (a). (b) shows the average Raman spectrum of two polar measurements, one in 0 ° (red) and one in 90 ° (blue).

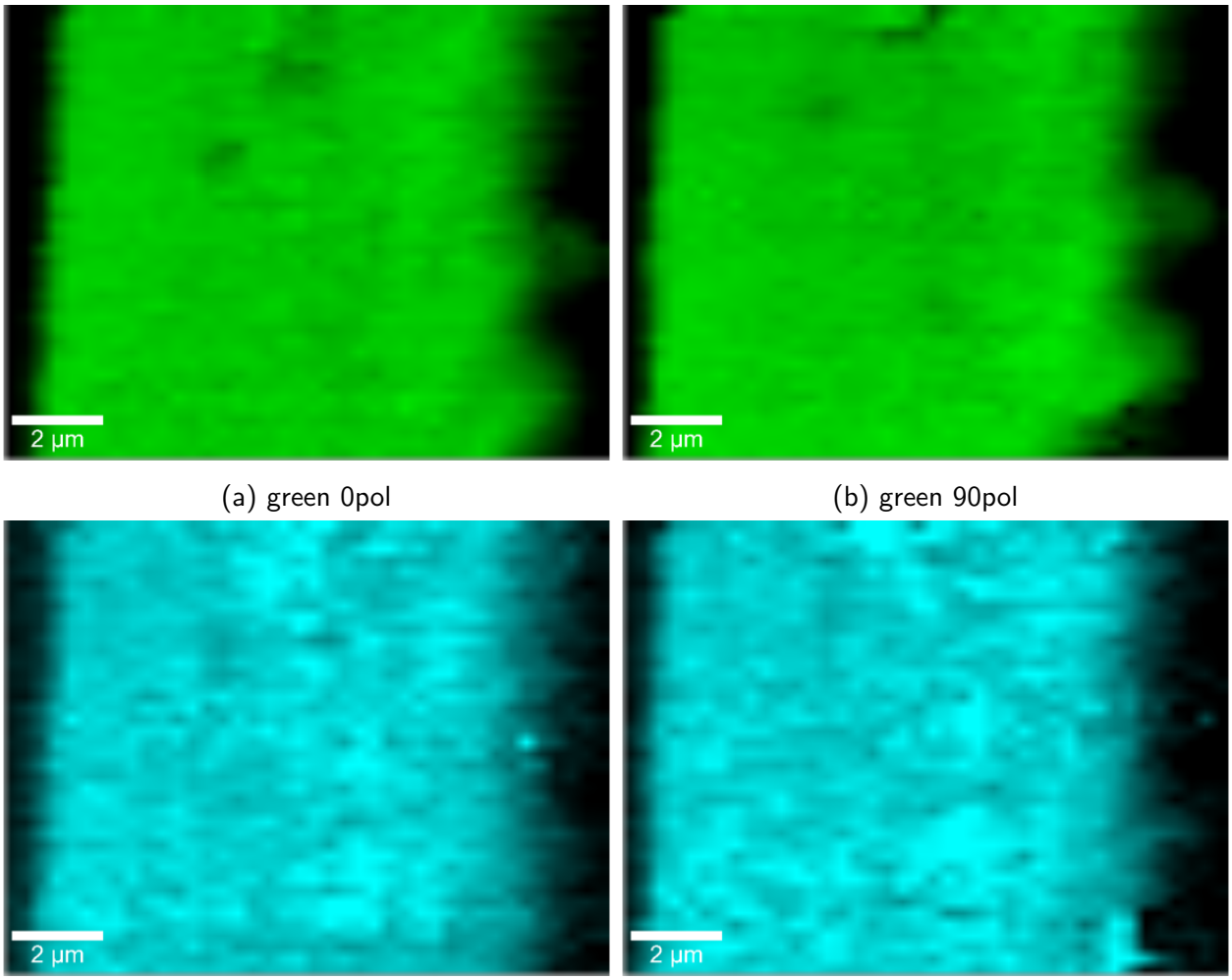

(a) green 0pol (b) green 90pol

(c) cyan 0pol (d) cyan 90pol

Figure 6.17: *S. scincus* dorsal scale in cross section scanned with Raman. Vibrations of two different bonds are shown. The C-H bond (green) and the C-O bond (cyan). Also two different polar measurements were done for these vibrations, 0° (a,c) and 90° (b,d).

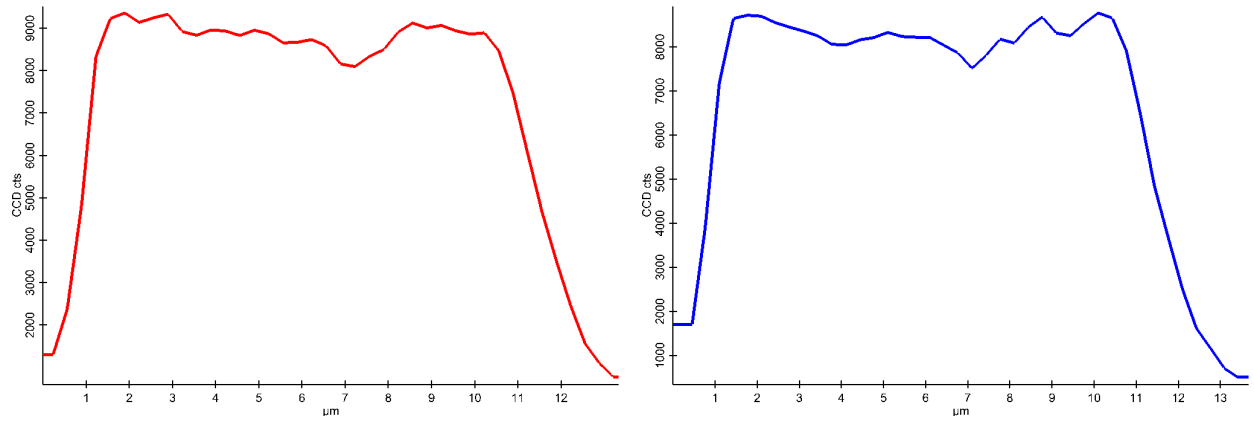

(a) (b)

Figure 6.18: A Raman intensity scan for a *S. scincus* dorsal scale in cross section is shown. Polar measurements for the C-H vibration were conducted in 0 ° (red) and 90 ° (blue).

Chapter 7 - Understanding and replication of the adhesion/friction reduction

7.1 Introduction

Bionics (also biomimetics) is an interdisciplinary field of research, bringing together biologists, engineers and other scientists. Its aim is not only the investigation of biological phenomena and the abstraction of the underlying principles, but also the conception of potential applications in new technologies. In this regard, despite that much fundamental research was performed, application development was ultimately the aim of this work. Also many experiments in the process of prototyping were used for proving the created hypotheses and the underlying principles. Up to this point structural, compositional, mechanical and superficial analysis was conducted, providing many data. Further evaluation and interpretation is now required to form a combined theory which explains as much of the data as possible.

Mechanical properties are very important in understanding abrasion resistance of a material. For this reason, tensile testing and nanoindentation, which show the deformation behaviour of a material were performed. Additional knowledge can still be acquired, to round up the data and facilitate a complete interpretation of sandfish skin mechanics, nevertheless, the gathered results can already be used to some extent. For future applications, it would be useful if a synthetic material with the same mechanical properties was constructed. Meanwhile, existing synthetic polymers, such as thermoplastics or elastomers with similar properties in respect to mechanics can be used for early prototypes. The problem existing polymers have, even if these have the exact same hardness and elasticity as the sandfish skin, is that most of them would also exhibit a high adhesion to sand. This would increase friction and drag, and consequently the abrasion by sandblasting, making the material utterly useless for the same function, realized by the sandfish skin. That is, unless the surface of these materials could be modified in a manner so that they would no longer "stick".

If previous research is correct, such modification may just be possible by coating a sample synthetic material with glycans, isolated from the sandfish epidermis. Previous studies show that if glycans were linked to a glass surface, the adhesion and friction angle for sand were significantly reduced compared to the control sample (Baumgartner et al., 2007; Staudt, 2012). As shown in chapter 6, N-glycans were found linked on the keratins in the exuviae of *S. scincus* and the

scaffolds of 5 structures were proposed. Since the animals only shed their skin every 3 months on average (Hartmann, 1989), the sandfish exuviae are a scarce source material to use for bulk modification of material. The isolation of larger glycan amounts is not sufficiently efficient, and the same is true for in vitro synthesis. However, the proposed high mannose structures are relatively simple, and may also be found in other sources.

In this chapter, the collection of sandfish-like N-glycans will be discussed, in addition to surface modification of synthetic polymers. M5 - M9 glycans may not necessarily be the native structures found in the sandfish epidermis, however, they are the closest known up to date. Therefore organisms with M5 - M9 glycans were searched for in the UniCarb databank (`http://unicarb-db.biomedicine.gu.se/`) and 3 alternative sources were chosen for analysis and the acquisition of glycans: baker's yeast (*saccharomyces cerevisiae*), leaves of the mistletoe (*Viscum album*) and sweet almond seeds (*Prunus dulcis*). For surface modification, Poly(methyl methacrylate) - PMMA, or plexiglass was chosen and its acrylic group targeted as the linking site. Additional tests were also performed on other acrylic surfaces and glass.

7.2 Methods

7.2.1 Glycan extraction from alternative sources

Baker's yeast

If the extraction of appropriate glycans was successful, yeast would make an excellent alternative for a glycan source since it can be cultivated in a fermenter. This would enable a year-round production on site, independent of external factors, like the weather or the market. Yeast contains all the structures proposed in the MS analysis: M5 - M9, in addition to many others (UniCarb DB). Similar to plants, yeast has a cell wall which is very stable, the protein extraction therefore requires harsh conditions in which the cell wall is "cracked".

The protocol developed by Printen & Sprague (1994) was used for this purpose. Fresh baker's yeast was acquired at the local market and 0.5g of it was added to 500μl of cracking solution [1], together with 0.1ml of glass beads with a radius of 500μm, 10μl mercaptoethanol and 50μl 50mM PMSF. The mix underwent incubation at 70°C for 10min, followed by vigorous vortexing for 1 min. At the end, the sample was centrifugated at 12300g for 5min and the supernatant containing the proteins was extracted.

The solution was transferred to ice-cold ethanol in a relation 1:4 (sample:ethanol) and incubated for 20min at 0°C while gently stirred. This was followed by centrifugation at 12300g for 5min. The solution was removed and the pellet containing the proteins was washed with 80% ethanol and vortexed again. The washing procedure was repeated twice. The pellet was resuspended with 200μl dH_2O, and 40μl of the solution were used for protein analysis by means

[1] 48g Urea, 5g SDS, 4ml of 1M Tris/HCl (pH 6.8), 20μl of 0.5M EDTA, 40mg bromphenol blue, ad 100ml dH_2O

of the Bradford test and lectin blotting (chapter 6). The rest was used for N-glycan extraction, which was performed as described for MS in chapter 6.

Mistletoe

Mistletoe is a wintergreen plant with thick and sappy leaves, making the extraction of proteins from them relatively fast and simple. Mistletoe contains different glycans from the high mannose family, but also complex and hybrid N-glycan structures and O-glycans (UniCarb DB). To facilitate extraction of glycoproteins, the cell walls had to be cracked, which can be (due to the large size of the structures) also done mechanically.

Fresh leaves were collected in the direct vicinity of JKU Linz in March 2014. The leaves were washed with detergent, under running tap water and thoroughly rinsed with dH_2O to remove any impurities on the surface. The clean leaves were cut into approximately 2x2mm pieces with a scalpel. 2g of chopped leaves were added to 4ml of dH_2O and the mixture was ground with a glass pestile for 5min. The mix was then vortexed for 1min and the solution containing the cytoplasma was collected.

The purification procedure was performed in the same way as for the baker's yeast, using ice cold ethanol and centrifugation. The extracted proteins and the glycosylation were analysed by means of the Bradford test and lectin blotting. Glycan extraction was performed as described above.

Sweet almonds

In addition to other structures (as mentioned for the organisms above), sweet almonds also contain high mannose glycans (Wilson et al., 2001). According to the Food and Agriculture Organization (FAOSTAT), in 2013 the world production of shelled almond seeds was about 2.9 million tonnes, which makes them a rich source of glycans.

The greatest advantage of sweet almonds used as an alternative glycan source, however, is that in addition to high mannose glycans, they also contain the enzyme PNGase A, which cleaves N-glycans (Takahashi, 1977). It only cleaves glycans from peptides (Roche Applied Science), and not from whole proteins, however, if the procedure is done correctly, this would eliminate the necessity to add extra deglycosylation enzymes such as PNGase F.

Whole almond cores were ground with a coffe grinder and 10g of the meal were added to a solution of 29ml dH_2O and 1ml 100% ethanol, containing PMSF with an 1mM end concentration. The sample was mixed for 4h at 4°C and the solution was transferred to a falcon and centrifugated at 112g for 10min. The centrifugation separated the sample into 3 phases, a precipitate of the remaining solid particles, a milky aqueous solution in the middle and a fat layer on top. The milky, presumably protein rich solution (also containing glycoproteins and PNGase A) was then transferred to a fresh container using a syringe and a long cannula and was filtered through a 0.4μl porous membrane. To preserve the PNGase as much as possible, no additional purification took place in this step. The samples were analysed by gel electrophoresis and lectin blotting.

Since PNGase A can only cleave glycans from small peptides, a sample was divided into two halves, one serving as the deglycosylation substrate (A), and the other as the deglycosylation source (B). The proteins in sample A were fragmented either by trypsin digestion, followed by trypsin inactivation at 60°C for 10min or β-elimination with NaOH (0.02M) for 10min, followed by neutralization with HCl.

7.2.2 Additional glycan purification

Mass spectroscopic analysis showed that the sandfish keratins contain high mannose glycans. Other structures may also be present, which is uncertain at this point. The materials used as alternative glycan sources also contain the wanted high mannose structures, however, in addition to all kinds of other structures. Sialic acids alone can due to their large diversity and many modifiable carbon atoms (Varki et al., 2009) complicate the analysis and influence the surface adhesion. To test the impact of different glycans, these were analysed separately. Firstly the uncharged glycans were tested, one category of which being high mannose glycans. Anion exchange resins can bind negatively charged carbohydrates, such as glycosaminoglycans, polyuronic acids, polysialic acids, or even charged neutral carbohydrates under alkaline conditions (Lee, 1990). To remove acidic and charged neutral glycans from the sample, a simple pipetting chromatography protocol was used: Pipette tips containing a strong anion exchange resin were used together with an automatic electronic pipette (Rainin) and the following protocol was performed:

1. Equilibration: 500μl dH_2O - slow pipetting 10x100μl
2. Capture: 100μl sample - slow pipetting 20x100μl (acidic sugars bind to the resin - the remaining fraction contains neutral and positive molecules, which we want to extract from the sample.)
3. Washing: 500μl dH_2O - slow pipetting 10x100μl
4. Elution: 100μl 0.1M NaCl - slow pipetting 20x100μl (acidic sugars are released)

7.2.3 Sample evaluation

Different samples, varying from isolated treated or untreated exuviae to various technical materials, partly modified with sandfish and other glycans, had to be evaluated for their interaction with the environment, especially sand. Many experiments could have been conducted for surface interaction evaluation, however, in this work, adhesion force measurements by means of AFM (atomic force microscopy) and friction angles with sand were performed. Two different atomic force microscopes were used throughout the studies (Thermo/Nanosurf), which resulted in a variation between the measured values. Therefore, only the measurements performed with the same device were compared to each other. The general procedure was the same for both devices: A contact mode cantilever (CONTR) with a silicon (Nanosurf) or silicon nitride (Thermo) tip was installed and the surface was scanned in static force mode. The topography and deflection were recorded and the surface image was evaluated during the procedure to ensure the settings

were reasonable. The approach and retraction curves of the deflection measurement were compared to each other and the adhesion peak distance was measured. Before technical surfaces were evaluated, a broader perspective on adhesion of the sandfish skin was needed. To gain this, sandfish exuviae were measured, treated with various solutions and enzymes:

- native sandfish skin, cleaned by air blowing
- native sandfish skin, washed 3x5min with dH_2O and dried at room temperature
- sandfish skin, treated with PNGase F in PBS, washed 3x5min with dH_2O and dried at room temperature
- sandfish skin, treated with O glycosidase in PBS, washed 3x5min with dH_2O and dried at room temperature
- sandfish skin, treated with sialidase, washed 3x5min with dH_2O and dried at room temperature
- native berber skink skin, cleaned by air blowing

In addition to adhesion force measurements by AFM, friction angles with sand were measured as described in previous studies (Rechenberg, 2004; Baumgartner et al., 2007; Saxe, 2008; Staudt, 2012). The procedure followed a simple protocol:

- A sample was secured on a see-saw with an integrated protractor for angle measurement.
- Through a plastic pipette, sand was gradually applied to the surface of the sample from a few mm above.
- The see-saw inclination was increased until all the sand has slipped and then slowly reduced until the sand began to stick to the sample. The angle of inclination at this point was measured and recorded.
- The measurement was repeated 10 times per sample, then the average and standard deviation were calculated.

7.2.4 Surface modification of glass

Already used in former analysis, glass was selected as one of the testing materials for modification, which would facilitate better data comparison with old results. Also the chemistry and mechanics of glass are known very well today.

Silanization

Silanization is the modification process of surfaces by the use of silanes - silicon molecules with three reactive alkoxy groups (react with -OH groups of a surface) and a functional group which determines new surface properties (Seed, 2001). Over the years, many protocols were developed

for the silanization of glass and metal oxides, using silane solutions in organic solvents. For this work, the procedure described by Karrasch et al. (1993) was adopted, using acetone.

Glass cover slips determined for modification were firstly washed in acetone 3 times for 5min and dried in air at RT. For the silanization, (3-aminopropyl)-triethoxysilane or APTES was used. The slides were incubated in a 2% APTES solution in acetone for 3 min at room temperature while gently stirred. The slides were washed with dH_2O 2x5min and dried at room temperature. If the silanization process was successful, the cover slips were slightly less hydrophilic than before and tended to swim on the water surface.

Glycan bonding

The silanization was used as the first part of the modification, the silanes thereby being used as linkers. The primary amine serving as APTES' functional group can be linked to a ketone found in a GlcNAc molecule through a reductive amination reaction (Abdel-Magid, 1996; de Boer et al., 2007; Song et al., 2009).

Sandfish glycans were extracted from 5mg of skin substrate as described before and suspended in 30μl of dH_2O. Silanized cover slips were placed on a heating plate with 60°C and a well on its edges was created, using dental silicone (President light body). The glycan sample was applied to the well along with 280μl dimethyl sulfoxide (DMSO), 120μl glacial acetic acid and 200μl sodium cyanborohydride ($NaBH_3CN$) and incubated for 2-3h during which the complete incubation buffer evaporated. Caution is advised during the procedure since a side product of the reaction is HCN (hydrogen cyanide or prussic acid). After the incubation, the glycan-modified slips were allowed to cool to room temperature. Afterwards, they were washed for 5min in PBS and 5 times for 5min in dH_2O. The samples were dried at room temperature and stored for further analysis. The modified glass surface was evaluated by measuring friction angles and the adhesion force by the use of AFM. Typically, 15 measurements were conducted for every sample. Compared to native or solely silanized glass, the glycan modified surfaces showed reduced friction and adhesion, which confirmed the results of Staudt et al. (2012).

Since the glycans seem to make a difference in adhesion on a modified surface, one question which needed answering was the correlation between the adhesion and the glycan density on mentioned surface. Therefore a larger sample of sandfish N-glycans was extracted from 20mg of clean, dry exuviae and resuspended in 30μl of dH_2O. A series of steps (0.25μl glycan sample per step) was covalently linked to a silanized glass surface with an area of $\sim$ 20mm^2. The samples were washed, dried and the adhesion was measured with an AFM.

7.2.5 Surface modification of PMMA

Polymethyl methacrylate (PMMA), acrylic glass or plexiglass is a very versatile material. It is strong but very lightweight (Brydson, 1999) and is being used in a wide variety of applications, extending from lighting, medical technologies and other uses (Kutz & Myer, 2002; Meyers, 1995). Due to its acrylic group, it shares some chemical properties with other materials, such as acrylic

varnishes or elastomers. It is thus a reasonable candidate for modification.

Amino-linking

Brown et al. (2006) reported that a free primary amine group can be attached to PMMA, by soaking it in a 1M solution of ethylene diamine (also ethane-1,2-diamine, with the formula $H_2N(CH_2)_2NH_2$, see figure 7.1) in DMSO for 20 min at room temperature. The organic solvent attacks the ester group of the acrylic, allowing the substitution of the amine nitrogen with the ester oxygen. A similar protocol for linking an amine to PMMA was also reported by Fixe et al. (2004). The procedure uses another amine-linker, namely hexamethylene diamine (also 1,6-diaminohexane with the formula $H_2N(CH_2)_6NH_2$, see figure 7.1), which reacts with the ester group in a solution of boric acid at high pH values. The acrylic is soaked into a 10% hexamethylene diamine solution of 100mM $B(OH)_3$/NaOH with a pH value of 11.5 and is incubated ON at 37°C. Both protocols were used in the preliminary experiments. Alternatively, a novel protocol was tested, using input from both of these studies. According to GHS (Globally Harmonized System of Classification and Labelling of Chemicals), ethylenediamine is highly toxic, reactive and hygroscopic. It requires careful handling and storage in a dry N_2 atmosphere. DMSO is a strong organic solvent and can attack thermoplastic surfaces, making them no longer smooth and transparent. Since the principle of amine linking seemed fairly simple, a novel protocol was developed using the solid and less toxic hexamethylene diamine as the amine-linker and the less aggressive 2-propanol (also isopropanol) as the organic solvent. A PMMA foil was cut into 3 by 4cm pieces, which were soaked in one of the following solutions and incubated accordingly:

- A) 10% hexamethylene diamine ($H_2N(CH_2)_6NH_2$) solution in 100 mM $B(OH)_3$/NaOH pH 11.5, incubated ON at 37°C
- B) 10% ethylene diamine ($H_2N(CH_2)_2NH_2$) solution in DMSO, incubated for 20min at room temperature
- C) 10% hexamethylene diamine in 2-propanol, incubated for 20min at room temperature

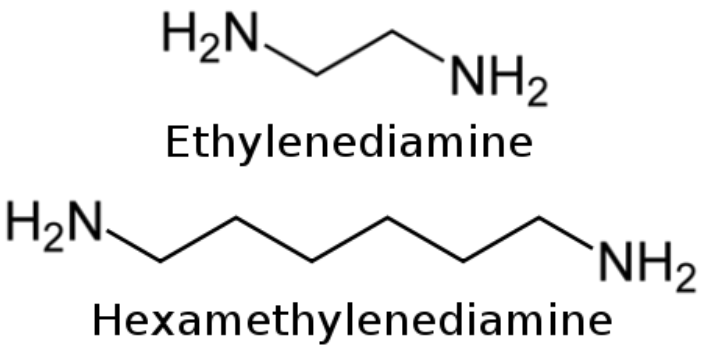

Figure 7.1: Structural formulas of ethylene diamine (ethane-1,2-diamine) and hexamethylene diamine (1,6-diaminohexane).

After incubation, the PMMA slides were washed with dH_2O 3x5min and dried in air at room temperature. Before proceeding the amine linking needed to be evaluated, which proved rather difficult. If it were successful, the amines would form a monolayer, which would require a very sensitive method to detect it. EDX (Energy-dispersive X-ray spectroscopy) analysis might have been suitable, however, the plexi glass could not sustain the electron beam. Raman spectroscopy is also a suitable method for surface analysis, but has also proved unsuccessful. The reason for that being either an unsuccessful modification or insufficient sensitivity. A difference between treated and untreated surfaces could be determined by measuring the contact angles. The advantage of this method is that it depends strongly on surface chemistry and is very sensitive, however, it does not provide detailed information about the chemistry itself. Because all other methods were unsuccessful, contact angles with dH_2O were measured and, as shown in Figure 7.2, changes could be observed.

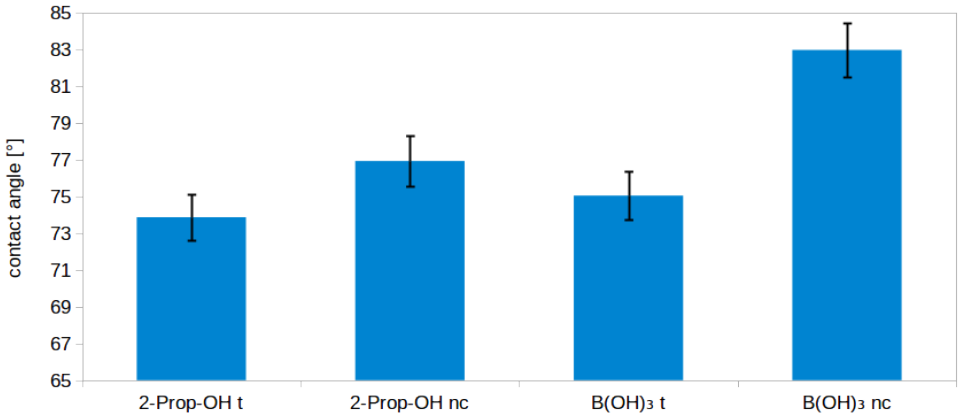

Figure 7.2: Contact angle measurement for amine modification of PMMA with hexamethylene diamine. Four samples are shown in this preliminary experiment: 2-Prop-OH (incubated as in protocol C - 2-propanol for 20min at room temperature) test (t) and negative control (nc) and $B(OH)_3$ (incubated as in protocol A - boric acid at pH 11.5 ON at 37°C), also test (t) and negative control (nc). Hydrophobicity increased after both procedures. The contact angle difference between test and negative control is significant in both samples, $p < 0.05$.

Methods A and B have been verified before, yet it would be rather interesting to investigate the performance of the newly developed method C. If the amination proved successful, the contact angle should change slightly when compared to untreated PMMA. The sheets treated with ethylene diamine, dissolved in DMSO (B), have become rough and milky, which made the surfaces very hydrophobic while they remained dry, but retained the water well once they were wet. While this procedure might have accomplished the linking of a primary amine to the PMMA surface, it had drastically changed its properties, making other methods preferable. Samples A (hexamethylene diamine, borate buffer) and C (hexamethylene diamine, 2-propanol) both showed a significant ($p < 0.05$) change in contact angle between the test (t) and the negative control (nc), suggesting that the amine-linking was successful. The difference in contact angle was thereby larger for sample A, which can be explained by either better linking and/or change of micro

structure. AFM analysis of the PMMA test sheets has shown that while untreated, they exhibit a micro structure of 0.3μm wide and 25nm high cylinders. When treated with borate buffer, the micro cylinders remain intact, however, if treated with 2-propanol for 20min, their edges are smoothed and their height reduced to approximately half, see figure 7.3. Micro structure has a strong impact on contact angle, amplifying the effect of the substrates interaction with a liquid (Jung & Bhushan, 2006). If modified surfaces were to be tested for friction angles in later experiments, smoother samples would be more appropriate for comparison with other technical surfaces. For this reason, method C (hexamethylene diamine, 2-propanol) was used for further procedures.

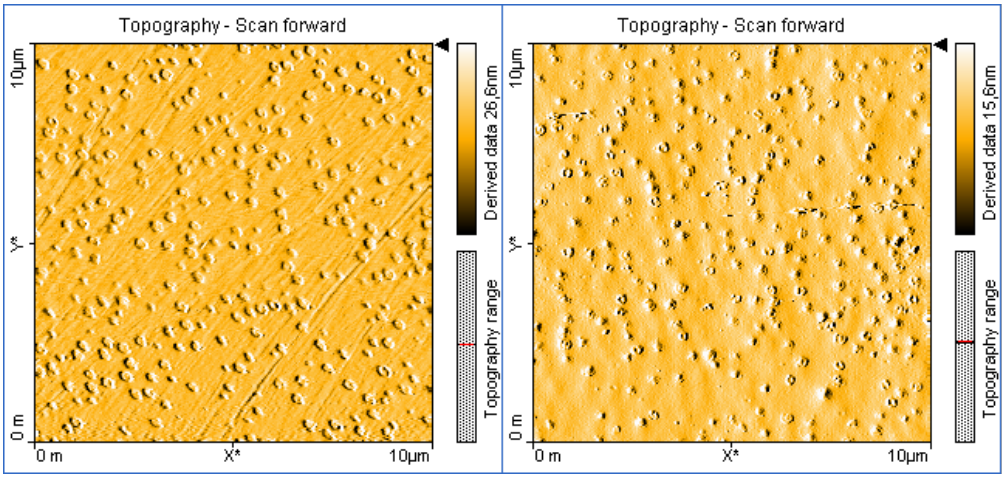

Figure 7.3: PMMA sheet topography comparison. The surface of untreated (left) and 2-propanol (right) soaked PMMA sheets was evaluated using AFM. 2-propanol has a mild etching effect on the material, smoothing the micro structure.

Glycan bonding

The final step in the modification of PMMA was to link the carbohydrates to the prepared surface. Reductive amination is the reaction forming covalent bonds between aldehydes and amines and is typically used for linking glycans to glass surfaces with a free primary amine (Abdel-Magid, 1996). The reaction usually takes place in a waterless solvent (DMSO) with the catalyst sodium cyanborohydride ($NaBH_3CN$), which is activated by acetic acid (de Boer et al., 2007; Song et al., 2009). DMSO has been shown to attack PMMA, therefore this reaction solution may damage the surface. For this reason, alternative reactions were devised, in which DMSO was exchanged for another waterless solvent, but other procedures were also tested. In 1997, Bulmuș et al. were working on the modification of PMMA by the use of borate buffer at high pH values. They found that in the same environment, later used by Fixe et al., reductive amination can take place between primary amines and aldehyde groups. For the preliminary experiments, three reaction solutions were prepared:

- A) 5μl glacial acetic acid + 45μl DMSO + 50μl $NABH_3CN$

- B) 5μl glacial acetic acid + 45μl Ethyleneglycol + 50μl $NABH_3CN$
- C) 100μl 100 mM $B(OH)_3$/NaOH pH 11.5

As in the labelling process for capillary electrophoresis, maltose was used as the aldehyde containing carbohydrate sample. For every protocol, 2 samples were created. A test sample contained 10μl 100mM maltose, and the control sample none. Two variations of incubation were tested for all samples, one at 60°C for 1h, and another at 37°C overnight. Afterwards, the samples were washed with dH_2O three times for 5 min and dried in air at room temperature. The presence of carbohydrates was tested in two different ways. A lectin fluorescence protocol was used, as described in lectin blotting (chapter 6), and contact angles with dH_2O were measured and compared. The lectin fluorescence protocol did not yield useful results, because the surface was damaged during the analysis, probably due to the peroxide in the the ECL buffer. Moreover, Concanavalin A adhered very well to the plastic surface and thereby dramatically increased the background noise, even though the surface was blocked beforehand with PBS tween. For the above listed reasons, lectin blotting seems as an inappropriate method for glycan determination on acrylic surfaces. On the other hand, contact angle measurement did show differences between samples, which were treated or untreated with maltose. The results of the contact angle measurement are shown in figure 7.4. Because of the many hydroxylic groups found in carbohydrates, maltose has very polar properties, and should therefore reduce the contact angle for water on the PMMA surface. When compared side by side, the results for procedure C, performed at 37°C, showed the greatest difference between its two samples. Therefore, this procedure was selected for further work.

While after repeated washing and drying no optical differences could be observed between the samples in procedure C, the difference in contact angle remained permanent. The contact angle alone is, however, not sufficient to determine the detailed change in surface constitution. Therefore it cannot be concluded whether maltose was indeed covalently bound to the surface or not.

Nevertheless, we propose a mechanism for PMMA modification with glycans, based on the work of Brown et al. (2006), Fixe et al. (2004) and Bulmuș et al. (1997), which is shown in figure 7.5. First, the amino linker hexamethylene diamine is attached to the acrylic surface by attacking the methoxy group, creating a free primary amine on the surface. In the second step, a glycan is linked to the amine through a reductive amination reaction. For this to work, the first GlcNAc has to undergo a ring-opening, thus creating a free aldehyde group, which can react with the free primary amine on the acrylic surface. The acrylate group, which is the target of the modification on PMMA, can also be found in other materials, like acrylic lacquers, elastomers and rubbers. If the method is confirmed, these should therefore also be modifiable by using the same protocol.

After seemingly successful plexiglass coating, glycans were purified from different sources and used for the modification of PMMA. In addition to sandfish glycans, the plexiglass sheets were also treated with *Viscum album* and *Prunus dulcis* glycans. For every source material, N-glycans were extracted and partially separated into neutral and acidic glycans, using anion exchange

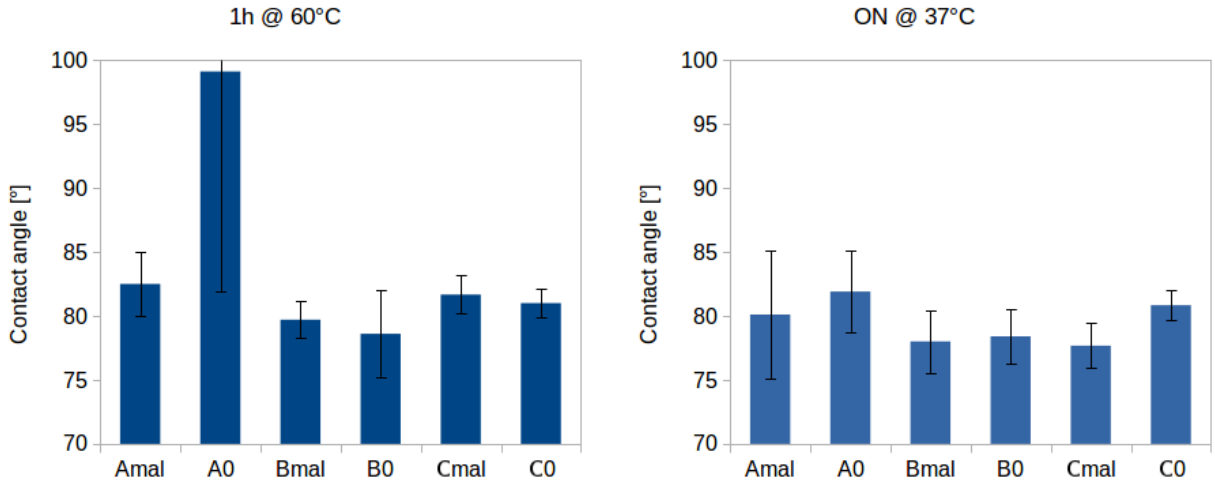

(a) (b)

Figure 7.4: PMMA modification. The modification protocols A (DMSO, Acetic acid, $NABH_3CN$), B (Ethyleneglycol, Acetic acid, $NABH_3CN$) and C ($B(OH)_3$) were tested with a 1h at 60°C (a) and an ON at 37°C (b) incubation. Every protocol was tested with and without the additional maltose. Afterwards, contact angles were measured for all samples.

chromatography as described before. For the sandfish glycans, a concentration series (glycan amount per surface area) was created on PMMA, as was done on silanized glass. Because the biochemical analysis of the sandfish epidermis indicated that it contains high mannose glycans, a simple high mannose glycan, Man5 was purchased from Sigma-Aldrich and used for PMMA modification. An image of a sample plexiglass sheet, partially modified using *Viscum album* N-glycans, is shown in figure 7.6. The modified sheets were analysed in friction angle and AFM measurements, where the friction coefficient and the adhesion force were measured. In addition, the protocol was used to modify metal plates, coated with acrylic lacquers (kindly provided by BASF).

7.3 Results and discussion

A series of synthetic steps was performed during this work, which was based on data found in literature and has theoretical legitimacy, it would, however, also require analytical confirmation. Methodology often limits scientific research because of the lack of detection and/or sensitivity of some techniques. The aim of the work described in this chapter was the modification of acrylic surfaces with glycans found in the sandfish epidermis. Unfortunately, the success of each step in the modification could not be directly measured by analytical methods. Therefore indirect means of evaluation such as wettability, adhesion measurements by AFM and friction angles with sand were performed. The reduction of adhesion and friction on acrylic surfaces was the main goal of the modification, which has provided the desired result. However, the proposed mechanism of the modification cannot be confirmed at this point.

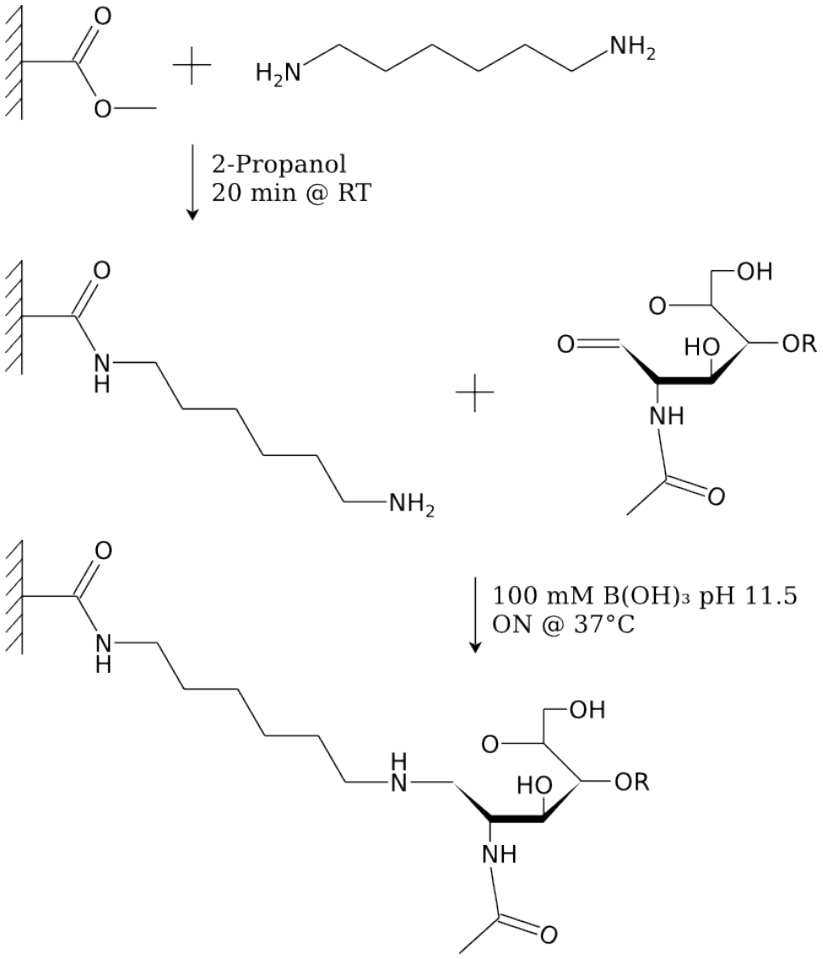

Figure 7.5: The proposed mechanism of PMMA glycosylation.

Before the modification and evaluation of technical surfaces was performed, the sandfish skin itself was evaluated in more detail. The contribution of glycans (or their absence) to adhesion was evaluated on the epidermis using adhesion force measurements. Sandfish skin exuviae, treated in different ways, and clean berber skink exuviae were measured with a ThermoMicroscopes AFM. The results are shown in figure 7.7.

Native sandfish skin exhibits the lowest adhesion among all tested materials. No difference was observed between dry-cleaned (air-blown) or washed skin, which was dried afterwards. Wetting and swelling therefore does not seem to have an influence on the adhesion. On the other hand, the sample treated with PNGase F showed significantly higher adhesion ($p < 0.01$), which was still significantly lower than the berber skink's. If the latter was due to the absence of N-linked glycans or due to keratin denaturation during the process, is difficult to say. It should be noted that no anomalies were observed on the topography of PNGase F treated samples. The sample treated with sialidase also showed higher adhesion, compared to the native skin ($p < 0.05$). The samples treated with O-glycosidase showed slightly higher adhesion, but were still in the normal range of native skin. O-linked glycans often link a sialic acid, which, if present, prevents enzymatic deglycosylation (Varki et al., 2009). If we assume that the adhesion change was purely due to deglycosylation, this opens up the possibility that the O-glycosydase treated sample would also

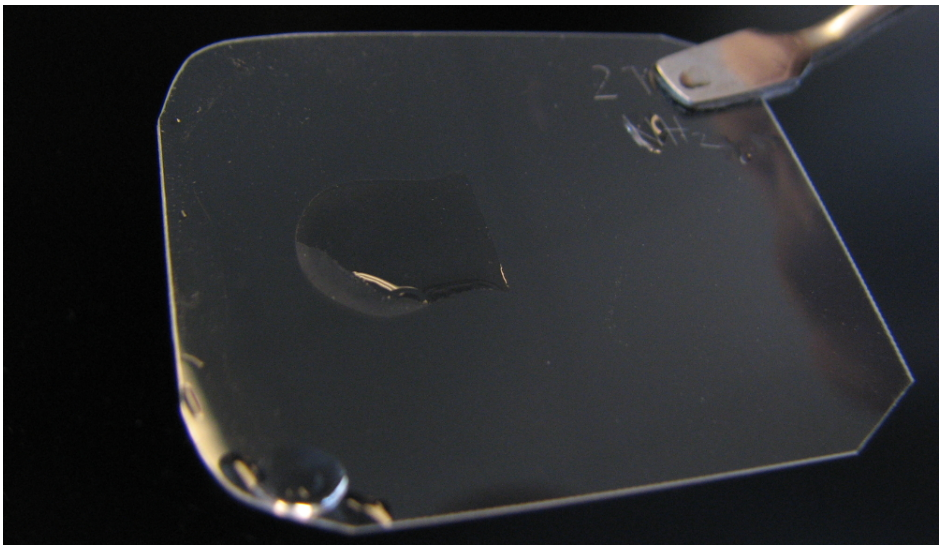

Figure 7.6: A wet glycan modified PMMA sample. On the left side of the sheet, approximately 1cm^2 was modified with glycans, the rest only with the amine linker. The sheet was washed 3x5min and dipped in water, to observe its wetting properties.

show a significant increase in adhesion if pretreated with sialidase. If the same sample was then to be treated with PNGase F, it is possible that the adhesion would be in the same range as the skin of the berber skink.

7.3.1 Glass

How the glycans are integrated into the keratins is still unknown and remains to be resolved by a structural analysis of the glycosylated keratins. However, previous studies suggest that if immobilized on a glass surface, the adhesion and friction of said surface is reduced (Baumgartner et al., 2007; Saxe, 2010; Staudt, 2012).

For the glycans to reduce adhesion on the surface, a certain amount of glycans would be required to sustain a homogeneous interaction with the environment. In this case, linking glycans to a surface should result in a gradual adhesion reduction of the surface until a minimum value is reached. To test this, a silanized glass slide was coated with a series of different amounts of glycans, extracted from the sandfish epidermis. The sample was then measured with a ThermoMicroscopes AFM. The results are shown in figure 7.8. As postulated, the adhesion of the modified glass was indeed reduced as a function of glycan amount. The function curve has a sigmoid shape and after an exponential decrease of adhesion, the minimum levels are approached asymptotically. The curve is placed between the levels of silanized glass and native sandfish skin which acts as the minimum. Due to the high standard deviation in samples 1-3, the curve seems to begin somewhat higher than the pure silanized glass value. It should be noted, that its value has a standard deviation of approximately 0.7nN, therefore the measurements may not necessarily be in contradiction.

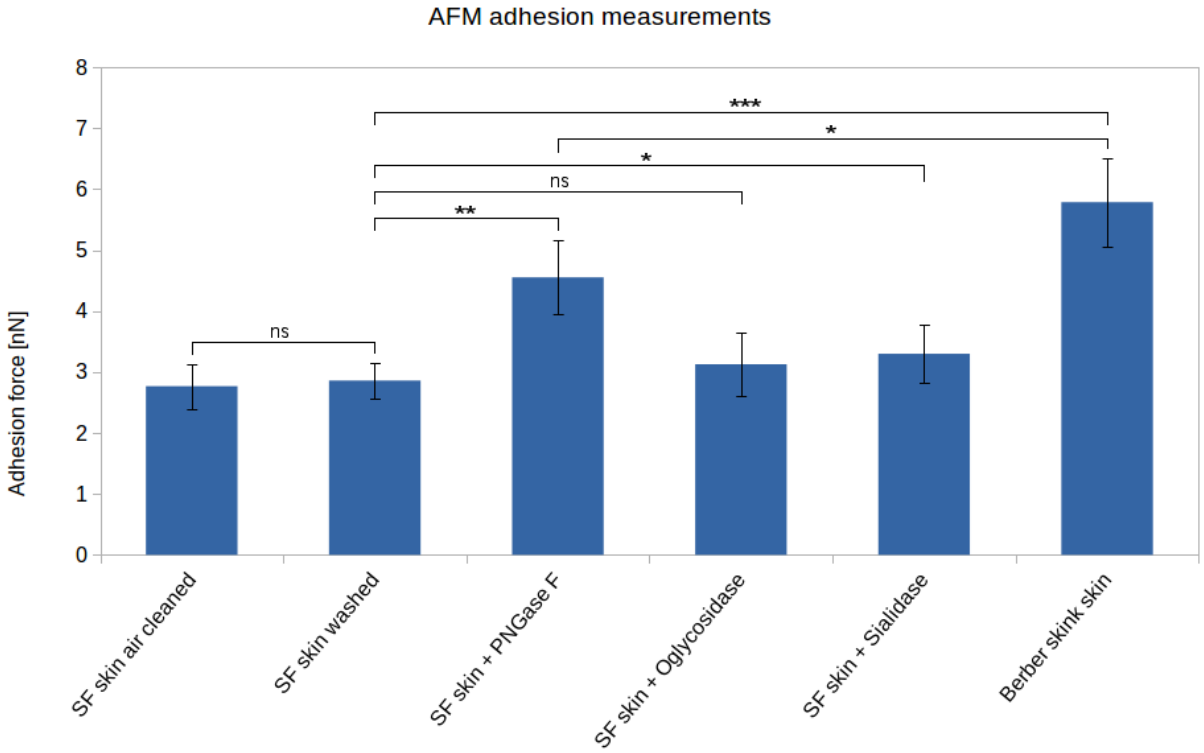

Figure 7.7: AFM adhesion force measurements comparison. The following samples were measured with a ThermoMicroscopes AFM: berber skink skin and sandfish skin, prepared in different ways: cleaned by air blowing, cleaned by washing with dH_2O, treated with PNGase F, treated with O-glycosidase and treated with sialidase. Approximately 1 square cm of exuviae was used for every type of sample, on which 10 measurements on different areas were recorded. A two-tailed T-Test of significance was calculated for the shown pairs.

7.3.2 PMMA

After what may be a successful modification of PMMA in the preliminary experiments, the glycan series experiment was also performed on this material. The adhesion force measurements were performed with a Nanosurf AFM with a silicon contact mode cantilever. Although the material properties and the modification process on PMMA are different than those of glass, a similar result would be expected concerning the form of the adhesion curve. The results are shown in figure 7.9. The adhesion force for native sandfish skin is approximately twice as high when measured with the Nanosurf device in comparison to the ThermoMicroscopes device. The reason for this is presumably the variability between the cantilevers. Interactions between materials are specific, therefore variation in measured adhesion is not surprising (silicon nitride tip (Thermo)/ silicon tip (Nanosurf)). The tip radius between cantilevers may also vary and can also influence the measurement. It is noteworthy that the absolute values are only valid for the according variables and settings. However, for this study, relative values were more important, since they display a comparison between different materials. In comparison with the glass sample, the resulting variation of the first few samples in the PMMA series was lower, therefore a better overlap of

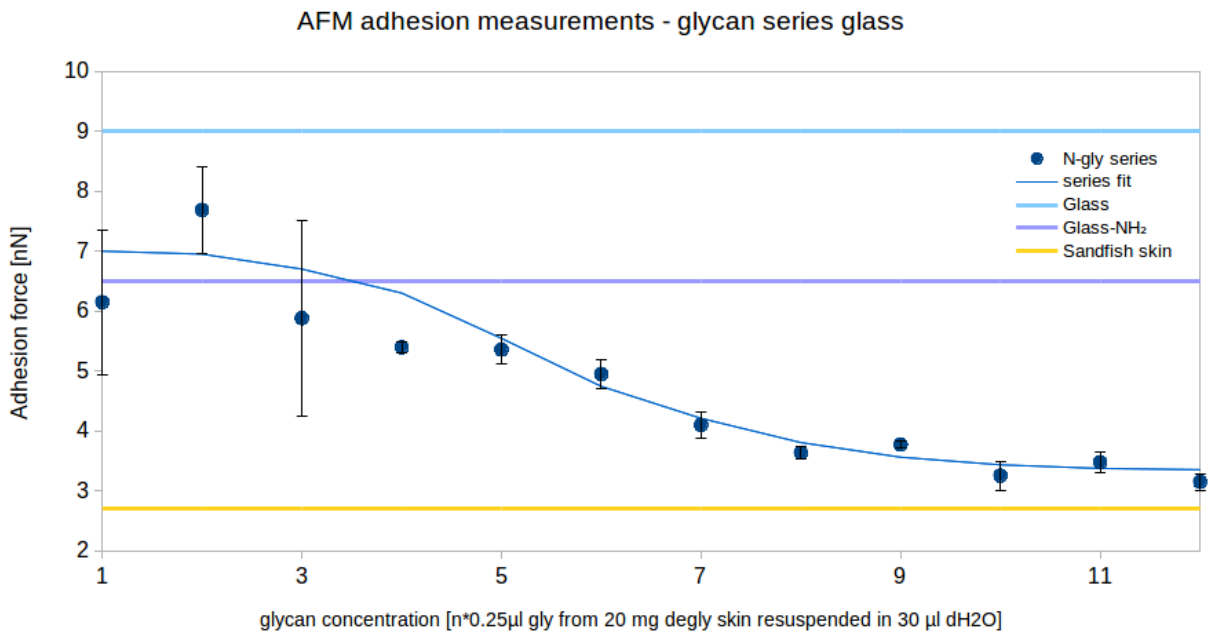

Figure 7.8: AFM adhesion force measurements of N-glycan series on glass. Different amounts of glycans were linked to a glass surface and measured by AFM. As a reference, the values of other samples are shown as the horizontal lines: yellow - native sandfish skin, light blue - glass, violet - silanized glass. 10 measurements per sample were recorded, each having a circular surface with a diameter of 5mm.

the fitted curve to the amine modified surface can be observed. Overall, the curve behaviour was the same. Maximum adhesion was measured on the sample without the glycans ($\approx$ 53nN). It was exponentially reduced at first and then asymptotically approached the minimum value at $\approx$ 10nN.

While AFM adhesion force measurements are suitable for quantitative analysis of surface - cantilever interaction, sand friction angles also have to be measured. Although primitive in the set-up, this kind of measurement is closest to simulating the sandfish's gliding through sand under controlled conditions. Firstly a PMMA sheet, modified with sandfish glycans was compared to native skin, untreated PMMA and amine-modified PMMA. The results are shown in figure 7.10. A glycan sample, purified from 5mg of clean, dry exuviae was used to modify an area of 2x3cm on a PMMA sheet, which was set as the standard glycan-PMMA sample for all measurements. Average Friction angles (left y-axis) and friction coefficients (right y-axis) were determined from 10 measurements for each sample. Untreated PMMA had the highest friction angle of approximately 35°, the angle for PMMA with the amino linker was for a few degrees smaller. Native sandfish skin had the expectedly lowest friction angle of 21°, which was already determined by Rechenberg et al. (2004). Glycan modified PMMA has shown significantly lower values in comparison with other PMMA samples, however, it did not reach the values of the skin. The average value was approximately 25°, with the lowest measured value at 23°.

While the friction of the modified PMMA samples did not reach the level of the sandfish

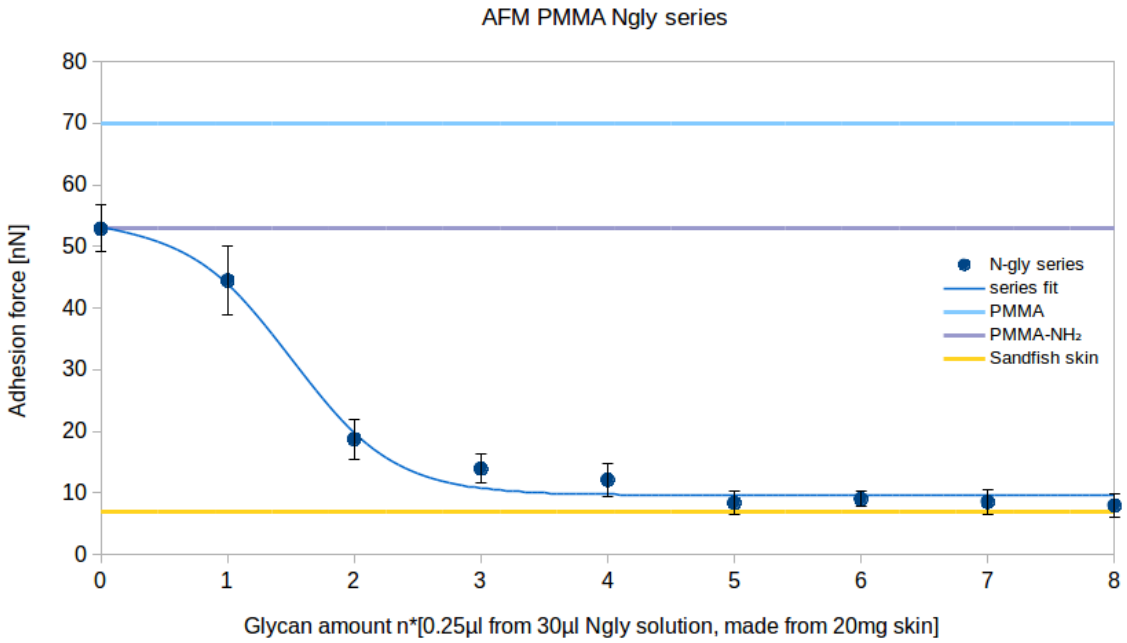

Figure 7.9: AFM adhesion force measurements of N-glycan series on PMMA. For comparison, the values of other samples are shown as horizontal lines: yellow - native sandfish skin, light blue - PMMA, violet - PMMA-NH_2. 10 measurements per sample were recorded, each having a circular surface with a diameter of 5mm.

skin, a friction reduction of up to 30% could be achieved. Next, acrylic lacquers (kindly provided by BASF) were tested in the same manner. Treated and untreated samples were compared, see figure 7.11. The untreated lacquers showed friction angles above 35°, while the samples modified with glycans, with the exception of R68, showed the same friction reduction as PMMA. Figure 7.12 shows a snapshot of a side by side comparison of a treated and untreated GW34 lacquer sample. Both were covered with sand and then tilted to approximately 30°. The untreated sample is fully covered with sand, while the treated sample is almost completely free from sand, except for the edges, which were covered with an incubation frame and were therefore not modified. As can be observed in the figure, the surface of the treated sample shows no stains or rough marks and is completely smooth and shiny. The modification therefore seemed to have no impact on the sample roughness.

The next challenge was to find suitable alternatives for glycan sources. Glycans were extracted as described in the methods section and used for PMMA modification. Afterwards, friction angles were measured, see figure 7.13. The PMMA sheets, modified with *Viscum album* and *Saccharomyces cerevisiae* glycans show no friction reduction compared to the control samples. The reason for this may be either the lack of appropriate structures which would facilitate friction reduction, or the presence of other structures, which would inhibit it. The high mannose glycans which were observed in the sandfish epidermis, should, according to UniCarb databank to some extent, also be present in both tested samples. The research was therefore continued by further purification of the samples. *Viscum album* glycans were separated into neutral and acidic struc-

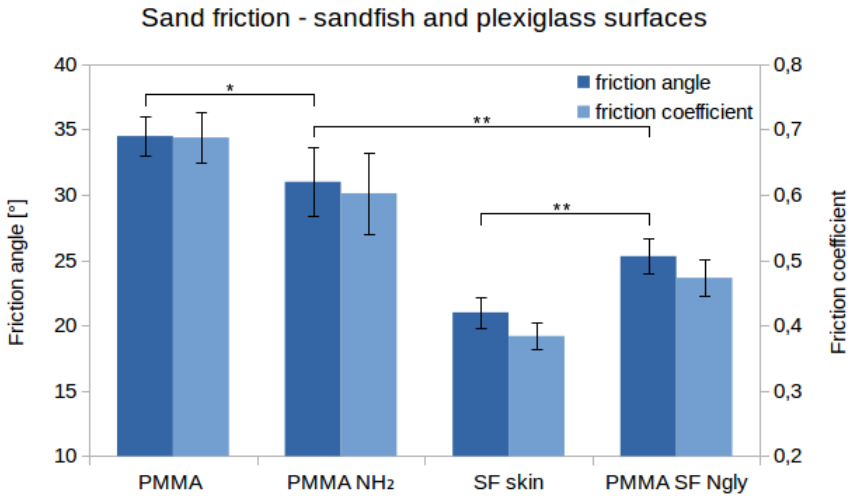

Figure 7.10: Friction measurements of sandfish epidermis and PMMA. Friction angle is shown on the left vertical axis, while the calculated friction coefficient is shown on the right. 10 measurements were performed for every sample.

tures by anion exchange chromatography as described in the methods section. the separated samples were then used for PMMA modification and friction angle measurement, see figure 7.14. The neutral *V. album* glycans show a friction reduction, almost to the same extent reached by sandfish glycans, however, the glycan amount in the sample, which was not measured, is probably different. Nevertheless, this suggests that friction reduction can be achieved by structures obtained from other sources.

Another alternative source of glycans are sweet almonds (*Prunus dulcis*). As mentioned above, in addition to high mannose glycans, almonds also contain the enzyme PNGase A, which cleaves N-glycans, therefore making the addition of other deglycosylation enzymes unnecessary. Glycans were extracted and further purified to obtain neutral structures by using anion exchange chromatography. These were used for PMMA modification and friction angle measurement. The results are shown in figure 7.15. The friction angles of neutral structures, obtained without additional deglycosylation enzymes, reached the friction levels of sandfish glycans on PMMA, which is very promising for the development of low friction surfaces on a larger scale.

The obtained results support the data from previous studies, which suggest that sandfish glycans can reduce the friction if immobilized on surfaces. It appears, such or similar structures can also be obtained from alternative sources, like almond seeds, by relatively simple means. As discussed in chapter 6, the detected structures could be products of peeling, but it is these same structures which were used for modification of glass and have produced lower adhesion and friction. It is questionable if all structures need to be present to sustain the effect and in what relation to each other. A simple purified Man5 glycan was purchased from Sigma-Aldrich and used for modification and friction angle measurements as described. The results are shown in figure 7.16. Surprisingly, the friction angle results of the Man5 glycan are indistinguishable from the sandfish glycan-modified sample. This is a strong indication that one structure may well be

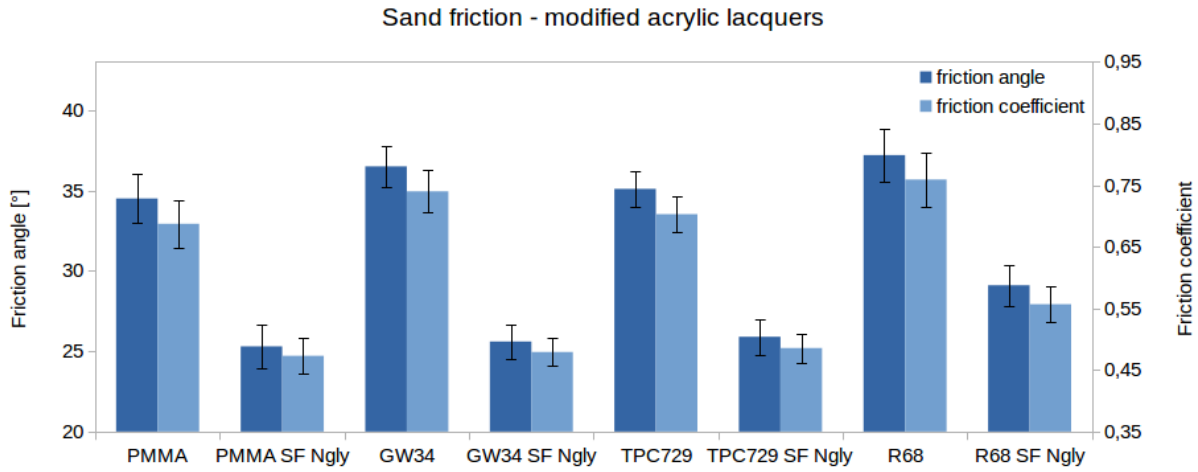

Figure 7.11: Friction angle measurements of modified BASF plates. Friction angle is shown on the left vertical axis, while the calculated friction coefficient is shown on the right. 10 measurements were performed for every sample. A sample pair is shown for every material in native or modified (SF Ngly) form.

enough to create a surface with low friction against sand if present in sufficient amount.

In retrospect, sandfish glycans can be used for modification of technical materials such as glass, or possibly even of organic polymers. For the latter, a method to modify PMMA and other acrylic surfaces, such as varnishes was devised. While the proposed mechanism of modification could not be confirmed yet, the treated surfaces show a substantial reduction in adhesion and friction in comparison to untreated samples. Furthermore the method does not seem to affect the overall appearance of the samples, which could be appropriate for industrial applications. The glycans found in the sandfish epidermis can be also obtained from other sources and used for modification, potentially making bulk production somewhat more viable. In principle, high mannose glycans suffice for substantial friction reduction, the results even suggest that one structure is enough to sustain the effect.

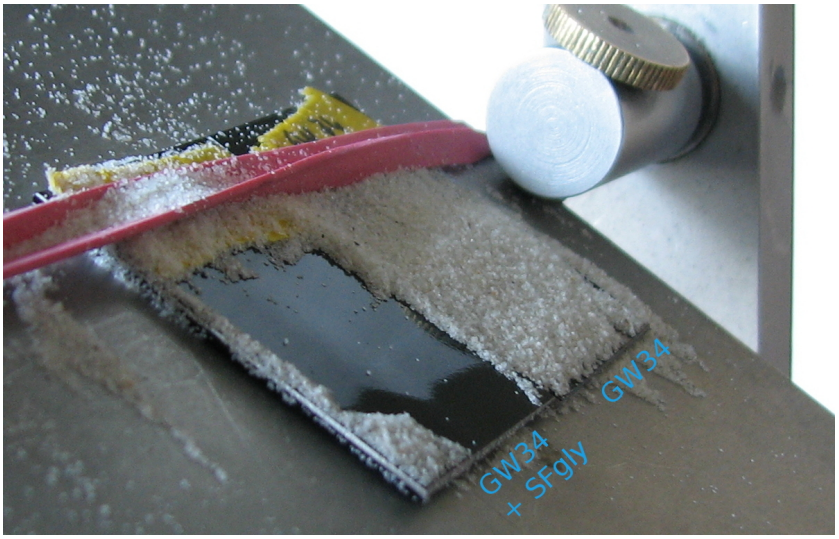

Figure 7.12: Friction comparison of modified and untreated BASF plates. A treated and an untreated sample were placed side by side on an inclined plane and completely covered with sand. The inclination was gradually increased until sand began to slide off. A photograph was taken at an inclination of approximately 30°.

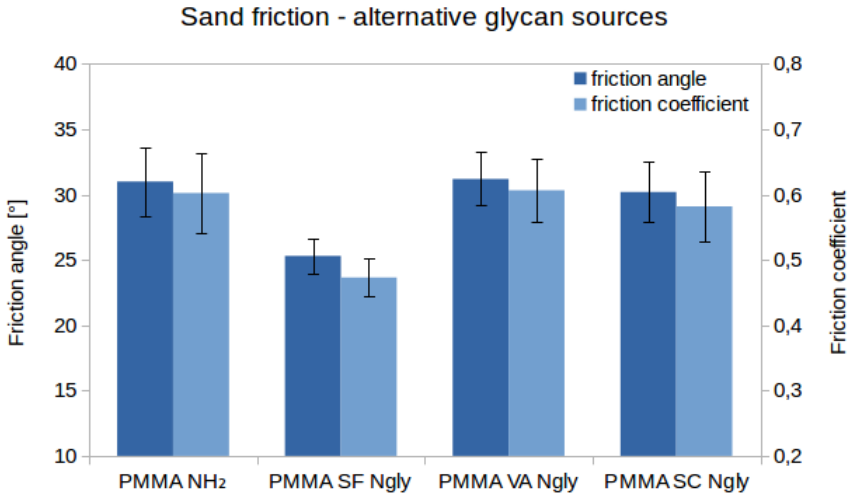

Figure 7.13: Friction measurements of modified PMMA with glycans from alternative sources. PMMA sheets with the following modification are shown from left to right: only amine linker (negative control), sandfsih (SF) glycans, *V. album* (VA) glycans and *S. cerevisiae* (SC) glycans. Friction angles were measured 10 times on every shown sample.

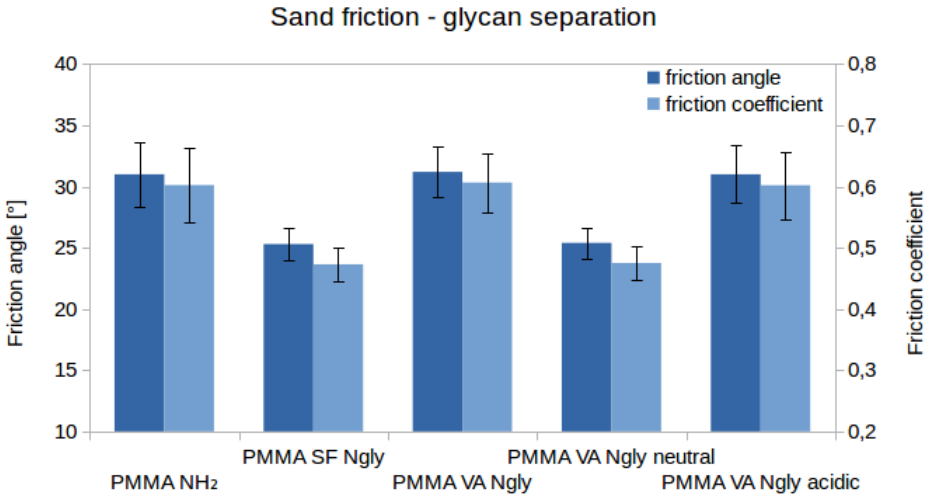

Figure 7.14: Friction measurements of modified PMMA with separated glycans from *Viscum album*. PMMA sheets with the following modification are shown from left to right: only amine linker (negative control), sandfsih (SF) glycans, unseparated *V. album* (VA) glycans, neutral VA glycans and acidic VA glycans. 10 measurements were performed with every sample.

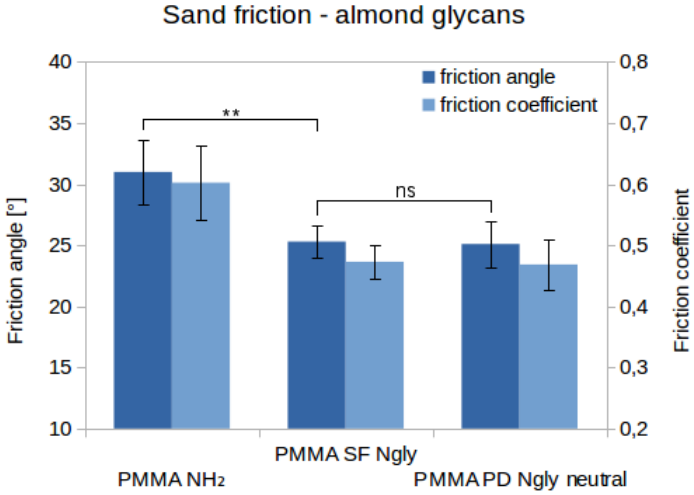

Figure 7.15: Friction measurements of modified PMMA with almond glycans.PMMA sheets with the following modification are shown from left to right: only amine linker (negative control), sandfsih (SF) glycans and neutral almond glycans. Friction angles were measured 10 times on every sample.

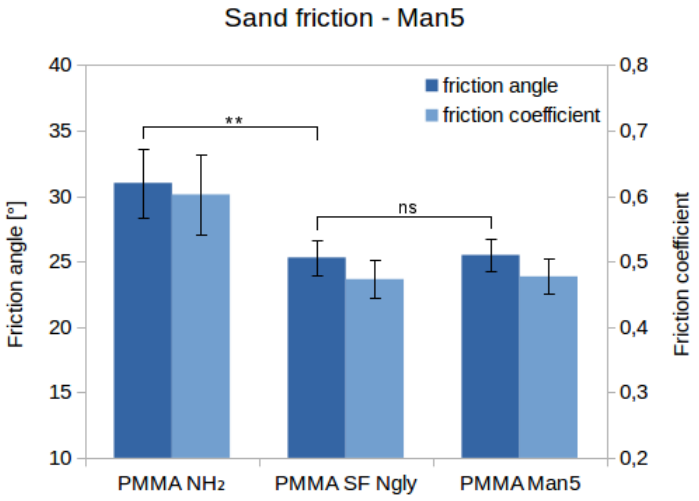

Figure 7.16: Friction measurements of modified PMMA with Mannose 5 N-glycan. The friction angles were measured 10 times on every sample.

Chapter 8 - Conclusion and outlook

This project was set out to continue the work previously performed by Saxe and Staudt on the friction and abrasion resistant sandfish epidermis. The aim was to further investigate on:

- detailed skin composition and
- further characterization of its main elements, keratins and glycans
- measuring additional aspects of friction reduction and abrasion resistance
- devising a theoretical model to describe and explain these features
- development of working prototypes and applications
- hypothesizing a strategy for bulk production of possible applications

Many of the planned experiments were performed successfully and new insights were gathered concerning the "sandfish effect", as it was named by Rechenberg (2009). Superficial properties were measured, like surface energy and Young's modulus and the results showed that the surface energy is low (23 - 27 $\frac{mN}{m}$) and comparable with low energy plastics such as PTFE, PE or PP (twi-global, accessed march 2015). Two different methods were used to determine the elastic modulus: tensile testing by stretching the material until rupturing and nanoindentation - pressing a very fine needle into the measured material. The methods showed very different results. While tensile testing showed Young's modulus' values of soft elastomers (Domininghaus, 1998) from 300 - 400MPa, Nanoindentation showed average values of a factor of 5 higher. Also, nanoindentation measurements provided a very broad spectrum of values, the majority of them lying between 0.7 and 1.7GPa, which is comparable with different hard plastics (Domininghaus, 1998). It is unclear whether the Young's modulus can be defined as such, for the material might behave as an elastomer and thereby not have a constant modulus of elasticity. In general, the measurements suggest that the sandfish's epidermis has material properties with stress-strain values which can be found in the spectrum of existing synthetic polymers. The appropriate combination of stiffness and elasticity remains to be found, however, the plasto-elastic behaviour of the sandfish skin might, to some extent, be explained by the interplay of the different types of keratin.

Structural and chemical analysis (TEM, RAMAN, SDS-PAGE) of the outer epidermal generation (exuviae) of the sandfish epidermis has shown that while it has basic reptilian structure (Toni et al., 2007; Paquin & Colomban, 2007; Cooper & Greenberg, 1992), there seem to be some deviations when compared to the epidermis of the average lizard. The exuviae have a typical

transition from whole cells to the outer oberhäutchen. However, no clear separation of α- and β- keratins was observed, which are normally found in clearly distinct layers with an intermediate mesos layer (Toni et al., 2007; Paquin & Colomban, 2007; Vitt & Caldwell, 2014). For the sandfish it rather seems, as if the different keratin types (the helical, elastic α- and the stiff packet forming β-keratins) are interlinked into a homogeneous composite. If the deformation resistance of the hard components could be embedded into a matrix with a long elastic recoil, this could also explain the largely different values between the tensile testing and nanoindentation. This is because it is likely that the tensile test would predominantly reflect the properties of the matrix, while the hard components would have a stronger impact on nanoindentation.

In addition to the epidermal structure, what separates the sandfish skin from those of other squamates, is the high level of glycosylation in the keratins, which was already described in previous studies. A detailed analysis of the glycans has shown that many different types of glycans may be found in the epidermis, however, only N-linked glycans of the high-mannose type were confirmed. The strongest signals were present for a Man5 and a Man9 structure, somewhat weaker, yet still significant, were the signals for Man6, Man7 and Man8 structures. As discussed above, it is not clear whether or in which amount these occur in the native state, or are products of peeling.

Based on the obtained information, we can propose a simple model of a low friction, abrasion resistant surface: Abrasion resistance typically correlates with high hardness (Rabinowitz, 1995), in this case the high hardness of the β-keratin packets. If these are interlinked with an elastic matrix composed of softer α-keratins, the composite could exhibit both, a hard surface and a prolonged bandwidth of elastic recoil, which seems ideal for a material with a high abrasion resistance. High hardness typically also correlates with high surface energy (Rabinowitz, 1995), however, the keratins are modified with the glycans, which were shown to reduce the surface interaction and thereby the friction coefficient. A graphical representation of the "low friction, abrasion resistant" epidermis model is shown in figure 8.1. Such architecture would seem homogeneous under TEM as well as Raman spectroscopy, despite consisting of different components. At the same time it would likely show different stress-strain behaviour, depending on the method of measurement.

In addition to skin analysis, surface modification of technical materials was tested, especially acrylic surfaces. A simple two-step protocol was developed, which shows promise according to indirect measurements (AFM, friction angles), however, its effectiveness could not be confirmed on a molecular level. The conducted experiments suggest that glycans, appropriate for friction reduction can be isolated from alternative sources, like almonds, which further eliminates the necessity to add deglycosylation enzymes. Exploiting new sources of N-linked high mannose glycans would be an important step towards mass production. As MS analysis has shown, 5 different high mannose structures could be found in the sandfish's epidermis (whether all are native remains questionable), however, sand friction and AFM adhesion experiments have shown that for sustaining low friction not all of these are necessary. In fact, the measurements suggest that a simple Man5 glycan is enough to mimic the effect to the same extent, although the

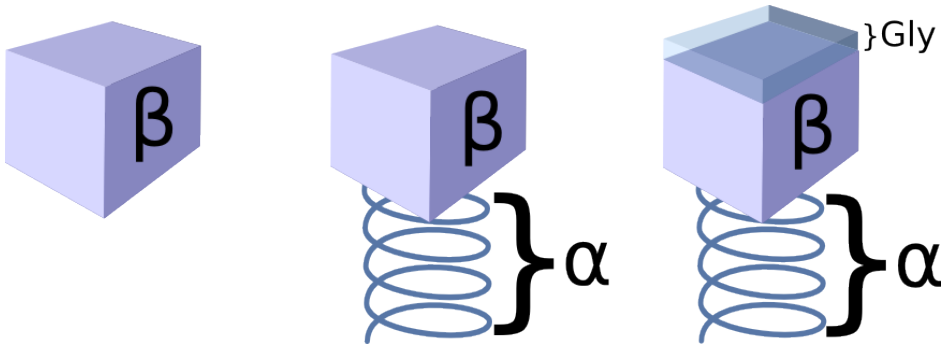

Figure 8.1: A model of the low-friction, abrasion-resistant sandfish epidermis. The hard β-keratin packets are represented by cubes, which could be interconnected with an elastic matrix, composed of α-keratins (spring). The glycans, responsible for friction reduction, are shown lying on top of the keratins.

question "why?" remains unanswered just yet.

Man5 is found in various tissues of other organisms (UniCarb database) and fortunately, there is enough extensive data on its composition and structure, available for comparison (GLYCAM database). The most interesting glycan feature for our research is the connection to the keratin and the glycans spatial structure. The latter can vary due to the environmental factors like solution and other neighbouring molecules, however, even a simplified molecular model might provide some insight into the glycan behaviour on a surface. Some models are found in the 3D structure library of the GLYCAM database. A calculated model of the Man5 glycan with the lowest minimized energy (34.187 $\frac{kcal}{mol}$) in a watery medium is shown in figure 8.2. While the angles and rotations of the single sugar rings may vary according to the milieu, the structure would due to its sequence presumably retain its tree-like form most of the time.

This offers an interesting thought experiment. As already discussed in chapter 2, when particles (but also surfaces of larger objects) are close, they are attracted to each other due to Van der Waals forces (Parsegian, 2005). The attraction is specific for every material pair, which has its own attraction constant, the so called Hamaker constant - A_{Ham} (Parsegian, 2005). According to Israelachvili (2011), A_{Ham} is defined as the scalar product of π^2, the interaction parameter C for particle-particle interaction and the number densities ρ_n of both materials. The number or particle density is defined as the number of atoms (N) in a physical volume (V). For example, silicon dioxide crystals usually have a number density of $50 \cdot 10^{27}$ atoms per m^{-3} (Filipovič, 2012).

$$A_{Ham} = \pi^2 \times C \times \rho_{n1} \times \rho_{n2} \qquad \rho_n = \frac{N}{V} \tag{8.1}$$

Now let us imagine a glass slide, modified with Man5 glycans that are interacting with a sand particle. The glass slide is approximated to have a perfectly flat surface, while the sand particle is a perfect sphere composed of pure silicon dioxide. For such a simple system, there is an existing mathematical solution for the attractive Van der Waals force (Parsegian, 2005), which is defined as follows:

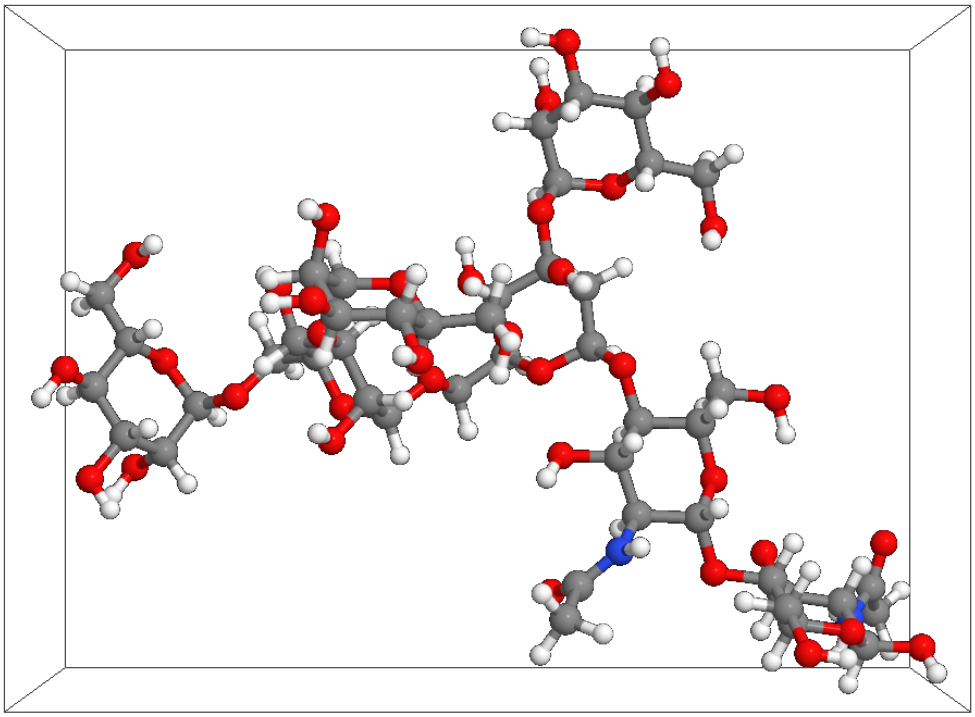

Figure 8.2: 3D Model of a Man5 glycan in a watery medium, obtained from GLYCAM database. All the atoms are labelled accordingly to their nature. All the sugars contain carbon (gray), oxygen (red) and hydrogen (white) atoms, the GlcNAcs also contain nitrogen (blue).

$$F_{VdW} = -\frac{A_{Ham}}{6}\frac{R}{l^2} \qquad R \gg l \tag{8.2}$$

Here, R is defined as the radius of the sand particle, which is much greater than the distance to the glass surface (l). If the glass slide is modified with glycans, we can assume that Man5 "trees" in blocks, as shown in figure 8.2, are lined up over the complete surface. A single block has the following dimensions: $2.25nm \times 1.65nm \times 1.24nm$, resulting in a total volume of approximately $4.6nm^3$. The number density can thereby be calculated from the block volume and the number of atoms in a glycan, which is approximately $35 \cdot 10^{27}$ atoms per m^{-3}. Chu & Dalgarno (2004) have determined the Van der Waals interaction coefficients for the same element atomic pairs and the data was later revised and confirmed by Tkatchenko & Scheffer (2009). Different methods have shown slightly different results, however, the order of attraction ranging from the strongest to the weakest is as follows: Si >C >O >H. The found coefficients apply only to free atoms and cannot be directly used for molecules, which contain covalent bonds, since these could alter the values. As there is no known data of Van der Waals' coefficient values for the carbohydrate - silicon dioxide interaction, the coefficient was held constant in this simple evaluation. When computing all the values, the result is very interesting. While the estimation may be inaccurate due to simplification, the A_{Ham}, which, is directly proportional to the Van der Waals force, is approximately 30% lower between the sand particle and a Man5-covered flat surface than between the sand particle and the pure glass surface. This is a rough estimation which ignores

many factors that could contribute to the reduction of adhesion. However, considering the data from Chu & Dalgarno (2004), which show a higher attraction for Silicon atoms, than for C, O or H, the difference may be even substantially larger. A lot of research is still necessary to create a more precise mathematical model, but it seems evident that reducing the particle density on the interface can considerably contribute to surface interaction. While this simple model could partly explain how the adhesion is reduced on a flat modified glass surface, the binding and position of the glycans in their native form is still not fully established. It is therefore difficult to deduce, how much influence the particle density reduction actually has in the natural model.

In spite of performing many different experiments, a lot of information is still required to fully understand and explain the interactions that the sandfish's epidermis has with a sandy environment while (at the same time) being able to efficiently produce effective applications that would mimic it. Further characterization of the keratins and the glycans is required, especially concerning their spatial structure. This would show the true nature of their interaction and how the glycans reduce the surface interaction of the skin's environment. To effectively achieve the latter, analysis such as X-ray crystallography or NMR (nuclear magnetic resonance) spectroscopy should be performed. Moreover, creating a detailed physical model of molecular interaction between the epidermis and its environment would also be required, which would help explain the underlying effect on the nanoscopic levels.

New prototypes need to be developed, combining both reduced friction and abrasion resistant properties. This would confirm or disprove the proposed mechanism and open new possibilities for mass production of practical applications. Native glycans can be prepared in larger amounts in reasonable levels of purity and could be used for some applications. Research by Saxe (2008) has shown that sandfish exuviae are sensitive to UV radiation, which causes the epidermis to change colour and crack. Proteins are known to absorb UV light, and N-glycosidic coupling can even increase a material's extinction coefficient (Berrens & Bleumink, 1966). However, carbohydrates normally do not exhibit significant absorption in the UV spectrum (Ikawa & Niemann, 1949). We can therefore assume that linked to a less UV sensitive material, an application, such as protective foil or lacquer (made with gylcans), could be used outdoors. On the other hand, carbohydrates succumb to many other environmental factors, such as high temperatures, chemical and biological degradation, etc. For the long term, a completely synthetic material would therefore likely be a better alternative.

References

[1] Abdel-Magid AF, Carson KG, Harris BD, Maryanoff CA, Shah RD (1996) Reductive Amination of Aldehydes and Ketones with Sodium Triacetoxyborohydride. Studies on Direct and Indirect Reductive Amination Procedures. J. Org. Chem., 61(11):3849–3862

[2] Alberts B, Bray D, Hopkin K, Johnson A, Lewis J, Raff M, Roberts K, Walter P, (2003) Essential cell biology (2nd ed), Garland science, New York & London, pp. 39-82

[3] Alibardi L, Valle LD, Toffolo V, Toni M (2006) Scale keratin in lizard epidermis reveals amino acid regions homologous with avian and mammalian epidermal proteins. The Anatomical Record, 288A:734-752

[4] Alpert AJ (1990) Hydrophilic-interaction chromatography for the separation of peptides, nucleic acids and other polar compounds. J. Chrom., 499:177–196

[5] Aminoff D, Gathmanna WD, McLeana CM, Yadomaea T (1980) Quantitation of oligosaccharides released by the β-elimination reaction. Anal. Biochem., 101:44-53

[6] Arnold EN, Leviton AE (1977) A revision of the lizard genus *Scincus* (Reptilia: Scincidae). Bull. br. Mus. nat. Hist. Zool., 31: 189–248.

[7] Askeland DR, Fulay PP, Wright WJ (2010) The Science and Engineering of Materials (6th Ed), Cengage Learning, London, pp. 197-234

[8] Askeland DR, Phulé PP (2006) The science and engineering of materials (5th Ed), Cengage Learning, Toronto, pp. 183-222

[9] Baumgartner W, Saxe F, Weth A, Hajas D, Sigumonrong D, Emmerlich J, Singheiser M, Böhme W, Schneider J M (2007) The Sandfish's Skin: Morphology, Chemistry and Reconstruction. J. Bionic Eng., 4:1-9

[10] Berrens L, Bleumink E (1966) The influence of sugars on the U.V. absorption spectrum of proteins. Recl. Trav. Chim. Pays-Bas, 85:59–69

[11] Beyak R, Meyer CF (1968) Elasticity and Tensile Properties Human Hair. I. Single Fiber Test Method. J. Soc. Cosmetic Chemisls, 20:615-626

[12] Breloy I, Pacharra S, Ottis P, Bonar D, Grahn A, Hanisch FG (2012) O-Linked N,N- diacetyllactosediamine (LacdiNAc)- modified glycans in extracellular matrix glycoproteins are specifically phosphorylated at subterminal N-acetylglucosamine. J. Biol. Chem. 287, 18275-18286

[13] Brown L, Koerner T, Horton JH, Oleschuk RD (2006) Fabrication and characterization of poly (methylmethacrylate) microfluidic devices bonded using surface modifications and solvents. Lab Chip, R. Soc. Chem., 6:66-73

[14] Brydson JA (1999) Acrylic Plastics In Plastics Materials (7th Edition). Butterworth Heinemann, Oxford, pp. 398-424

[15] Bulmuș V, Ayhan H, Pişkin E (1997) Modified PMMA monosize microbeads for glucose oxidase immobilization. Chem. Eng. J., 65:71-76

[16] Cho SM, Park JW, Han HS, Seok HK, Moon MW, Kim YC (2013) Multifunctional composite coating as a wear-resistant layer for the bearing in total hip joint replacement. ACS Appl. Mater. Interfaces, 5(2):395-403

[17] Chu X, Dalgarno A (2004) Linear response time-dependent density functional theory for van der Waals coefficients. J. Chem. Phys., 121:4083-4088

[18] Cooper WE Jr, Greenberg N (1992) Reptilian coloration and behavior. In "Biology of the Reptilia Vol 18" by Gans C, Crews D, The University of Chicago Press, Chicago, pp. 298–422

[19] de Boer AR, Hokke CH, Deelder AM, Wuhrer M (2007) General microarray technique for immobilization and screening of natural glycans. Anal Chem., 79(21):8107-8113

[20] Deckman HW, Wronski CR, Witzke H, Yablonovitch E (1983) Optically enhanced amorphous silicon solar cells. Appl. Phys. Lett., 42:968-970

[21] Dobkin D, Zuraw MK (2003) Principles of Chemical Vapor Deposition, Kluwer Academic Publishers/ Springer Netherlands, pp. 196-223

[22] Domininghaus H (1998) Die Kunststoffe und Ihre Eigenschaften (5th ed), Springer, Berlin Heidelberg, pp. 97-482

[23] Ettre LS (1993) Nomenclature for chromatography, Pure & Appl. Chem, 65(4):819-872

[24] Filipovič L (2012) PhD thesis: Topography Simulation of Novel Processing Techniques. Fakultät für Elektrotechnik und Informationstechnik, TU Wien

[25] Fixe F, Dufva M, Telleman P, Christensen CBV (2004) Functionalization of poly(methyl methacrylate)(PMMA) as a substrate for DNA microarrays. Nucleic Acids Res., 32(1):e9

[26] Food and Agriculture Organization of the United Nations (Faostat) database, available at `http://faostat3.fao.org/home/E`, accessed 09 March 2015

[27] Fujii T, Li D (2008) Preparation and properties of protein films and particles from chicken feather. J. Biol. Macromol., 8(2):48-55

[28] Gardiner DJ, Graves PR (1989) Practical Raman Spectroscopy. Springer, Berlin, Heidelberg, pp. 1-157

[29] Garsault FAP (1764) Les figures des plantes et animaux d'usage en medecine, décrits dans la Matiere Medicale. Geoffroy Medecin, Paris, pp. 85

[30] GLYCAM database - Complex Carbohydrate Research Center, University of Georgia, available at glycam.org, accessed 12 May 2015

[31] Greer AE (1970) A subfamilial classification of scincid lizards. Bull. br. Mus. comp. Zool., 139(3): 151-184

[32] Hartmann UK (1989) Beitrag zur Biologie des Apothekerskinks Scincus scincus. Herpetofauna, 11:17-39

[33] Hecht E (2002) Optics (4th ed.). Pearson, Harlow, pp. 86-140;325-378

[34] Hetherington TE (1989) Use of vibratory cues for detection of insect prey by the sandswimming lizard *Scincus scincus*. Anim. Behav. 37:290-297

[35] Hirtz D, Elling L (2012) N-Glykan Analyse Protokoll, Biomaterialien Praktikum, RWTH Aachen

[36] Holdich RG (2002) Fundamentals of Particle Technology, Midland Information Technology and Publishing, Shepshed, pp. 1-28

[37] Ikawa M, Niemann C (1949) A spectrophotometric study of the behavior of carbohydrates in seventy-nine per cent sulfuric acid. J. Biol. Chem., 180(2):923-931

[38] Israelachvili JN (2011) Intermolecular and surface forces (3rd ed.), Academic press, Amsterdam, pp. 415-467

[39] Jayo RG, Thaysen-Andersen M, Lindenburg PW, Haselberg R, Hankemeier T, Ramautar R, Chen DDY (2014) Simple Capillary Electrophoresis–Mass Spectrometry Method for Complex Glycan Analysis Using a Flow-Through Microvial Interface. Anal. Chem., 86(13):6479–6486

[40] Jones RM (1999) Mechanics of composite materials (2nd ed), Taylor & Francis, Philadelphia, pp. 2-26

[41] Jung YC, Bhushan B (2006) Contact angle, adhesion and friction properties of micro-and nanopatterned polymers for superhydrophobicity. Nanotechnology, 17:4970-4980

[42] Karrasch S, Dolder M, Schabert F, Ramsden J, Engel A (1993) Covalent binding of biological samples to solid supports for scanning probe microscopy in buffer solution. Biophys. J. 65:2437-2446.

[43] Kemp G (1998) Capillary electrophoresis: a versatile family of analytical techniques. Biotechnol. Appl. Biochem., 27:9-17

[44] Khosa MA, Ullah A (2013) A Sustainable Role of Keratin Biopolymer in Green Chemistry: A Review. J Food Processing & Beverages, 1(1):8

[45] Koch K, Bennemann M, Bohn HF, Albach DC, Barthlott W. (2013) Surface microstructures of daisy florets (Asteraceae) and characterization of their anisotropic wetting. Bioinspir Biomim., 8(3):036005

[46] Ko FK, Jovicic J (2004) Modeling of mechanical properties and structural design of spider web. Biomacromolecules, 5(3):780-785

[47] Krüss surface science, available at: http://www.kruss.de/services/education-theory/glossary/surface-free-energy/, accessed 16 January 2015

[48] Kutz M (2002) Handbook of Materials Selection. John Wiley & Sons, New York, pp. 341

[49] Laemmli UK (1970) Cleavage of Structural Proteins during the Assembly of the Head of Bacteriophage T4. Nature, 227:680-685

[50] Land MF (1972) The physics and biology of animal reflectors. Prog. Biophys. Mol. Biol., 24:75–106

[51] Leertouwer HL, Wilts BD, Stavenga DG (2011) Refractive index and dispersion of butterfly chitin and bird keratin measured by polarizing interference microscopy. Opt. Express, 19(24):24061-6

[52] Lee YC (1990) High-Performance Anion-Exchange Chromatography for Carbohydrate Analysis. Anal. Biochem., 189:151-162

[53] Maladen RD, Ding Y, Li C, Goldman DI (2009) Undulatory Swimming in Sand: Subsurface Locomotion of the Sandfish Lizard. Science 325(5938):314-318

[54] Mandal C, Mandal C (1990) Sialic acid binding lectins. Experientia, 46:433-441

[55] Mark Richard - Kinesiology (UTA): Mechanical properties of Materials course, available at: http://wweb.uta.edu/faculty/ricard/Classes/KINE-3301/Notes/Lesson-14.html, accessed 17 February 2015

[56] McKittrick J, Chen PY, Bodde SG, Yang W, Novitskaya EE, Meyers MA (2012) Structure, Functions and Mechanical Properties of Keratin. JOM, 64(4):449-468

[57] Meyers RA (1995) Molecular Biology and Biotechnology: a comprehensive desk reference, Wiley-VCH, pp. 722

[58] Nofziger DL (2003) Soil Temperature Variations With Time and Depth, available at: http://soilphysics.okstate.edu/software/SoilTemperature/document.pdf, accessed 26 March 2015

[59] Oliver WC, Pharr GM (2003) Measurement of hardness and elasticity by instrumented indentation, J. Mat. Res., 19(1):3-20

[60] Osorio D, Ham AD (2002) Spectral reflectance and directional properties of structural coloration in bird plumage. J Exp. Biol., 205(14):2017-27.

[61] Pack AA, Herman LM (1995) Sensory integration in the bottlenosed dolphin: Immediate recognition of complex shapes across the senses of echolocation and vision. J. Acoustical Society of America, 98(2): 722–733

[62] Paladino FV (1985) Temperature Effects on Locomotion and Activity Bioenergetics of Amphibians, Reptiles, and Birds. Am. Zool., 25(4):965-972

[63] Paquin R & Colomban P (2007) Nanomechanics of single keratin fibres: A Raman study of the α helix - β sheet transition and water effect. J. Raman Spectrosc. 38(5):504-514

[64] Parsegian VA (2005) Van der Waals Forces: A Handbook for Biologists, Chemists, Engineers, and Physicists, Cambridge University Press, Cambridge, pp. 1-37

[65] Patel TP, Parekh RB (1994) Release of oligosaccharides from glycoproteins by hydrazinolysis. Meth. Enzymol., 230:57-66

[66] Payne RS (1971) Acoustic location of prey by barn owls (*Tyto alba*). J. Exp. Biol., 54:535-573

[67] Peter JB (2013) Amontons' Laws of Friction in "Encyclopedia of Tribology" by Wang QJ, Chung JW, Springer, New York, pp. 71

[68] Plotkin M, Boden SA, Galushko D (2010) Solar energy harvesting in the epicuticle of the oriental hornet (*Vespa orientalis*). Naturwissenschaften, 97:1067-1076

[69] Printen JA, Sprague GF (1994) Protein interactions in the yeast pheromone response pathway: Ste5p interacts with all members of the MAP kinase cascade. Genetics, 138:609-619.

[70] Rabinowicz E (1995) Friction and wear of materials (2nd ed), Wiley, New York, pp. 1-50

[71] Rechenberg I, El Khyari AR (2004) Reibung und Verschleiß am Sandfisch der Sahara, available at: `http://www.bionik.tu-berlin.de/institut/festo04.pdf`, accessed 15 January 2015

[72] Rechenberg I, Zwanzig M, Zimmermann S, El Khyari AR (2009)Tribologie im Dünensand - Sandfisch, Sandboa und Sandschleiche als Vorbild für die Reibungs- und Verschleißminderung, available at: `http://www.bionik.tu-berlin.de/institut/TriboDueSa.pdf`, accessed 13 February 2015

[73] Renewable Resource Data Center Databank, available at: `http://rredc.nrel.gov/solar/spectra/am1.5/`, accessed 12 April 2014

[74] Rhode RA (2007) Global Warming Art project, available at: `http://www.globalwarmingart.com/wiki/File:Atmospheric_Transmission_png`, accessed 02 April 2015

[75] Riedl M (2001) Optical Design Fundamentals for Infrared Systems (2nd Ed), SPIE Press, Bellingham, pp. 74

[76] Ripamonti A, Alibardi L, Falini G, Fermani S, Gazzano M (2009) Keratin-Lipid Structural Organization in the Corneous Layer of Snake. Biopolymers 91:1172–1181

[77] Roche Applied Science PNGase F activity, available at: http://lifescience.roche.com/shop/en/global/products/n-glycosidase-f-311153-1, accessed 18 December 2012

[78] Rothman LS, Jacquemart D, Barbe A, Benner DC, Birk M, Brown LR, Carleer MR, Chackerian C, Chance K, Coudert LH, Dana V, Devi VM, Flaud JM, Gamache RR, Goldman A, Hartmann JM, Jucks KW, Maki AG, Mandin JY, Massie ST, Orphal J, Perrin A, Rinsland CP, Smith MAH, Tennyson J, Tolchenov RN, Toth RA, Vander Auwera J, Varanasi P, Wagner G (2004) The HITRAN 2004 molecular spectroscopic database. J. Quant. Spectrosc. Radiat. Transfer, 96: 139-204

[79] Saxe FPM (2008) Diploma Thesis: Functional and morphological investigation of the epidermis of the sandfish. LuFG Zelluläre Neurobionik, RWTH Aachen

[80] Schmied H (2007) Rasterelektronenmikroskopische Analyse der Oberflächenstruktur der Schuppen verschiedener Arten von Glattechsen (Scincidae) der Gattungen *Scincus*, *Scincopus*, *Eumeces* und *Acontias*. Blockpraktikum, Zoological Research Museum Alexander Koenig.

[81] Scott RPW (1986) Liquid chromatography detectors (2nd Ed), Elsevier, New York, pp. 7-48

[82] Seed B (2001) Silanizing Glassware. Curr Protoc Protein Sci., A.3E.1

[83] Sever DM, Hopkins WA (2005) Renal sexual segment of the ground skink, *Scincella laterale* (Reptilia, Squamata, Scincidae). J. Morphol., 266(1):46-59

[84] Shental-Bechor D, Levy Y (2008) Effect of glycosylation on protein folding: A close look at thermodynamic stabilization. PNAS, 105(24):8256-8261

[85] Sigma-Aldrich Life Science: Alkaline beta elimination, available at: http://www.sigmaaldrich.com/life-science/molecular-biology/molecular-biology-products.html?TablePage=19365078, accessed 10 March 2015

[86] Simmons JA, Stein RA (1980) Acoustic Imaging in bat sonar: echolocation signals and the evolution of echolocation. J. Comp. Physiol. A, 135(1):61–84

[87] Krüss liquid properties datasheet, available at: http://www.kruss.de/services/education-theory/substance-data/liquids/, accessed 16 January 2015

[88] Smythe CV (1936) The reactions of Iodoacetate and of Iodoacetamide with various Sulfhydryl groups, with Urease, and with Yeast preparations. J. Biol. Chem., 114(3):601-12

[89] Song X, Lasanajak Y, Xia B, Smith DF, Cummings RD (2009) Fluorescent glycosylamides produced by microscale derivatization of free glycans for natural glycan microarrays. ACS Chem Biol., 4(9):741-50

[90] Staudt K (2012) PhD thesis: Comparative surface and molecular investigations of the sandfish's epidermis (Squamata: Scincidae: *Scincus scincus*). LuFG Zelluläre Neurobionik, RWTH Aachen

[91] Staudt K, Böhme W, Baumgartner W (2012) Comparative Investigations of the Sandfishs β-Keratin(Reptilia: Scincidae: *Scincus scincus*). Part 2: Glycan-Based Friction Reduction. JBBTE, 16:1-9

[92] Staudt K, Saxe FPM, Schmied H, Soeur R, Böhme W, Baumgartner W (2012) Comparative investigations of the sandfish's β-keratin. Part 1: Surface and molecular examinations. JBBTE, 15:1-16

[93] Storch V, Welsch U (2003) Systematische Zoologie (6th Ed), Spektrum, München, pp. 652-667

[94] Takahashi N (1977) Demonstration of a new amidase acting on glycopeptides. Biochem. Biophys. Res. Commun., 76(4):1194-1201

[95] The Engineering ToolBox: Tensile Modulus - Modulus of Elasticity or Young's Modulus - for some common Materials, available at: `http://www.engineeringtoolbox.com/young-modulus-d_417.html`, accessed 20 February 2015

[96] The Welding Institute surface energy data sheet, available at: http://www.twi-global.com/technical-knowledge/faqs/material-faqs/faq-what-are-the-typical-values-of-surface-energy-for-materials-and-adhesives/, accessed 16 January 2015

[97] Tkatchenko A, Scheffer M (2009) Accurate Molecular Van Der Waals Interactions from Ground-State Electron Density and Free-Atom Reference Data. PRL, 102:0730051-4

[98] Tolivia J, Navarro A, Tolivia D (1994) Polychromatic staining of epoxy semithin sections: a new and simple method. Histochemistry, 101(1):51-55

[99] Toni M, Dalla Valle L, Alibardi L (2007) Hard (Beta-)Keratins in the Epidermis of Reptiles: Composition, Sequence, and Molecular Organization. Journal of proteome research reviews, 6(9):3377-92

[100] UniCarb Database, available at: `http://unicarb-db.biomedicine.gu.se/`, accessed 19 March 2015

[101] Varki A, Cummings RD, Esko JD, Freeze HH, Stanley P, Bertozzi CR, Hart GW, Etzler ME (2009) Essentials of Glycobiology (2nd Ed), Cold Spring Harbor, New York, pp. 101-280

[102] Vihar (2012) M.Sc. thesis: The subharenal (under sand) respiration of the Sandfish (*Scincus scincus*). LuFG Zelluläre Neurobionik, RWTH Aachen

[103] Vitt LJ, Caldwell JP (2014) Herpetology (4th Ed). Academic Press, Amsterdam, pp. 68;

[104] Wilson IBH, Zeleny R, Kolarich D, Staudacher E, Stroop CJM, Kamerling JP and Altmann F (2001) Analysis of Asn-linked glycans from vegetable foodstuffs: widespread occurrence of Lewis a, core α1,3-linked fucose and xylose substitutions. Glycobiology, 11(4):261-274

[105] Wredenberg F, Larson PL (2009) Scratch testing of metals and polymers: Experiments and numerics. Wear 266(1-2):76-83

[106] Zangwill A (1988) Physics at surfaces, Cambridge university press, Cambridge, pp. 185-203

[107] Zhang Q, Qi Y, Hector LG, Cagin T, Goddard WA (2007) Origin of static friction and its relationship to adhesion at the atomic scale. Phys. Rev. B 75(144114):1-7

[108] Zhu J, Hsu CM, Yu Z, Fan S, Cui Y (2010) Nanodome Solar Cells with Efficient Light Management and Self-Cleaning. Nano Lett., 10(6):1979–1984

Materials list

A.1 Materials

A.1.1 Chemicals

2,2-Thiobisethanol	Sigma-Aldrich, München, GER
2-Dodecenylsuccinic acid anhydride (DDSA)	Serva GmbH, Heidelberg, GER
2-Mercaptoethanol	Carl Roth GmbH, Karlsruhe, GER
2-Propanol	Carl Roth GmbH, Karlsruhe, GER
2,5-dihydroxy benzoic acid	Sigma-Aldrich, München, GER
3-aminopropyltriethoxysilane (APTES)	Sigma-Aldrich, München, GER
8-Aminopyrene-1,3,6-Trisulfonate (APTS)	Beckman Coulter, Krefeld, GER
Acetic acid	Carl Roth GmbH, Karlsruhe, GER
Acetone tech.	Applichem GmbH, Darmstadt, GER
Acetone p.a.	Carl Roth GmbH, Karlsruhe, GER
Acetonitrile (ACN)	Carl Roth GmbH, Karlsruhe, GER
anti-ß-keratin AB	Prof. Dr. Lorenzo Alibardi, University of Bologna, ITA
Ammonium persulfate (APS)	Sigma-Aldrich, München, GER
Boric acid	Carl Roth GmbH, Karlsruhe, GER
Bradford reagend (roti quand)	Carl Roth GmbH, Karlsruhe, GER
Bromphenole blue	Carl Roth GmbH, Karlsruhe, GER
Bovine serum albumin (BSA)	Carl Roth GmbH, Karlsruhe, GER
BSAc	Provided by Agnes Weth, RWTH Aachen, GER
$CaCl_2$	Carl Roth GmbH, Karlsruhe, GER
Cacodylate	Serva GmbH, Heidelberg, GER
carbol gentiana violet	Chroma - Waldeck, Münster, GER
carbol methylene blue [1]	
Chlorophorm	Carl Roth GmbH, Karlsruhe, GER
Citric acid	Carl Roth GmbH, Karlsruhe, GER
Coomassie blue staining solution [2]	

[1] Carbol methylene blue: 2% methylene blue (dissolved in dH_2O) + 0.5% phenole (also dissolved in dH_2O)
[2] 2.5g Serva Blau G250, 454ml 2-Propanol, 454ml dH_2O, 92ml glacial acetic acid

Coomassie blue destaining solution [3]	
Concanavalin A HRP	Sigma-Aldrich, München, GER
Cracking buffer for yeast protein extraction [4]	
$CuSO_4$	Merck, Darmstadt, GER
Diethylenglycol	Sigma-Aldrich, München, GER
Diethylpthalate	Sigma-Aldrich, München, GER
Dimethyl sulfoxide (DMSO)	Carl Roth GmbH, Karlsruhe, GER
Dowex 50W-X8	Sigma-Aldrich, München, GER
ECL 1 [5]	
ECL 2 [6]	
EDTA (Ethylenediaminetetraacetic acid)	Carl Roth GmbH, Karlsruhe, GER
Electrophoresis buffer [7]	
Ethylenediamine	Sigma-Aldrich, München, GER
Ethyleneglycol	Sigma-Aldrich, München, GER
Ethanol (Et-OH) p.a.	Carl Roth GmbH, Karlsruhe, GER
Euparal (Eucalyptol)	Chroma - Waldeck, Münster, GER
Fetuin	Sigma-Aldrich, München, GER
Film developer	Kodak, Stuttgart, GER
Film fixative	Kodak, Stuttgart, GER
Formvar	Science Services GmbH, München, GER
Glucose	Sigma-Aldrich, München, GER
Glutaraldehyde	Sigma-Aldrich, München, GER
Glycerol	Serva GmbH, Heidelberg, GER
Glycidyl ether 100	Serva GmbH, Heidelberg, GER
Glycin	AppliChem, Darmstadt, GER
Goat-anti-rabbit AB HRP	Jackson ImmonoResearch, West Grove, USA
H_2O (tap, distilled, double distilled)	
H_2O_2	Carl Roth GmbH, Karlsruhe, GER
HCl	Carl Roth GmbH, Karlsruhe, GER
HEPES	Carl Roth GmbH, Karlsruhe, GER
Hexamethylenediamine	Sigma-Aldrich, München, GER
Hexamethyldisilazane (HMDS)	Carl Roth GmbH, Karlsruhe, Deutschland
Iodoacetamide	Sigma-Aldrich, München, GER
KCl	Carl Roth GmbH, Karlsruhe, GER
KH_2PO_4	Carl Roth GmbH, Karlsruhe, GER

[3] 50ml glacial acetic acid, 75ml Et-OH, ad dH_2O

[4] 48g Urea, 5g SDS, 4ml of 1M Tris/HCl (pH 6.8), 20μl of 0.5M EDTA, 40mg bromphenol blue, ad 100ml dH_2O

[5] 1ml 250mM Luminol(DMSO), 0.44ml 90mM p-Cumaric acid(DMSO), 10ml 1M Tris pH8.5, ad 100ml H_2O

[6] 64μl 30% H_2O_2, 10ml 1M Tris pH 8.5, ad 100ml H_2O

[7] 10g SDS, 144g Glycin, 30g Tris, ad 2l dH_2O - diluted 1:5 with dH_2O before use.

Lead citrate	Sigma-Aldrich, München, GER
Luminol	Sigma-Aldrich, München, GER
LR White *	Sigma-Aldrich, München, GER
Methyl iodide	Sigma-Aldrich, München, GER
Methylnadic anhydride (MNA)	Serva GmbH, Heidelberg, GER
$MgCl_2$	Carl Roth GmbH, Karlsruhe, GER
Milk powder	Applichem, Darmstadt, GER
$MnCl_2$	Carl Roth GmbH, Karlsruhe, GER
$NaBH_4$	Sigma-Aldrich, München, GER
NaCl	Carl Roth GmbH, Karlsruhe, GER
Na_2CO_3	Carl Roth GmbH, Karlsruhe, GER
Na_2HPO_4	Carl Roth GmbH, Karlsruhe, GER
NaOH	Carl Roth GmbH, Karlsruhe, GER
Nitrocelulose (NC) membrane	Amersham, Freiburg, GER
NH_4CO_3	Local apothecary
O-glycosidase	Roche Applied Science, Mannheim, GER
Osmium tetroxide	Science services, München, GER
Panceau red	Carl Roth GmbH, Karlsruhe, GER
Pararosaniline	Chroma - Waldeck, Münster, GER
p-Cumaric acid	Sigma-Aldrich, München, GER
Pentanediol	Sigma-Aldrich, München, GER
Phosphate buffered saline (PBS) [8]	
Phenole	Carl Roth GmbH, Karlsruhe, GER
Phenylmethylsulfonyl fluoride (PMSF)	Carl Roth GmbH, Karlsruhe, GER
PNGase F (N-glycosidase)	Roche Applied Science, Mannheim, GER
Polyacrylamide gel (Rotiphorese)	Carl Roth GmbH, Karlsruhe, GER
Pyridine	Sigma-Aldrich, München, GER
R-Gent SE-EM Activator	Aurion, Wageningen, NED
R-Gent SE-EM Enhancer	Aurion, Wageningen, NED
R-Gent SE-EM Initiator	Aurion, Wageningen, NED
Sample buffer - PAGE [9]	
Sodium dodecyl sulphate (SDS)	Carl Roth GmbH, Karlsruhe, GER
Serva Blau G250	Serva GmbH, Heidelberg, GER
Sodium citrate	Carl Roth GmbH, Karlsruhe, GER
Sodium cyanoborohydride ($NaBH_3CN$)	Sigma-Aldrich, München, GER
Streptavidin gold particles	Jackson Immuno Research, Newmarket, UK
Sucrose	Serva GmbH, Heidelberg, GER
Tetramethylethylenediamine (TEMED)	Carl Roth GmbH, Karlsruhe, GER

[8] 137mM NaCl, 2.68KCl, 9.58mM $Na_2HPO_4x2H_2O$, 1.47mM KH_2PO_4

[9] 3x concentrated: 0.454g tris, 1.2g SDS, 7.56g glycin, 400μl bromphenol blue (2mg/ml), ad. 20ml dH_2O

Transfer buffer for blotting [10]	
Trifluoroacetic acid (TFA)	Sigma-Aldrich, München, GER
Tris	Carl Roth GmbH, Karlsruhe, GER
Tris(dimethylaminomethyl) phenol	Serva GmbH, Heidelberg, GER
Trypsin	Serva GmbH, Heidelberg, GER
Tween	Carl Roth GmbH, Karlsruhe, GER
Uranyl acetate	Sigma-Aldrich, München, GER
Urea	Sigma-Aldrich, München, GER
WFA biotin antibody	Linaris GmbH, Dossenheim, GER
WGA biotin antibody	Linaris GmbH, Dossenheim, GER

A.1.2 Laboratory equipment

AFM	Thermo Microscopes, Sunnyvale, CAN
AFM	Nanosurf, Liestal, SUI
Centrifuge	VWR, Wien, AUT
Curing forms for resins - silicone	
Curing forms for resins - PET	
CE Analysator P/ACE MDQ	Beckman Coulter, Krefeld, GER
Digital camera Canon PowerShot S3 IS	Canon, Osaka, Japan
Dissicator	
Electrophoresis chamber	Bio-Rad, München, GER
Electrophoresis semidry blotting device	Bio-Rad, München, GER
Electrophoresis gel stand	Bio-Rad, München, GER
Heating Plate 150W	Medax, Olching, GER
Laboratory oven	Memmert, Schwabach, GER
Laboratory shaker	Gesellschaft for Labortechnik, Burgwedel, GER
Magnetic stirrer	VWR, Wien, AUT
MALDI MS	Bruker Daltonics, Bremen, GER
Table top Centrifuge	VWR, Wien, AUT/ Eppendorf, Hamburg, GER
Goniometer	
pH-meter	Mettler Toledo, Wien, AUT
Pipettes (10,100,100μl)	Eppendorf, Hamburg, GER
Pipettes (10,100,100μl)	VWR, Wien, AUT
Pipette (automatic - 1000μl)	Mettler Toledo
UHU power glue gel	UHU, Baden, GER
Ultramicrotome	Reichert, Wien, AUT
TEM	Zeiss, Oberkochen, GER
Speed vacuum concentrator	Eppendorf, Hamburg, GER

[10] 3.03g tris, 14.41g glycine, 10g SDS, 200ml methanol, 800ml dH_2O

Raman Spectrometer
Vortex

A.1.3 Miscellaneous

Baker's yeast (*saccharomyces cerevisiae*)	Local supermarket in Linz, AUT
Dental silicone - President light body	Coltene, Altstätten, SUI
Dialysis tubing (MWCO 3500)	Serva
Diamond knife	Diatome, Hatfield, USA
Glass beads (d=0.5mm)	Lactan, Graz, AUT
Glass knives	
Glass plates	
Glass slides	Paul Marienfeld, Königshofen, GER
Grid incubation chamber	
Kimtech wipes	Kimberly-Clark, Irving, USA
Magnetic stir bars	
Measuring cylinders	
Mistletoe leaves (*Viscum album*)	
Ni grids for TEM	
Parafilm	Pechiney Plastic Packaging Company, Chicago, USA
Petry dishes (glass, plastic)	
Photo film	Fuji, Minato, Japan
Pipette tips (10,100,1000μl)	Eppendorf, Hamburg, GER
PMMA sheets	Evonik, Essen, GER
Sandfish exuviae (*Scincus scincus*)	
Saran foil	Saropack, Rorschach, SUI
Sodium soap (non parfumated)	
Spacers (teflon)	
Sweet almonds (*Prunus dulcis*)	Local supermarket in Linz, AUT
Syringes (5,10,20ml)	
Terrarium lightbulb (solar spectrum), 60W	Terra Exotica, Alfeld, GER
Tabletop light	
Wet chamber	

A.1.4 Software

Contact angle measurement software	self written
GChemPaint	open source
Gedit	open source
GIMP	open source
GNU Octave	open source

ImageJ	open source
Inkscape	open source
LibreOffice	open source
Maple	Maplesoft, Waterloo, USA
Matlab	MathWorks, Natick, USA
TeXmaker	open source
VLC media player	open source

A.1.5 Animal care

The 3 sandfish specimen were raised in a terrarium, sized approximately $50 \times 60 \times 120$cm, with a rough imitation of a sandy desert landscape. The terrarium was filled with approximately 30cm of Sahara sand and additional surface shading objects were added such as logs, a seed bowl and a small drinking well. Heating and lighting was provided with 1 150W (switched on/off every 60min) and 1 100W (switched on all day) solar spectrum terrarium bulbs and 1 50W Osram Vitalux UV lightbulb (switched on all day). The lamps were active from 8.00 till 19.00 and created a day time temperature of 30 to 45°C and a night time temperature of 17 to 20°C. The animals were fed with steppe crickets 3 times per week.